Towards Chiralomics:

Targeted and Untargeted Gas Chromatography-Mass Spectrometry based Enantioselective Metabolome Analysis

Dissertation

zur Erlangung des Doktorgrades der Naturwissenschaften (Dr. rer. nat.)

an der Fakultät für Chemie und Pharmazie

der Universität Regensburg

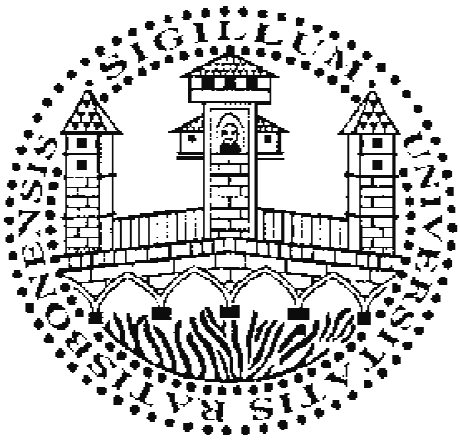

vorgelegt von

Magdalena C. Waldhier

aus Neustadt a. d. Donau

im Jahr 2015

Diese Doktorarbeit entstand in der Zeit vom Mai 2009 bis Oktober 2014 (mit Ausnahme der Mutterschutz- und Elternzeit vom August 2012 bis September 2013) am Institut für Funktionelle Genomik der Universität Regensburg.

Die Arbeit wurde angeleitet von Prof. Dr. Peter J. Oefner.

Promotionsgesuch eingereicht am 16.10.2015

Kolloquiumstermin: 18.12.2015

Prüfungsausschuss:	Vorsitzender:	Prof. Dr. Jörg Heilmann
	Erstgutachter:	Prof. Dr. Frank-Michael Matysik
	Zweitgutachter:	Prof. Dr. Peter J. Oefner
	Drittprüfer:	Prof. Dr. Joachim Ruther

Für meine Familie

Danksagung

Nach all der getanen Arbeit, den Anstrengungen und den unzähligen niedergeschriebenen Worten darf ich nun endlich danke sagen für eine Zeit auf die ich mit Freude zurückblicke. Es ist schwer in Worte zu fassen wie sehr mich die Jahre bereichert haben an Erfahrungen, Erkenntnissen, Vorbildern und Freundschaften. Es ist ein Privileg für mich an dieser Stelle auf meine Zeit in der Forschung zurückblicken zu können und den Personen die sie mir ermöglicht haben, sie begleitet und mitgestaltet haben von Herzen “DANKE” sagen zu dürfen.

Mein aufrichtiger Dank geht an erster Stelle an **Prof. Dr. Peter Oefner** der es mir ermöglichte am Institut für funktionelle Genomik meine Dissertation zu einem äußerst interessanten Themengebiet anzufertigen, welches in der Metabolomik bisher wenig Beachtung gefunden hatte. Ich bedanke mich für Ihr Vertrauen, die Unterstützung und den Mut, die nötig waren um in diesem Themenbereich neue Akzente setzen zu können. Danke auch für Ihre Ehrlichkeit und Fairness.

Des Weiteren gilt mein Dank **Prof. Dr. Frank-Michael Matysik** für die bereitwillige und freundliche Übernahme des Erstgutachtens. Danke für Ihr aufrichtiges Interesse an meiner Arbeit.

Prof. Dr. Joachim Ruther und **Prof. Dr. Jörg Heilmann** danke ich für die Übernahme des Drittprüferschaft bzw. des Prüfungsvorsitzes. Ich weiß Ihre Zeit und Ihr Interesse zu schätzen.

Mein herzlicher Dank geht an **Dr. Katja Dettmer-Wilde** und **Dr. Michael Gruber** die mir mit Rat und Tat während meiner Zeit in der Forschung zur Seite standen. Danke dass Ihr Euren großen Erfahrungsschatz zu GC Anwendungen mit mir geteilt habt und für das ‘Handauflegen’ am Gerät wenn gerade nichts mehr so lief wie es sollte. Danke auch für die aufbauenden Worte wenn ich mal den Glauben an meine Fähigkeiten verloren hatte. Von Euch durfte ich sehr viel lernen.

Prof. Dr. Claus Hellerbrand, **Dr. Christoph Dorn**, **Dr. Karin Landfried**, **Dr. Ernst Holler** und **Anja Thomas** danke ich für die großzügige Bereitstellung von Probenmaterial und für den guten Informationsfluss bei Fragen.

Ich danke **Nadine Nürnberger** für die Hilfe im Labor, für deine ‘freien Spitzen’ und deine flinken Hände. Es hat Spaß gemacht mit dir im selben Labor zu arbeiten. Denn mit deinen stets amüsanten Anekdoten und deiner Spitzenperformance als Labor DJ sorgst du immer für gute Stimmung. Auch die Kaffeepausen mit dir bleiben unvergesslich.

Auch bin ich dankbar für die Hilfe von **Claudia Samol**, **Carry Louis** und **Annkathrin Immervoll** sowie **Dr. Joerg Reinders und Dr. Yvonne Reinders**. Danke für Eure guten Tipps und Euren Zuspruch. Ich freue mich sehr euch kennen zu dürfen. Ich habe die Zeit mit euch genossen und hoffe unsere Freundschaft bleibt erhalten.

Ich bedanke mich bei allen ehemaligen Doktoranden des Institutes: **Dr. Birgit Timischl, Dr. Hannelore Kaspar**, **Dr. Axel Stevens**, **Dr. Martin Almstetter, Dr. Nadine Aßmann und Sophie Schirmer** und bei **Dr. Wentao Zhu** für die herzliche Aufnahme in die Gruppe, die stets lockere und heitere Arbeitsatmosphäre und für eure Vorbildfunktion. Dr. Martin Almstetter danke ich insbesondere für die fruchtbare und für mich sehr lehrreiche Zusammenarbeit am GC×GC. Es war sehr angenehm mit dir zu Arbeiten. Danke für deine Geduld, deine Komplimente und für das Teilen des “Pegasus” und des “Jean Pierres” mit mir.

Bei **Dr. Prof. Wolfram Gronwald** und seinen Doktoranden, hierbei insbesondere bei **Dr. Matthias Klein** und **Jochen Hochrein** bedanke ich mich für die Hilfe mit ‘R’ und die interessanten Diskussionen zur Datenauswertung, sowie für eure geduldigen Erklärungsversuche wenn ich mit meinen Statistik-Latein am Ende war. Ihr ward immer für Fragen offen.

Auch ohne **Christian Kohler** wäre diese Arbeit nicht möglich gewesen, da ich dank ihm optimal vernetzt war. Dein IT support hat mir das Leben oft einfacher gemacht. Ein herzliches merci für deine Hilfe.

Auch bei allen anderen ehemaligen und aktuellen Mitarbeitern des IFG und des KFB bedanke ich mich herzlich für die gute Zusammenarbeit und Eure kollegiale Art. Insbesondere gilt mein Dank hierbei **Dr. Christoph Moehle** für das bereitwillige Teilen seines Büros und für die angenehmen Gespräche. Ich habe mich immer willkommen gefühlt.

Dr. Alexander Riechers, **Franziska Vogl** und mein ‘Arbeitsehemann’ **Christian Wachsmuth**, bei Euch bedanke ich mich für Eure aufrichtige Freundschaft, das stets offene Ohr in allen Belangen und Eure überaus großzügige Hilfsbereitschaft. Ihr habt mich menschlich bereichert. Glaubt an Euch! Ihr seid herausragende Persönlichkeiten und hervorragende Wissenschaftler. Als Kollegen und Freunde seid ihr Gold wert.

Auch meinen neuen Kollegen von der Agrolab Laborgruppe, hierbei insbesondere , **Barbara Maier**, **Philipp Schaffler**, **Gregor Patschky** und **Elizabeth Liebsch** danke ich für das Verständnis und die Geduld wenn ich manchmal unausgeschlafen in der Arbeit erschien, weil ich zulange in die Nacht gearbeitet habe. Ich gelobe Besserung.

Wie groß meine Dankbarkeit meiner Familie gegenüber ist, ist kaum in Worte zu fassen. Mama (**Christine Orschulik**) und Dad (**Josef Orschulik**) – Eure bedingungslose Liebe definiert mich. Danke für euren unermesslichen Einsatz um mir und meinen Geschwistern ein besseres Leben bieten zu können. Auch meine bessere Hälfte **Matthias Waldhier**, seine Liebe und Unterstützung sind unersetzlich für mich. Du bist mein Fels in der Brandung. Bei meinem Lieblingsmenschen **Benjamin Albert Waldhier** entschuldige ich mich für zu wenig Zeit zum Spielen. Du bist das Beste was mein Leben bisher hervorgebracht hat.

1 Table of Contents

2 Abbreviations and Acronyms

Standard 3-letter abbreviations for proteinogenic amino acids:

Ala	alanine
Arg	arginine
Asn	asparagine
Asp	aspartic acid
Cys	cysteine
Gln	glutamine
Glu	glutamic acid
Gly	glycine
His	histidine
Ile	isoleucine
Leu	leucine
Lys	lysine
Met	methionine
Phe	phenylalanine
Pro	proline
Ser	serine
Thr	threonine
Trp	tryptophan
Tyr	tyrosine
Val	valine

Other abbreviations and acronyms:

2-HG	2-hydroxyglutaric acid
2-KG	2-ketoglutarate
4-HPA	4-hydroxyphenylacetic acid
AA	amino acid

AAE	amino acid enantiomer
ACL	ATP-citrate lyase
APCI	atmospheric pressure chemical ionization
ATP	adenosine triphosphate
BsrV	broad spectrum racemase *Vibrio*
CD	cyclodextrin
CE	capillary electrophoresis
CSF	cerebrospinal fluid
DAO	D-amino acid oxidase
E. coli	*Escherichia coli*
EI	electron impact ionization
FA	fatty acid
fc	fold change
FDR	false discovery rate
FMOC	9-fluoroenylmethyl chloroformate
FWHM	full widths at half maximum
GC	gas chromatography
GC×GC	comprehensive two-dimensional gas chromatography
GlcNAc	N-acetyl-glucosamine
HFB	heptafluorobutanol
HICA	hydroxyisocaproic acid
HMDB	Human Metabolome Database
HPLA	3-(4-hydroxyphenyl)-lactic acid
HPLC	high performance liquid chromatographie
ICA	independent component analysis
IDH	isocitrate dehydrogenase
IS	internal standard

LA	lactic acid
LC	liquid chromatography
LLOQ	lower limit of quantification
LOD	limit of detection
LTP	long-term potentiation
MCF	methyl chloroformate
MDGC-MS	multidimensional gas chromatography-mass spectrometry
MeOH	methanol
MM	master mixture
MS	mass spectrometry
MSD	mass selective detector
MSTUS	MS total useful signal
MurNAc	N-acetylmuramic acid
NAA	N-Acetyl-aspartic acid
NAFLD	non-alcoholic fatty liver disease
NASH	non-alcoholic steatohepatitis
NBD-F	4-fluoro-7-nitro-2,1,3-benzoxadiazole
NIST	National Institute of Standards and Technology
NMDA	N-methyl-D-aspartic acid
NMR	nuclear magnetic resonance
PAG	phenylacetylglycine
PBP	penicillin binding protein
PCA	principal component analysis
PCF	propyl chloroformate
PFPA	pentafluoropropionic acid
PG	peptidoglycan
PGA	pyroglutamic acid

PLA	3-phenyllactic acid
PLOT	porous layer open tubular
PLP	pyridoxal-5-phosphate
PTV	programmed-temperature vaporization
qMS	quadrupole mass spectrometry
R_s	resolution
RSD	relative standard deviation
S/N	Signal-to-noise ratios
SCT	stem cell transplantation
SD	standard deviations
SIBO	small intestinal bacterial overgrowth
SIM	selected ion monitoring
TNF	tumor necrosis factor
TOFMS	time-of-flight mass spectrometry
t_R	retention time
ULOQ	upper limit of quantification
w_b	to base peak width
WCOT	wall coated open tubular

3 MOTIVATION

Metabolomics aims at the reliable and quantitative acquisition of the complete set of endogenous and exogenous small-molecule compounds present within a biological sample in response to environmental and genetic factors. Metabolomics methods should therefore be ideally capable of determining simultaneously thousands of organic molecules with distinctly different but also very similar physicochemical properties. This ambitious goal has so far eluded us, as available techniques suffer from insufficient selectivity and sensitivity. They do not distinguish enantiomers of chiral metabolites and lack in accessibility to all present metabolites. Thus, a variety of complementary analytical tools, including enantioselective methods, is required to comprehensively cover the metabolome[1, 2].

Gas chromatography coupled to mass spectrometry (GC-MS) is widely used in metabolomics studies. GC-MS combines high peak capacity separation, analyte-characteristic detection, and the opportunity to structurally identify biomarkers[1]. Applied to metabolic profiling, GC-MS is used for the sensitive and selective determination of components of metabolite classes or metabolic pathways[1]. Commonly, however, the methods employed lack the selectivity required for the separation and quantitation of chiral metabolites. Chirality is not a rare phenomenon in the metabolome. Sugars, some lipids, most amino acids (AAs) and many organic acids contain one or more chiral centers. Enantiomers behave like image and mirror image. They are not identical but have similar chemical and physical properties with few exceptions. Their different interaction with a chiral environment constitutes the basis for their chromatographic resolution using chiral stationary phases. This is commonly referred to as direct approach. Diastereomers contain more than one chiral center with not all centers having the opposed configuration. They possess different physicochemical properties. This is used for indirect approaches that add chiral centers by derivatization. By means of these strategies the presence of both enantiomers of chiral metabolites, mainly AAs, has been demonstrated in all organisms from bacteria to human. Still, the high requirements on sensitivity and selectivity render the comprehensive stereoselective analysis challenging and call for the continued development of new methodology.

Based on this general motivation, this doctoral thesis set out for the following aims:

Aim 1. Optimization of a previously developed one-dimensional gas chromatography-quadrupole mass spectrometry method for the targeted determination of methyl chloroformate derivatives of selected amino acid enantiomers.

Aim 2. Application of comprehensive two-dimensional gas chromatography - time-of-flight mass spectrometry for improved resolution and detectability of amino acid enantiomers as their methyl chloroformate derivatives.

Aim 3. Application of one-dimensional gas chromatography in combination with both electron ionization quadrupole mass spectrometry and atmospheric pressure chemical ionization time-of-flight mass spectrometry to the untargeted detection, resolution and identification of metabolic enantiomers that differentiate experimental groups.

Aim 4. Application of the methods developed to a mouse model of fatty acid liver disease with the goal of identifying urine based biomarkers in that allow the non-invasive differential diagnosis between reversible fatty liver disease without inflammation and fatty liver disease accompanied by progressive inflammation, which leads, if not recognized and treated in time, to fibrosis, cirrhosis and, ultimately, liver cancer. Such biomarkers are in great need, as with the recent introduction of effective remedies for the treatment of viral hepatitis, fatty liver disease as one of the manifestations of metabolic syndrome, characterized by diabetes, hypertension, obesity and dyslipidemia, is expected to become the leading cause of liver cancer.

4 Background

4.1 Metabolomics

The ultimate goal of functional genomics is the elucidation and prediction of the function and interaction of genes and their interaction in biological entities such as cells, tissues and entire organisms under a given set of genetic and environmental conditions. To that end, methods and technologies are required that allow to capture ideally all gene products at a given molecular level such as gene transcripts, proteins and metabolites in a single analysis[3]. The respective investigation fields are depicted in Figure 1, with metabolomics capturing the nonstructural phenotype of a biological entity[1].

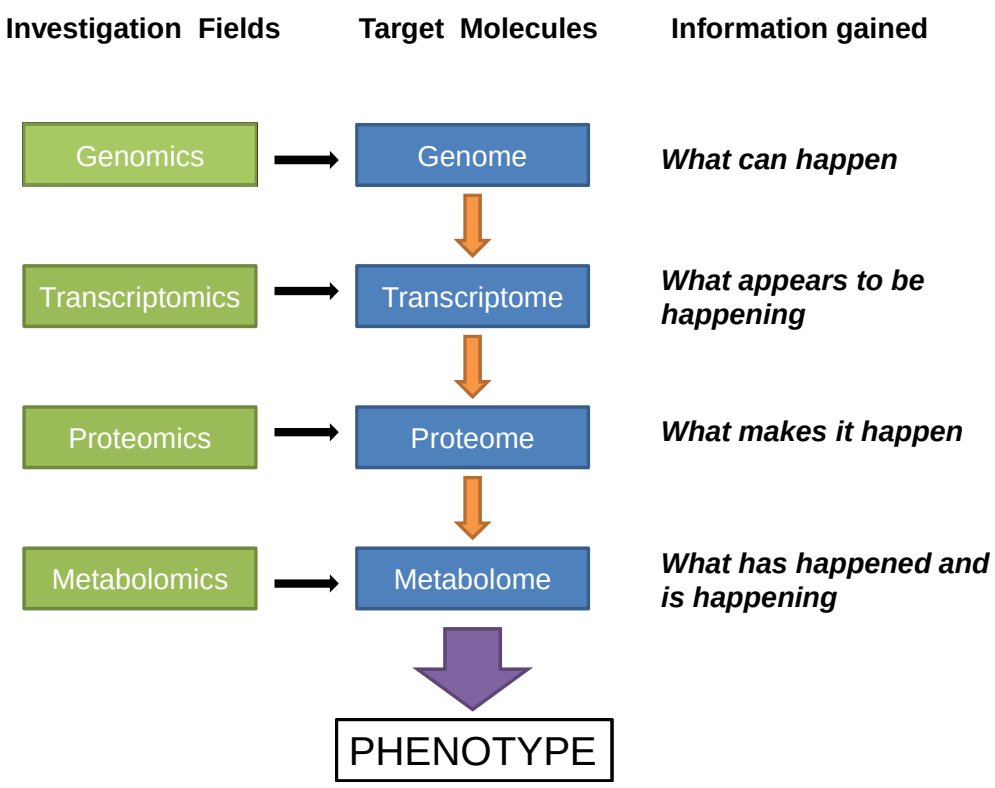

Figure 1. The 'omics' cascade of investigation fields and their molecular targets and associated information gained. The metabolome is very predictive of phenotype. Adapted with permission from[1].

Genes are used to control the synthesis of proteins in organisms. Proteins regulate abundances of metabolites via transport and catalysis of metabolic reactions. The metabolome (all metabolites of a living system) is predictive of phenotype as its alteration reflects the response of an organism to genetic, pathogenic and other

influences[2]. Analyses comparing and combining information gained at different levels of the 'omics' cascade suggest a high discriminatory power of metabolic profiles when used for characterization of organisms into groups[4].

4.1.1 The Fundamentals of Metabolomics

Metabolomics and metabonomics are the two terms applied often interchangeably for the discipline aiming at the comprehensive, systematic and quantitative study of all metabolites in a living system. Materials under investigation are mostly physiological fluids, tissues or cells. The obtained results help to characterize metabolite function, interactions, reactions and their dynamic response to biological stimuli, genetic modification or other events[5]. Therefore, metabolomics generates knowledge about the way living systems function and provides potential for understanding the pathogenesis of disease[6]. Early diagnosis and development of novel therapeutic strategies are chances of a founded interpretation of metabolomics data sets. Furthermore, information gained by metabolomics methodologies allowed, together with the results from the other 'omics' disciplines, mapping the complex pathway network of energy metabolism, and understanding the underlying redox metabolism as well as the biosynthesis of physiologically active macromolecules and their precursors. Beyond, flux analyses of the metabolome aim at the detection of the reaction rates in the network and their regulation as response to specific biological circumstances.

Metabolites are low molecular-weight molecules (typically< 1500 Da) that participate in metabolic reactions. Comparing physicochemical properties there are great differences between representatives of different metabolite classes whereas they can be similar for metabolites of the same class especially for isobaric metabolites like e.g. L-Leu and L-Ile and almost identical for enantiomers. Thus the biggest challenge in metabolomics studies remains the development of a method that is capable of capturing and resolving the whole metabolome. Currently used detection techniques like nuclear magnetic resonance (NMR) and mass spectrometry (MS) suffer from insufficient detectable concentration range [1] and selectivity, and thus do not allow to monitor all metabolites, not even of a simple organism like *Escherichia coli* (*E.coli*) holding about 750 metabolites[7]. The disciplines above metabolomics in the 'omics'

cascade (Figure 1) are less affected by molecular diversity as investigated macromolecules are basically build up from a manageable number of molecules. In contrast metabolomics deals with small target molecules that can be easily modified and transported through the whole organism.

Metabolites can be synthesized by one or more anabolic reactions (endogenous metabolites) or they are exogenous and therefore are not part of any anabolic pathway. Metabolites can be altered and degraded by one or more catabolic pathways and can be excreted from the organism. The complexity of physicochemical properties, pathways, interactions and fluxes renders the acquisition, analysis and interpretation of metabolome data sets challenging. Different strategies, explained in the next chapter, try to tackle these problems.

4.1.2 Strategies in Metabolomics Studies

Metabolomics studies are mainly based on two different strategies: Targeted (Metabolic profiling, Target analysis) and untargeted analysis (metabolic fingerprinting, metabolic footprinting).

Metabolic profiling methods concentrate on a number of metabolites related to a biochemical pathway or a metabolite class[1]. They often use selective sample preparation (e.g. extraction), separation (e.g. stationary phases with specific selectivity) and detection (e.g. selected ion monitoring mode of quadrupole mass selective detectors) to remove 'irrelevant' analytes and to obtain high-quality data that allow absolute quantification of target metabolites with high accuracy, precision and low LLOQs[8]. The objective is to investigate well-defined hypotheses.

Targeted analysis focuses on very few metabolites like on substrates or products of enzymes or biomarkers of specific diseases. It aims at the direct study of primary effects of genetic alterations or serves as a diagnostic tool[1, 9].

Metabolic fingerprinting refers to holistic analysis of as many metabolites as possible and therefore is the nearest to a real metabolomics approach. It uses a straightforward universal sample preparation, provides low-quality data and therefore is only semi-quantitative. It is hypothesis-generating. The intention is to classify samples into groups by their metabolite patterns or 'fingerprints' that differ due to

disease, genetic or environmental perturbations[1]. In order to achieve this, chemometric or comparative visualization strategies are required to handle large and complex datasets[10]. The final goal is to identify discriminating metabolites that are often investigated more closely in follow-up targeted studies.

Metabolic footprinting is a special metabolic fingerprinting approach analyzing extracellular metabolites in cell culture medium to study metabolite excretion or uptake by cells[1, 11].

4.1.3 Chiral Metabolomics

If entered into pubmed the expression ‘chiral metabolomics’ yields 24 results and the number increases continuously, with some publications using the term in their title[12] . As no consistent ‘-omics’ expression was introduced so far, other names like enantioselective or stereoselective metabolomics can be used interchangeably. Subfields of metabolomics like lipidomics and glycomics reduce the scope of recorded metabolites. In contrast chiral metabolomics should expand the field of view by the resolution of stereoisomers. However, until today chiral metabolomics has relied exclusively on targeted analysis focusing on the separation of a few selected enantiomers. Researchers first competed for the development of separation strategies as the similarity of enantiomers in structure and physicochemical properties makes their resolution by conventional approaches impossible. The application of chiral stationary phases or alternatively the creation of diastereomers by a chiral derivatization reagent are established and routinely used approaches in chromatography, electrophoresis and NMR based chiral metabolomics. While biological applications have been accomplished, it became clear that not only selectivity but also sensitivity and linear range are major concerns in chiral metabolomics. Thus, preseparation steps have been included routinely in order to separate targets from the biological matrix. Other problems are high costs of chiral materials and fast aging of chiral selectors. The motivation of chiral metabolomics was to demonstrate the presence of rare enantiomers, and moreover to elucidate their biological functions. The most frequently targeted molecules in chiral metabolic profiling methods are AAs. The importance of the L-enantiomer is obvious as they are building blocks of proteins, whereas biological functions of its antipode were

unknown for decades for eukaryotes and are still not fully understood. Further metabolite classes of interest in enantioselective metabolomics have been organic acids[13], lipids[14] and metabolic degradation products of drugs[15] [16]. A real chiral metabolomics approach, recording the most detailed metabolic fingerprint of a biological system, is the next step to go and long overdue, since the importance of stereo-differentiation in biochemical processes is well-known[7] for a long time[17]. Today with several enantioselective methodologies being successfully tested and established, it is insufficient to conjointly analyze and interpret enantiomers in metabolic fingerprints.

4.2 Significance of D-AAs and other Chiral Metabolites in Organisms

Traditionally AAs were thought to be synthesized and applied exclusively in their L-configuration in all kingdoms of life[18]. Today we know that D-AAs are present in all kinds of organic materials even in fossils, plants and inorganic materials like e.g. meteorites. They are examined in fossils for age determination or in meteorites for the purpose of understanding the origin of life[19-21]. The following two chapters focus on existing knowledge of D-AA presence, origins and biological functions in bacteria and mammals including humans. These organisms comprised the D-AA sources of biological samples analyzed in this thesis. The last chapter of this section emphasizes the significance of enantiomers, others than AAs, in mammals. It indicates the broad scope of target molecules in chiral metabolomics.

4.2.1 D-AAs in Prokaryotes

Bacteria produce the highest D-AA content among all organisms and possess an extensive D-AA metabolism. Regulatory functions of free D-AAs and their presence in the peptidoglycan (PG) of the cell wall contribute essentially to the remarkable resistance of bacteria to physical, chemical and biological insults[17]. Their distribution, metabolism and functions in bacteria are summarized in this section.

4.2.1.1 Distribution and Metabolism

D-AAs can be found in the cytoplasm, in the cell wall as building blocks of the PG, in the periplasm, in peptides and the supernatant of bacteria[17]. D-AAs are released in the cytoplasm after their conversion from the L-configuration by several AA racemases, each able to catalyze the isomerization of one AA type. There are five types of AA racemases known. They are classified into cofactor-dependent and cofactor –independent. Ala racemases and Ser racemases share a similar pyridoxal-5-phosphate (PLP)-dependent catalytic mechanism[17, 22]. In contrast, Glu racemases, Asp racemases and Pro racemases catalyze cofactor-independent conversions.

The PG is a netlike macromolecule situated on the outside of the cytoplasmic membrane in almost all bacteria[17]. It maintains cell shape, strength and the resistance to osmotic pressure and is composed of linear glycan chains holding repeated units of a disaccharide that consists of N-acetyl glucosamine (GlcNAc) and N-acetylmuramic acid (MurNAc)[17, 18]. These strands are crosslinked by D-AA containing peptides. The synthesis of the PG monomers occurs in the cytoplasm where the, mostly D-Ala and D-Glu containing, pentapeptides are build up directly on a uridine diphosphate-activated MurNAc by adenosine triphosphate(ATP)-dependent synthetases[17, 23, 24]. Required D-AAs are provided with the help of D-AA transaminase[25] and AA racemases[17, 18]. In the next step the peptide bound MurNAc is linked to GlcNAc and translocated to the periplasm where it is finally incorporated into the PG polymer via transglycosylation and transpeptidation by penicillin binding proteins (PBPs)[17, 24]. Besides the above mentioned most frequently found D-AAs in the PG, there are some bacteria known to hold other D-AAs in their cell wall like e.g. *Enterococcus faecium* holding D-Asp [26] and *Lactococcus lactis*, which utilizes both D-Asp and D-Asn[27]. In *Vibrio cholera* D-Met and D-Leu have been found to replace D-Ala on the fourth position of the peptide bridge in 3-4% of cases in stationary phase[17]. This is one effect of the remarkable production and release of D-Met, D-Leu, D-Val, and D-Ile in and from the periplasm, yielding in sum a D-AA concentration of about one millimolar in the stationary phase supernatant of these bacteria[18]. A broad spectrum racemase that was thus called BsrV (V stands for in *Vibrio*) was found to be responsible for the extensive release of these D-AA types. It is contrary to single AA recemases located in the periplasm and likely only active in stationary phase. Millimolar D-AA levels in stationary phase media are not confined to *Vibrio cholera*

but are also detected in case of other species of diverse phyla (e.g. *Streptomyces lividans*, *Staphylococcus aureus* and *Deinococcus radiodurans*). This suggests that many bacterial phyla encode broad-spectrum racemases, able to produce D-AAs different to those required typically for PG construction[17, 18]. Finally, there are also enzymes that catalyze the degradation of D-AAs like the membrane-bound, cytochrome-linked D-Ala dehydrogenase[28].

The bridge-peptides of the PG are not the only peptides in prokaryotes that benefit from the incorporation of D-AAs. Most free peptides holding D-AAs are built by nonribosomal peptide synthetases. There may be many more D-AA containing, biologically active peptides in prokaryotes, but they are probably often overlooked[17].

4.2.1.2 Biological functions

Free D-AAs in bacteria are known to be utilized as carbon and energy sources for bacterial growth[17, 28]. D-AAs as components of the cell wall and of free peptides provide protection against degradation by proteases that catalyze mostly a cut between two L-AAs. Due to this protective property and the fact that most free bacterial peptides holding D-AAs bear antimicrobial functions, D-AAs are an important factor of bacterial defense mechanisms. Furthermore D-AAs bear several regulatory functions concerning sporulation and adaption to harsh environmental conditions[17, 18]. In 1949 D-Ala was found to be a potent inhibitor of spore germination and an antagonist of the highly specific germinant L-Ala in many *Bacillus* species. The promoting action of L-Ala was impeded strongly by a D-Ala portion as low as 3% of the present L-Ala medium concentration[29]. In case of a *Bacillus anthracis* infection in murine macrophages a complete inhibition of germination required the presence of D-Ala together with D-His[30]. In contrast, in *Myxococcus xanthus* eleven D-AA types including D-Ala, D-Gln, D-Asn, D-Met and D-Trp were capable to induce starvation-independent sporulation. Among tested D-AAs only D-Asp, D-His, D-Lys and D-Pro did not effect starvation-independent sporulation[31]. D-AAs are not only building blocks of the bacterial cell wall, moreover they were found to manage the adaption of PG structure and content to stationary phase conditions [17, 18]. Due to this influential function they also determine the shape and the strength of the cell. This remodeling regulation of the PG by D-AAs was investigated in detail for species releasing D-AAs

in the millimolar range from their periplasm to the stationary phase medium. In the respective study, the stationary phase PG content was doubled in a mutant lacking BsrV, the enzyme responsible for elevated D-AA synthesis. However, the PG of the wild type was 20 times more resistant to osmotic pressure and thus differed clearly in its structure and architecture from the mutant's PG. The authors gathered from their results that D-AAs might be substrates and regulators of enzymes (PBPs) synthesizing and rearranging the PG network in the periplasm, and may trigger therefore growth inhibition when population density reaches saturation. The incorporation of high abundant unusual D-AAs into the cell wall was also suggested to contribute to the regulation of PG remodeling[17, 18]. A further regulatory role was discovered recently. It concerns biofilms being communities of bacteria. When biofilms age, waste products start to accumulate and nutrients become rare. Therefore, it becomes advantageous for biofilm-connected bacteria to leave this association. A mixture of D-Leu, D-Met, D-Tyr and D-Trp induced biofilm dissolution or could prevent biofilm formation by *Bacillus subtilis* at a concentration of about ten nanomolar. This function seems to be based on the replacement of the terminal D-Ala in the peptide side chain of PG by the named active D-AAs, which inhibited the anchoring of amyloid fibers that connect cells in biofilm assembly. This effect was also reported for *Staphylococcus aureus* and *Pseudomonas aeruginosa* [32].

4.2.2 D-AAs in Mammals

Homochirality of AAs in proteins is essential for all known organisms as it allows the protein its specific folding that determines its active sites and biological functions. However, as D-AAs were excluded from the ribosomal protein synthesis it was concluded that they were in general excluded from higher organisms. This assumption was revoked when D-AA analysis was expanded from prokaryotes to eukaryotic organisms. Until now D-AAs were detected in various living higher organisms, among others in human and other mammals in the form of free D-AAs, peptides and proteins[33]. Biochemical pathways and functions were identified and D-AAs were suggested as biomarkers for disease and potential therapeutical targets[34-39]. The so far gained knowledge about the relevance of D-AAs in mammals is summarized in this chapter.

4.2.2.1 DISTRIBUTION AND METABOLISM

Pätzold et al detected D-Ala , D-Asx (D-Asn+D-Asp), D-Glx (D-Gln+D-Glu) and D-Ser in the brain of various mammals like wallaby, mole, monkey and cow, with D-Ser being clearly the most abundant D-AAs in mammalian brains. The highest D-Ser concentration was found in the brain of monkey (4.2 µmol/g). Relative and absolute amounts of D-Ser were distinctly higher in the cerebrum than in the cerebellum of rabbit and pig[40]. This is consistent with the findings by Nagata et al., who found D-Ser amounts to be high in the forebrain of rat, mouse and bull (approximately 400 nmol/g wet weight) and low in the hindbrain. D/L ratios of Ser were approximately constant (~0.4) in all regions of the forebrain of rats except for the olfactory bulb where it was lower (~0.12)[41]. Significant D-Ser amounts were found to be produced in glial cells and neurons from L-Ser by serine racemase[42]. Moreover an age dependency of D-Ser absolute and relative levels in the fore- and hindbrain of mice and rat was observed [41, 43]. Another D-AA found at significant concentrations in mammalian brains is D-Asp. High D-Asp levels were present in the cerebrum of young rats (≥100 nmol/g) that decreased with increasing age as did the D-Asp amounts in the cerebellum, kidney, liver and blood even though they were lower from the beginning and decreased more slowly[43, 44]. In contrast, in the pituitary gland D-Asp levels increased continuously in rats over 42 weeks after birth, while in testis, spleen and thymus D-Asp levels increased until 14 weeks after birth[43]. In human frontal cortex D-Asp concentrations were shown to be low during lifetime but high at week 14 of gestation and continuously falling until birth whereas D-Ser levels stayed high during embryonic and postnatal life and were approximately halved in the frontal cortex of adolescent and aged people[45]. Immunostaining with a specific antibody revealed that D-Ala was localized to insulin producing β-cells in pancreas from rats [46]. In addition, its location to adrenocorticotropic hormone-secreting cells of the anterior pituitary gland was shown[47]. In urine, serum and faeces D-Ala and D-Ser were found to be the most abundant free D-AA types in the majority of analyzed mammalian specimens including physiological fluids of humans[48, 49,40]. Urine is the mammalian matrix with the highest relative and absolute D-AA amounts, with D-Ala and D-Ser ratios around 50% and even higher in some cases (e.g. D-Ser ratios in urine of chimpanzee, rabbit, cat and man[40, 48]. Human urinary D-Ser ratios were

constantly high over lifetime. In rat, in contrast, excretion of D-Ser and D-Ala was age dependent with decreased relative and absolute amounts in urine of aged animals[50]. Moreover, high D-ornithine ratios were detected in urine specimens from mammals including humans. In contrast, relative D-AA blood level were found to be in the low percentage range except for the D-Ala ratio detected in the blood coagulate of wallaby (13.3%)[40, 48]. Hamase et al. demonstrated, that the detected *allo*-Ile in rat, mouse and dog urine referred to the D-form exclusively. Moreover, high levels of the D-form of Val and Ile were observed in rat urine, whereas in plasma branched D-AAs were not detected or detected in trace amounts except for D-Leu[51]. D- Amino acid oxidase (DAO) was the first enzyme discovered in mammalian tissues, mainly in the kidney, brain and liver (except for mouse liver). It is responsible for D-AA metabolism in mammals [52, 53]. It catalyzes the catabolism of various neutral and basic D-AAs by oxidative deamination. The oxidative deamination of acidic D-AAs such as D-Asp and D-Glu is catalyzed by D-Asp oxidase, an enzyme similar to DAO that is expressed in the mammalian liver, kidney and the brain[52, 54]. Besides their enzymatic degradation mammalian organisms get rid of excessive D-AAs by renal excretion which explains high urinary D-AA contents[40, 48, 51, 55]. Ser racemase was the first enzyme discovered in mammals able to form a D-AA, namely D-Ser from L-Ser and vice versa[56]. The conversion of the stereo center with the help of the prosthetic group pyridoxal 5'-phosphate (PLP) of Ser racemase is shown in Figure 2. Additionally, it has been shown that the enzyme can catalyze the degradation of D- and L-Ser by α,β-elimination of water, to form pyruvic acid. Ser racemase was detected predominantly in neurons, but also in protoplasmic astrocytes, cerebral cortex, hippocampus, striatum and olfactory bulb [52, 56]. Recently, a second AA racemase was discovered in mammalian tissues namely Asp racemase. It is present mainly in brain, heart and testis and at low levels in the adrenal glands. Besides, its racemase function there is so far little known about other possible reactions catalyzed by the enzyme or underlying mechanisms [52, 57].

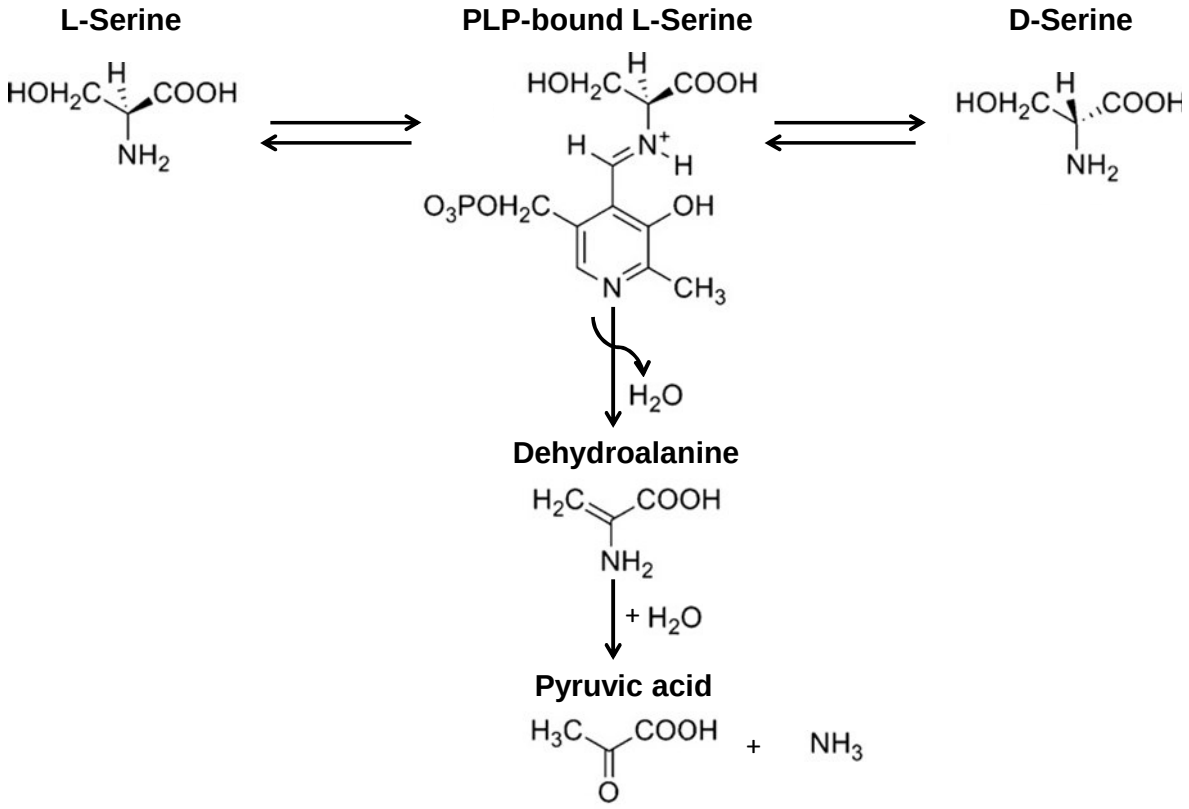

Figure 2. PLP-dependent reactions catalyzed by Ser racemase. Adapted with permission from[52]

The enzymes responsible for the creation of the other detected D-AA types have not been discovered yet and, therefore, they may be exogenous. Main D-AA sources of mammalian organisms are the intestinal and oral microbial flora as well as food treated with bacteria for fermentation and maturation[58-61]. Also in non-fermented food, like milk, vegetable and fruit juices, D-AA have been detected at relevant quantities[58, 62, 63].

Besides their free form, D-AAs were also identified as constituents of mammalian peptides and proteins[64-67]. The number of detected D-AA containing mammalian peptides is small. Probably many of these peptides remain undiscovered as conventional approaches like sequencing techniques or non-stereoselective chromatography coupled to MS do not determine the configuration of AAs. Therefore, they may be easily overlooked[65] .

4.2.2.2 BIOLOGICAL FUNCTIONS

Physiological functions of D-AAs in mammals are under investigation. They are still not clarified for many detected D-AA types. So far researchers have been able to demonstrate important functions for D-Ser and D-Asp in the nervous system. D-Asp has been recently demonstrated to be a potent neurotransmitter[68] and D-Ser was suggested already in 2000 as neurotransmitter[69]. The latter was reported to bind effectively to the 'glycine site' of the N-methyl-D-aspartic acid (NMDA) subtype of glutamic acid receptors and therefore is a potent co-agonist and is, in addition to the agonist glutamate, required for NMDA receptor activation in the brain[70]. NMDA receptors are key mediators for the excitatory transmission in the nervous system [71]. Ca^{2+} dependent release of D-Ser from astrocytes enables NMDA receptor activation, which is obligatory for synaptic long-term potentiation (LTP) that alters synaptic strength, on the basis of synaptic plasticity. Therefore D-Ser contributes to learning and memory processes, which are inter alia considered to be based on LTP mechanisms[71, 72]. Both stereoisomers of Asp can bind to the Glu site of NMDA receptors and elicit thereby excitation. D-Asp was additionally found to be a precursor of NMDA that represents a potent agonist of NMDA receptors[73, 74]. NMDA was shown to be a product of methyl transfer from S-adenosyl-methionine to D-Asp[73]. D-Asp was detected in mammalian endocrine and neuroendocrine tissues and testis [43, 44, 75] and was reported to regulate the synthesis and secretion of various hormones like growth and luteinizing hormones[73, 76], testosterone and progesterone[68,77], melatonin[78] and oxytocin[79] directly or indirectly as a part of dependent events or as precursor of NMDA. This hormone regulation was also shown to be NMDA receptor mediated[73]. Testosterone is involved in the regulation and maintenance of spermatogenesis[80]. Therefore D-Asp levels comprise an element of spermatogenesis regulation in testis [81, 82]. Since D-Ala was visualized to be localized to insulin producing β-cells in pancreas[46] and to adrenocorticotropic hormone-secreting cells of the anterior pituitary gland and both hormones adjust blood glucose, D-Ala was suggested to be involved in blood glucose control[47]. Characterization of D-AA functions in mammals is an ongoing field of research and most probably there exist further D-AA activities awaiting discovery.

4.2.2.3 D-AAs as biomarkers and potential therapeutics

The gained knowledge about D-AA distribution, metabolism and function led to the general assumption that D-AAs can serve as biomarkers and therapeutics for diseases affecting gut, liver, kidney or the nervous system. Indeed, researchers were able to demonstrate that D-AAs in physiological fluids, such as blood or urine, can be indicators of kidney dysfunctions[34, 83]. Furthermore, Ketting et.al found augmented D-Ala ratios in urine of a patient with short bowl syndrome when compared to controls[35]. Because of their important role in the activation of NMDA receptors, D-Ser and D-Asp levels and those of their degrading enzymes (DAO and D-Asp oxidase) in the brain have been associated with diseases that are believed to be based on NMDA receptor dysfunction. For example decreased D-Ser levels in cerebrospinal fluid (CSF)[36, 84], as well as increased DAO expression[85] and DAO activation[86] in the brain have been linked to schizophrenia. However, other studies failed to confirm these findings [52, 87, 88]. Nevertheless, the administration of D-Ser in addition to other antipsychotics has been shown to improve schizophrenia symptomes[36-38]. D-Asp in the brain has been reported to act like an antidepressant. The respective study was based on experiments with mutant mice, lacking D-Asp oxidase[39].

4.2.3 Other chiral Metabolites in Mammals

Also for chiral metabolites other than AAs, enantioselective detection is a prerequisite for the accurate characterization of metabolic changes in the pathogenesis of diseases and for the meaningful use of enantiomers as diagnostic markers. To that end, especially small acids and hydroxy acids have been monitored. The following examples show that enantiomers, which were initially thought to be the ’unnatural’ and meaningless form of a chiral metabolite (mostly the D-enantiomer), were finally found to be important not only as biomarkers but also as participants in mammalian metabolism. D-lactic acid acidosis was detected in cases of short bowel syndrome. It was caused partly by bacterial overgrowth of D-lactic acid (D-LA) producing bacteria [13, 89, 90]. As another source for the D-LA excess its production in the methylglyoxal pathway was suggested, which was reported to be increased in individuals with thiamin deficiency [89, 91]. D-LA showed neurotoxic properties and the neurotoxic concentration was observed to be different for different patients[89]. Unlike the L-form,

D-LA was shown to be oxidized very slowly in mammalian organisms including humans[92]. However, like L-LA dehydrogenase catalyzing the formation or degradation of L-LA, with pyruvate as substrate or product, a respective enzyme for the metabolism of D-LA was characterized namely D-α-hydroxy acid dehydrogenase [93]. Furthermore, high ratios of D-2-hydroxyisocaproic acid (D-HICA), D-3-phenyllactic acid (D-PLA) and D- 3-(4-hydroxyphenyl)-lactic acid (D-HPLA) were present in the urine of short bowel syndrome patients. The D/(D+L) ratios were around 50% for the latter metabolite and even higher for D-HICA (81-100%) and D-PLA (60-86%)[13, 94]. These D-forms were considered as products of bacterial AA metabolism and therefore, they were suggested to be indicators of bacterial overgrowth in short bowel disease[13]. The appearance of L- PLA and L-HPLA, being metabolites of L-Phe and L-Tyr, in urine was characteristic for patients suffering from phenylketonuria or tyrosinaemia[13, 94]. In maple syrup urine disease HICA was detected in the L-configuration[94]. Moreover, both pyroglutamic acid (PGA) enantiomers were detected in human urine specimens[13]. PGA results from a pH dependent intramolecular reaction of Glu or Gln to form the cyclic lactam. L-PGA was found to be a member of the γ-glutamyl cycle[13, 95]. The γ-glutamyl cycle, with glutathione as key metabolite, was suggested to be involved in AA transport[95]. However, Heil et al. found D-PGA to be the predominant enantiomer in urine (63-79%) of healthy probands. A patient that exhibited glutathione synthetase deficiency excreted predominantly L-PGA (>99%) and showed an overall increased PGA urinary level[13]. The origin, potential physiological functions and metabolism of D-PGA in mammals still await elucidation. The metabolism of malic acid enantiomers in rats was investigated by the administration of radioactive labeled L-malate or the equally labeled racemate. Both cases yielded comparable results including a fast metabolism of both substrates that was demonstrated by the excretion of radioactive carbon dioxide in the expired air. There was no indication for bacterial metabolism of malic acid enantiomers in the gut as the way of administration had little impact on the metabolic outcome[96]. The enzyme capable of metabolizing D-lactate (D-α-hydroxy acid dehydrogenase) was also shown to oxidize other substrates like D-malate and meso-tartrate[93]. For 2-hydroxyglutaric acid (2-HG) enantiomers, there were identified two different enzymes catalyzing their stereoselective conversion to α-ketoglutaric acid[97, 98]. Mutations on either of the responsible genes were accompanied with the respective L- or D-aciduria[97, 99]. Mutations on the genes encoding isocitrate dehydrogenase (IDH)1or 2

were shown to be associated with cancer types like glioma or acute myeloid leukemia and resulted in the production of D-2-HG from α-ketoglutarate by the altered enzyme[100-102]. D+L 2-HG serum quantity (cut-off 2 µM) was applied as indicator for these mutations. The stereospecific quantification of 2-HG enantiomers led to a more specific biomarker namely the D/ L 2-HG ratio[102].

Albeit one enantiomer of chiral metabolites is usually the predominant in mammalian organisms the other was present, too. Furthermore, there were enzymes identified that metabolize enantiomers stereospecifically. This makes stereoselective analysis a necessity to achieve a more precise specification of metabolic disorders. As several 'unusual' stereoisomers have been considered as bacterial metabolites they may serve as markers for diseases affecting the gut. The so far gained knowledge about antipodes of chiral metabolites demonstrates the chances of enantioselective techniques allowing the assignment of abundances, metabolism and functions of single enantiomers in mammals. Finally, chiral analysis is essential for the characterization of the active enantiomer of chiral drugs. They improve the understanding of the enantiospecific metabolism and therefore of possible side effects or toxicity caused by the administration of racemic drugs[15, 103] .

4.3 Separation of Enantiomers

4.3.1 History and Nomenclature

History. It took until 1848 for molecular chirality to be visualized for the first time, although we are daily surrounded by chirality, because objects like our hands, a corkscrew, or a sea shell are nonsuperimposable to their mirror picture. In 1848 Louis Pasteur observed the spontaneous resolution of racemic sodium ammonium tartrate tetrahydrate during its crystallization from aqueous solution. He sorted the resulting two crystal forms that were nonsuperimposable and therefore chiral[104, 105]. He detected the opposite rotation of the plane of polarized light for the two solved crystal groups. The angle of rotation, however, was the same[104]. The respective property of enantiomers, called optical activity, had been already recognized in the early nineteenth century by Biot and other scientists, but they had not understood the cause for the rotation. Fresnel's discovery of circularly polarized light was inevitable for the explanation of optical activity. Enantiomers show different refractive indices for

left and right circularly polarized light that overlaid results in linearly polarized light[104, 106]. Therefore, the velocity of left- and right-circularly polarized light was different after passing a solution with an optical active substance, leading to the rotation of the polarization plane of the two overlaid light rays[106]. These are the fundamentals of the first method for the determination of enantiomer ratio, which were summarized by the term 'optical rotatory dispersion'. In 1874 Van't Hoff and Le Bel independently postulated the tetrahedral structure of four substituents on a carbon atom and therefore the asymmetry of the shape in consequence of four different substituents. These reports provided the explanation for Pasteur's mirror image crystals and for molecular chirality in general[104, 105]. Louis Pasteur was also the first to demonstrate the importance of stereochemistry in biochemical processes by showing that enantiomers of ammonium tartrate were metabolized with different velocity by a mold fungus[105]. The invention of gas chromatography finally provided a technique with sufficient resolution for the separation of enantiomers. However, the first gas chromatographic separation of enantiomers was not realized until 1966. Gil-Av et al. separated Ala, Val and Leu stereoisomers, applying an optically active stationary phase[107, 108].

Nomenclature. In 1891 Emil Fischer invented the so-called Fischer projection as a simple way of illustrating chiral structures of molecules to describe the configuration of an asymmetric C center. On the basis of this projection and the model molecule glyceraldehhyde, he introduced the Fisher nomenclature. In the Fischer projection horizontal bonding lie above the paper plane, vertical ones below and the asymmetric (chiral) center lies in the paper plane. This two-dimensional way of displaying a three-dimensional structure is shown exemplarily in Figure 3 by applying Fisher's rules to AAEs in their physiological form. Fischer assigned the (+)-stereoisomer, rotating the polarization plane to the right, to D- glyceraldehyde and the (-)-stereoisomer, rotating the polarization plane to the left, to L- glyceraldehydes. When a moiety of a chiral molecule, considered to be the equivalent to the C_α hydroxy group of glyceraldehydes, is situated on the left side of the chiral center in Fischer projection the configuration is described by the prefix L. When it is on the right side the prefix D is used.

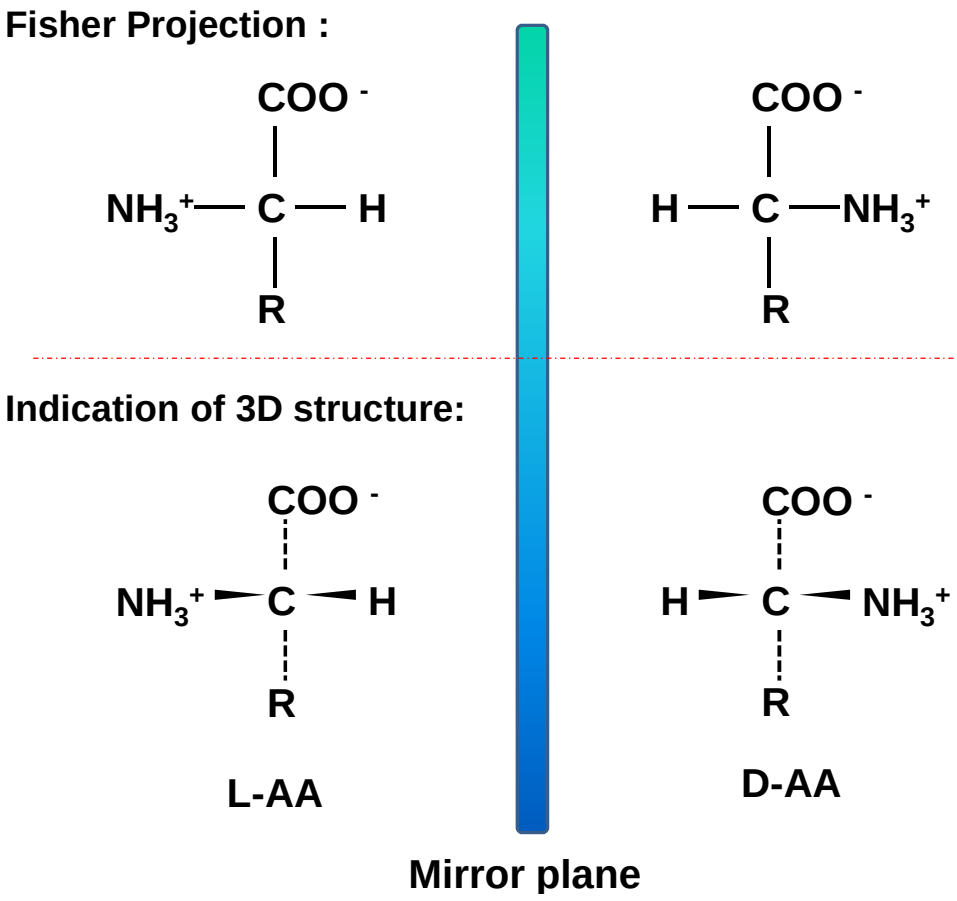

Figure 3. Fisher projection, applied to the structure of AAEs. DL-configuration was assigned according to the example of glyceraldehyde enantiomers. R refers to the characteristic moiety of each AA types except Gly which is achiral.

However, Fischer's assignment was arbitrary as he had no means to determine the absolute configuration of glyceraldehyde enantiomers[109]. Sixty years later Bijvoet et al. were able to clarify by means of x-rays, using a phase lag, that Fischer's assumption represented the true stereochemical situation[110]. Recently, the innovative technique of foil-induced Coulomb explosion allowing to image the positions of substituents of chiral centers was presented, in order to directly determine the absolute configuration of small molecules from the gas phase[111]. Nevertheless, Fischer's nomenclature is only definite for one chiral center and requires the invention of additional prefix (e.g. *allo*) or terms for the description of diastereomers (e.g. threonic acid enantiomers are diastereomers of erythronic acid enantiomers) and becomes unclear for multiple asymmetric centers within a molecule. In consequence, the Cahn-Ingold-Prelog priority rules were defined for substituents of chiral C atoms as the basis for the RS nomenclature allowing a definite description of configuration of all chiral centers in a molecule. They include sequence rules for

complex moieties and are based on the positive correlation of priority with the atomic number. With the view from the asymmetric C atom to the moiety of lowest priority, the R configuration is assigned when priority of the other three moieties, decreases clockwise. Prefix S describes the opposed stereochemical situation. Albeit the RS nomenclature offers a more detailed and clear assignment of configuration, the DL nomenclature has prevailed for biomolecules. However, the RS system is essential for the description of enzymatic reaction mechanisms[109]. Since the analyses of this work focused on small metabolites, including at maximum two asymmetric C atoms, the DL nomenclature was used.

4.3.2 Principles of Enantiomer Separation

One of the first strategies to determine AAE ratios in complex biological specimens employed immobilized enzymes that stereospecifically catabolize AAs. Appropriate detection techniques allow the sensitive quantification of produced α-ketoacids. However, these sensors have limitations such as short life times of the active layer and distinctly different sensitivity for different AA types because of individual reaction kinetics. The quantification of both antipodes required the immobilization of two different stereospecific AA oxidases[112-115]. Column chromatographic and electrophoretic approaches prevail for the separation of enantiomers and are generally based on two different strategies. Indirect approaches separate diastereomeric derivatives of target enantiomers, which possess different physical and physico-chemical properties, using achiral selectors or columns [108, 116, 117]. Limits of this strategy can be the absence of chemical groups amenable for the reaction with chiral reagents, the occurrence of kinetic resolution or racemization during derivatization and a lack of availability of enantiomerically pure reagents. The latter problem can be solved by applying correction factors to obtain accurate quantification results[117, 118]. Direct approaches use chiral nonracemic (pseudo) stationary phases that form diastereomeric association complexes with derivatized or underivatized enantiomers. The chiral selector does not have to be enantiomerically pure[117]. Different stabilities of the two complexes, resulting in different partition coefficients, enable the resolution of enantiomers[108, 117]. In the first direct GC based approach Gil-Av et al. applied N-trifluoroacetic –L-Ile lauryl ester groups in the liquid stationary phase to enable resolution of branched chain α-AAEs[107]. This strategy had some

drawbacks for the analysis of complex samples like time-consuming method optimization due to high sensitivity to chromatographic conditions and low selectivity for nonchiral chemical functionalities. Nevertheless, the direct approach is currently used most frequently for the gas chromatographic analysis of AAEs. Further limitations and chances of both strategies were discussed recently for the separation of AAEs[116].

4.3.3 Outstanding Methods for enantioselective Metabolic Profiling

Based on the direct or indirect approach several relevant column chromatographic and electrophoretic methodologies were described and discussed in my diploma thesis and in a trend article in view of the suitability for biomedical AAE analysis. These publications list and comment the most commonly used chiral stationary phases and derivatization reagents[116, 119]. The following chapters highlight outstanding methods, performing best, not only in the resolution of AAE and other stereoisomers, but also with regard to precision, accuracy, sensitivity and applicability to biological matrices.

4.3.3.1 Column Chromatography Methods for AAE Analysis

The most innovative high performance liquid chromatography (HPLC) based methods for the resolution of AAEs were presented by Hamase et al. and Barbaro et al., who applied chiral columns for the separation of fluorescent derivatives or underivatized AAEs[51, 120]. Hamase et al. achieved resolution of all proteinogenic branched chain AAE and of *allo*-Ile enantiomers by their two-dimensional approach. They used a conventional reversed phase column for the first and an enantioselective column for the second dimension. Overall, the method showed good performance with appropriate within-day and day-to-day precision and recoveries between 95.5 and 100.2 % of AAE amounts spiked into blood plasma. Fluorescence detection resulted in a LLOQ of 5 fmol of injected D-AA. The method was applied to the analysis of rat urine, plasma and tissues and urine of dog and mouse. However, the method was time-consuming due to derivatization, 60 minutes of reversed phase analysis and five minutes of enantioselective analysis for each AAE pair[51]. Other two-dimensional HPLC approaches allowed the precise and sensitive quantification of Ala

or Ser enantiomers after fluorescence derivatization with 4-fluoro-7-nitro-2,1,3-benzoxadiazole (NBD-F), and 30 or 40 minutes of analysis, respectively[121]. Barbaro et al. achieved the resolution of 19 AAE pairs (thereof 16 proteinogenic AA types) within a single chromatographic run. Two different mass selective detectors were tested. The LTQ-Orbitrap XL offered high mass accuracy, whereas the triple quadrupole mass spectrometer showed superior limits of detection (4 - 200 ng/L instead of 0.4-7µg/L with the Orbitrap detector). The use of isotopically labeled AAEs reduced matrix effects for all analytes except for D-Ser. Therewith, the method proved to be the most effective for the simultaneous analysis of a large number of AAEs in biological specimens within 35 minutes. However, the applied chiral column did not allow the separation of Ile/Leu isomers. Furthermore, spike-in experiments revealed that the method was not applicable to the quantitative analysis of D-Ser, D-Orn, L- and D-Trp as matrix effects hampered their accurate determination. Nevertheless, the method using the Orbitrap promised high potential for future untargeted analysis of chiral metabolomics[120].

From the published GC based methods for AAE analysis the one presented by Zahradníčková et al. showed notable enantioselectivity and sensitivity. It was validated in detail in respect of its applicability to biological specimens. An appropriate separation was achieved for 15 proteinogenic AAE pairs within 47 minutes using pentafluoropropylchloroformate and pentafluoropropanol reagent for derivatization and Chirasil-L-Val as chiral selector. AAE were extracted from biological samples using a cation exchanger. Resulting limits of detection (LODs) ranged between 0.29 and 3.25 µM and the method showed sufficiently low relative standard deviations (RSDs) and good recoveries for all AAEs except for Glu, Gln, Asp and Asn enantiomers. Several D-AAs could be detected in samples of cyanobacteria[122]. Schurig et al. demonstrated the superior enantioselectivity of L-Val based chiral stationary phase when applied to AAEs as their N-pentofluoropropanoyl isopropyl ester derivatives using hydrogen as the mobile phase. Seventeen proteinogenic types of AAE pairs could be separated in less than 35 minutes with most of them showing baseline resolution. Histidine enantiomers required further modification of the imidazol-N by an ethylbutoxycarbonyl group to allow their separation and elution from the chiral column. The competitive counterpart of the L-Val-*tert*-butylamide modified polydimethylsiloxane phase for successful AAE analysis were alkylated –γ-cyclodextrins (CDs), as chiral selectors, solved in (Lipodex E) or

linked to (Chirasil-γ-Dex) a polydimethylsiloxane backbone. Thirteen proteinogenic types of AAE pairs were baseline separated by Schurig's group as their trifluoroacetyl ethyl ester derivatives using a Chirasil-γ-Dex kind of stationary phase and hydrogen as carrier gas. This selector was thermally more stable than the L-Val selector as e.g. racemization of all chiral centers of the glucose molecules is very unlikely. Furthermore, the γ-CD selector was contrary to the L-Val derivative able to separate β- and γ-AAs as well as N-methyl-α-AAs. Despite their excellent AAE resolution, Schurig et al. did not pursue the applicability of these methods to biological matrices and unfortunately their self-made stationary phases were not made commercially available[123].

4.3.3.2 Capillary Electrophoresis Methods for AAE Analysis

Han et al. presented a straightforward method for the direct analysis of the 19 proteinogenic pairs of AAEs that can be automated due to efficient on-column derivatization with 9-fluoroenylmethyl chloroformate (FMOC) for UV detection. Applying 30 mM β-CDs in the buffer, the method achieved baseline separation of 17 pairs of AAEs and partly separated Ala and Arg enantiomers. However, the method was validated exclusively for Asp and Glu enantiomers that showed good linearities and recoveries when spiked into human serum as well as RSDs <5.4 % for peak areas, as a figure of merit for interday precision. The determined LODs of Glu (4.0 µM) and Asp (3.2 µM) were insufficient for the detection of D-Glu and D-Asp in serum of healthy volunteers. The limited linear range and insufficient sensitivity for the application to human serum remain major drawbacks of the method, although at the chosen pH other D-AA yielded higher peak intensities than D-Glu and D-Asp[124].

4.3.3.3 GC-MS Method for Organic Acid Analysis

Multidimensional (heart-cut) gas chromatography-mass spectrometry (MDGC-MS) was successfully applied for the separation of five enantiomer pairs of organic acids (LA, HICA, PLA, PGA and HPLA) as their methyl esters using a modified β-CD as chiral selector in the second dimension. The enantiomers were separated within a single chromatographic run of 100 minutes using hydrogen as mobile phase. Even

though no validation data were reported, the application of the method to urine of patients suffering from inborn errors of metabolism was demonstrated and enantiomer ratios, characteristic for the disorders, were found[13].

4.4 GC-MS Techniques for enantioselective Metabolomics

This chapter explains how the analytical techniques employed in the course of this thesis function and which operation modes and detectors were used. Further, it points out chromatographic parameters meaningful for a successful separation of chiral and non-chiral metabolites.

4.4.1 Gas Chromatography – Quadrupole Mass Spectrometry (GC-qMS)

Gas chromatography is an analytical technique that is used, beyond the separation of complex samples, for the study of reaction kinetics or for analyte characterization by assessment of physicochemical properties[125]. It uses an inert gas as mobile phase that transports analytes in gas phase along the solid or liquid stationary phase[126]. Therefore, the technique is amenable only for volatile and thermally stable analytes. However, vapor pressure of polar analytes like AAs and other small metabolites can be increased by derivatization with less polar chemical groups, which allows GC analysis of non-volatile molecules[1]. Typical mobile phases in GC applications are helium, argon, nitrogen or hydrogen. Nowadays, capillary columns are mostly employed. PLOT (porous layer open tubular) columns are capillary columns with a solid stationary phase coated on the inner wall of the capillary, whereas WCOT (wall coated open tubular) capillary columns feature a liquid coating on the inner wall as the discriminating stationary phase. Column diameter, film thickness of the active layer, and column length are the key parameters affecting separation efficiency. The partitioning coefficient K is characteristic for the analyte-stationary phase interactions and therefore determines the degree of retention. It is temperature dependent ($\ln K \sim 1/T$)[127]. Thus, the adjustment of temperature for isothermal analysis or the implementation of a temperature program (recommended for analytes with a wide boiling point range) is an important issue in method optimization in order to obtain baseline separation[125, 126]. Chromatographic resolution is defined as follows:

$$R_s = \frac{2*(t_{R2}-t_{R1})}{w_{b1}+w_{b2}} = \frac{1.18*(t_{R2}-t_{R1})}{FWHM_1+FWHM_2} \quad (1)$$

where R_s refers to resolution, t_R to retention time, w_b to base peak width, and FWHM to full widths at half maximum. Index 1 labels the first eluting compound, index 2 the successive one.

For accurate quantification of stereoisomers and other isobaric substances, a chromatographic resolution ≥1.5, that marks baseline separation, is required if a mass selective detector is applied. For a non-selective detection technique, all target peaks require baseline resolution for proper quantification.

Samples are introduced onto GC columns by means of an injector. Commonly, split/splitless or programmed-temperature vaporization (PTV) injectors are used. In both cases, the sample is injected by a syringe through a septum into the liner, which is a small chamber in which evaporation takes place. Both injectors are able to perform split and splitless injection. The whole injected sample amount is transferred onto the column in case of splitless injection, whereas only a definite split ratio of the injected amount reaches the column in split mode while the remaining volume is purged to the split outlet. PTV injection refers to a cold injection with a subsequent fast temperature program and is therefore a mild injection that is suitable for targets of low thermal stability.

Mass analyzers are more and more favored as detectors for GC applications of complex matrices as they offer high sensitivity and selectivity and help to identify ‘unknown’ structures. Quadrupole mass spectrometric detection after electron impact ionization (EI) is a robust detection technique that is widely used for the analysis of metabolomes. Electron impact ionization is a hard ionization technique in which electrons are emitted with a standard energy of 70 eV. The impact of the energy-rich electron causes fragmentation and ionization of analytes eluting from the column. Consequently, obtained mass spectra usually do not contain the molecular ions but fragment ions indicate chemical groups and therefore provide essential information on molecular structure. The standardized electron energy and high reproducibility and robustness of quadrupole detectors facilitate structure identification as spectra

can easily be compared e.g. with created libraries[1] using algorithms that search for spectral matches.

The quadrupole detector uses four parallel rods, usually of 15 cm length, with constant direct current and alternating radio-frequency voltages applied to them, to filter ions of different masses[126]. The resolution of a quadrupole detector is dependent on the ratio of the alternating voltage and the direct current voltage and a ratio tightly below 6 was identified for maximal resolution. The detector can be applied either in scan mode, in which both alterating and direct current are continuously increased to allow every ion mass to pass the filter at a given time[126], or in SIM (selected ion monitoring) mode that allows the selection of target ion masses in retention time windows. SIM mode is often applied to metabolic profiling, because it provides improved sensitivity due to a longer acquisition time per ion. Scan mode is used for fingerprinting analysis and during method optimization to asses an appropriate temperature program for a given aim.

4.4.2 Comprehensive Two-Dimensional Gas Chromatography – Time-of-Flight Mass Spectrometry (GC×GC-TOFMS)

Significance. To separate complex metabolomes from physiological fluids or tissues is challenging and one-dimensional GC methods often lack in selectivity, which results in coelutions. Mass spectrometric detection helps to quantify overlapping metabolites based on their characteristic mass fragments or (quasi-)molecular ions. Nevertheless, isobaric metabolites like structural isomers or stereoisomers cannot be differentiated by their mass spectra and require baseline separation. For metabolic profiling or targeted analysis selective sample pretreatment or selective detection techniques can help, if target monitoring is impeded by matrix peaks. However, if two target isomers overlap, a more selective technique which offers multiple separation mechanisms has to be chosen such as multidimensional GC (MDGC or GC-GC) or comprehensive two-dimensional GC (GC×GC). The latter technique is preferable for complex matrices and trace analysis due to its multiplicative peak capacity and improved sensitivity. In contrast heart-cut multidimensional GC allows the transfer of only few effluent portions of coeluting peaks to a second stationary phase.

Basics. The innovative analytical technique of GC×GC was invented in 1991[128]. It transfers the complete sample from the first column to the second dimension column by means of modulation. A schematic setup of the technique is shown in Figure 4.

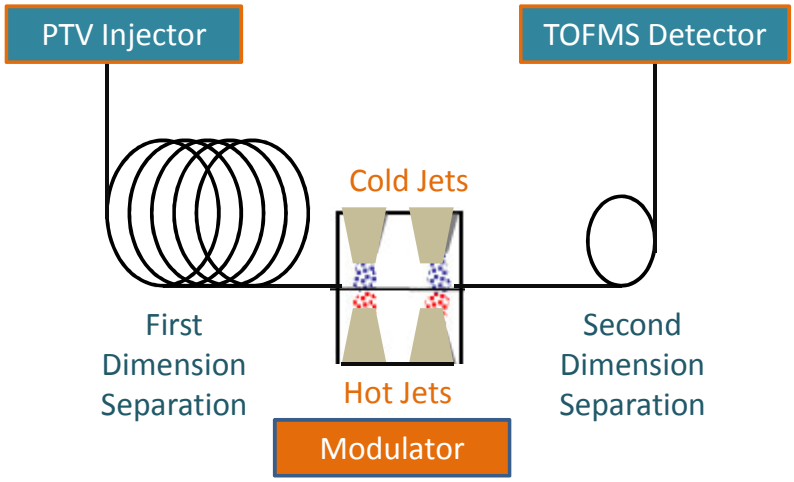

Figure 4. Schematic GC×GC-TOFMS setup. Adapted with permission from[10, 129].

A so-called "orthogonal" separation is based on two serially coupled stationary phases with distinctly different interaction mechanisms yielding a significant improvement of the overall selectivity. Both columns are operated typically temperature programmed in two individual ovens or in one shared. Analytes reaching the modulator are retained and therefore focused before they are released as sharp peaks to the second dimension analysis. Since the second dimension separation is very fast, nearly no peak broadening occurs until peak detection. This narrow peak shapes are typically accompanied by a considerable gain in peak height and therefore increased Signal-to-noise ratios (S/N)[130]. A high modulation frequency (2-8 seconds of modulation time) is required to maintain first dimension resolution. Therefore, a minimum of three modulations per first dimension peak is recommended. Also the preceding fraction should be eluted before the next is released to avoid a so-called 'wrap around' that hampers a well-arranged and structured separation space. Consequently narrow short columns are used for the second dimension analysis keeping retention times to a few seconds[131].

Data visualization. Typically only one detector is used at the end of the set-up that records a continuous signal of serially linked second dimension chromatograms. The obtained picture is complex and difficult to interpret. For a better visualization the acquisition software provides contour plots or 3D plots by cutting the raw

chromatogram at each fraction release based on modulation time and by combining the individual second dimension chromatograms in parallel.

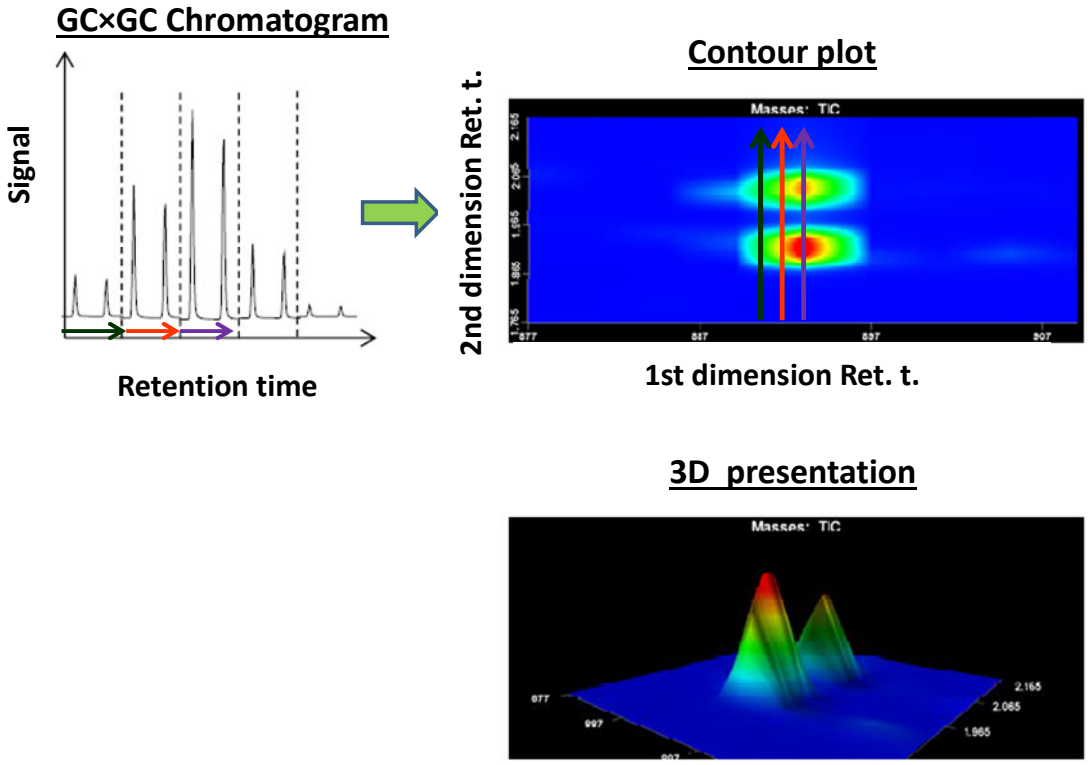

Figure 5. Raw GC×GC chromatogram, contour plot and three-dimensional presentation. Green, orange and purple arrows indicate how the contour plot is constructed from the cut raw GC×GC chromatogram pieces. The arrow length in the raw chromatogram refers to the modulation time. Adapted with permission from[10, 129].

The resulting 3 D picture displays the retention time of the first dimension separation on the x-axis, second dimension retention time on the y-axis and peak intensity on the z-axis. In a contour plot there is no z-axis but intensity is coded by colors[130, 132]. The concept of generating a contour plot and the 3D plot, respectively, from the actual GC×GC raw chromatogram is depicted in Figure 5.

Modulation. Different modulation strategies have been developed that enable two-dimensional separation. In pulse flow modulation, analytes eluting from the first column into the transfer line are focused by two successive gas pressure pulses, one in the beginning and one in the end of the transfer line, introduced via T connecters. Chemical bands are stored in the modulator capillary for a few seconds before their re-injection into the second column[133]. Although the method provided effective sample focusing and an appropriate re-injection frequency, thermal modulation strategies prevailed in the short history of GC×GC. The inventors of the GC×GC

technique were the first to trap fractions applying heat to the modulator tube by a rotating sweeper[128, 134]. Cryogenic modulators induce local clocked temperature changes realized at two nearby capillary regions either by a periodically moving cooler device or by two fixed cryogenic jets using liquid CO_2 for retention[135-137]. This refers to the so-called dual stage modulation, which was also realized in the set-up with four jets installed pairwise, which was applied in the course of this thesis. It mediates the injection-like launch of narrow bands by alternating cold/heat pulses. The jets are triggered in a way that the moment one trapping station is heated, the other is cooled and vice versa in the next pulse period. This is illustrated in Figure 6.

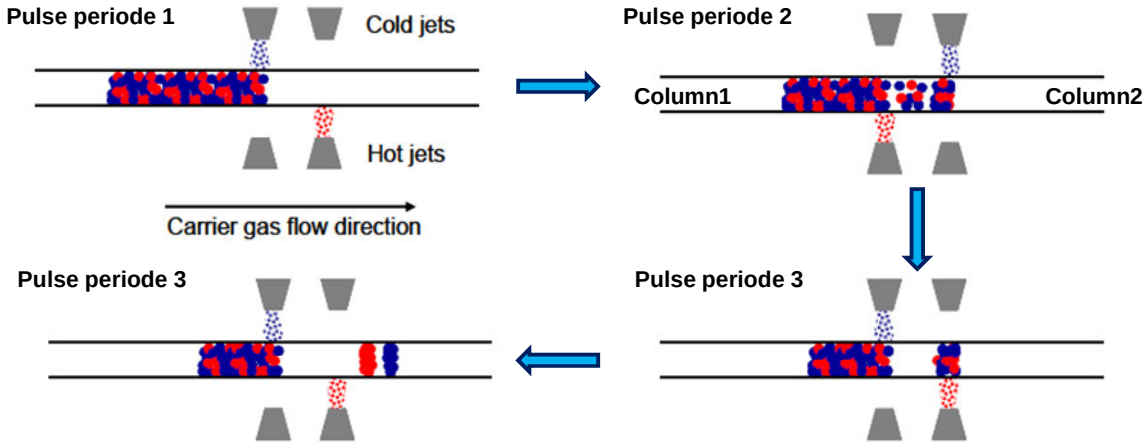

Figure 6. Simplified presentation of a hot/cold pulse sequence of one modulation by a dual-stage four-jet modulator. Adapted with permission from[10, 129].

This pulse sequence prohibits the breakthrough of an unfocused chemical band. Cold nitrogen gas is produced via heat exchange with liquid nitrogen and transported to the cold jets and hot air is directed to the trapping region through the hot jets[136]. The omission of moving components has proven to be preferable for robust high-throughput analysis by GC×GC.

Detectors. All of the above explained modulators provide efficient band focusing and therefore narrow peaks typically between 0.1 and 0.6 s of baseline peak width[131]. At least 15 points have to be recorded to quantitatively describe a peak. For peaks yielded from two-dimensional analysis, detection techniques with high acquisition rates (at least 150 Hz) need to be chosen. Flame ionization detectors and microelectron capture detectors were demonstrated to meet this challenge[131, 136]. However, to reach the maximum grade of selectivity, MS detectors have to be employed. Mostly time-of-flight mass spectrometers (TOFMS) were applied with EI

and nominal mass resolution. Instruments like the here used Pegasus IV GC×GC-TOFMS from LECO (Corporation, St. Joseph, MI, USA) are able to generate up to 500 spectra per second and therefore accomplish precise peak mapping for accurate and reproducible semi-quantification or quantification applications in complex matrices.

4.4.3 Gas Chromatography – atmospheric Pressure chemical Ionization – Time-of-Flight Mass Spectrometry (GC-APCI-TOFMS)

To couple GC to high-resolution MS and gain a powerful tool for structure elucidation of discriminating compounds in untargeted analysis, a soft ionization technique is inevitable to maintain molecular shape. APCI is suited to fulfill this requirement. Formation of protonized molecular ions proceeds via a series of ionization and clustering reactions initiated by a corona discharge electrode exposed to a high electric field. Electrons are emitted from the tip of the needle that ionize surrounding nitrogen gas. After cluster formation of the nitrogen ions, the positive charge is transferred to water molecules from air moisture that in the following associate in water clusters holding an excessive proton[138-140]. The assimilation of such protons by eluting compounds finally yields the quasi-molecule ions amenable for accurate molecular mass analysis. The respective reactions can be displayed as follows:

$$
\begin{aligned}
&N_2 + e^- \rightarrow N_2^{\bullet+} + 2e^- \\
&N_2^{\bullet+} + N_2 \rightarrow N_4^{\bullet+} \\
&N_4^{\bullet+} + H_2O \rightarrow H_2O^{\bullet+} + 2N_2 \\
&H_2O^{\bullet+} + H_2O \rightarrow H_3O^+ + HO^{\bullet} \\
&H_3O^+ + nH_2O \rightarrow H_3O^+ \cdot (H_2O)_n
\end{aligned}
\qquad (2)
$$

$$H_3O^+ \cdot (H_2O)_n + M \rightarrow MH^+(H_2O)_b + (n+1-b)H_2O$$

M describes a compound subjected to soft ionization in the APCI source. Reproduced with permission from[141]

Although this concept was introduced already in 1973 by Horning et al., it attracked little attention as a GC coupling device to accurate mass detection, possibly because of the expensive setup using a β-emitter (^{63}Ni) foil instead of the corona needle[139, 142].

It took another 30 years until new variants of the interface, actually commercialized for LC-MS coupling, offered its universal usage for both GC and LC connection to MS[143, 144] and initiated its breakthrough in the field of GC analysis. The promising coupling device was optimized and launched by Bruker Daltonics and Waters Corporation, simultaneously. Later, also Agilent Technologies provided an appropriate interface. GC-APCI-TOFMS was validated initially for profile analysis by researchers interested in the quantitation of pharmaceutical impurities[145], phenolic compounds in olive oil[146] or metabolites in human CSF[142, 147]. It offered satisfactory repeatability, sensitivity and ionizeable polarity scope for their objectives. Wachsmuth et al. established the feasibility of GC-APCI-TOFMS for the fingerprinting of methoximated and silylated metabolites. First, the performance of the technique was evaluated for 43 chemically diverse metabolites in comparison to the routinely applied hard (EI) and soft (chemical ionization) ion sources for the coupling of one- or two-dimensional GC to fast-scanning low-resolution TOF or quadrupole mass detection. GC×GC-EI-TOFMS was the only technique that provided wider linear ranges for quantitation. The new coupling performed as good as commonly used metabolomics instrumentations with respect to repeatability and linearity except for GC-EI-qMS that showed lower RSD for derivatization replicates. Moreover, APCI-based metabolic fingerprints of different *E. coli* strains outperformed the comparable GC×GC-TOFMS study in the number of structure elucidated discriminating features. Six additional metabolites were assigned due to selective adduct formation in the APCI source and sum formula prediction based on accurate mass and isotopic pattern[141, 148].Next, Wachsmuth et al. optimized the $M\text{-}H^+$ yield of MeOH/MCF derivatives in the APCI source by continuously injecting water into the ionization space at a rate of 0.4 mL/h. As a consequence, the variance of fingerprints within experimental groups was reduced, which helped to distinguish differently treated cancer cells by a greater number of detected and statistically discriminating features. $M\text{-}H^+$ abundance, however, was not influenced by water infusion in case of methoxime-trimethylsilyl derivatives[149].

4.5 How to gain relevant enantioselective Information

4.5.1 Pre-Separation from the biological Matrix

What essentially drives method optimization in chiral metabolomics is the objective of baseline separating as many pairs of enantiomers as possible, to monitor their ratios and contents. The price that many researchers had to pay was low overall selectivity provided by chiral selectors and therefore high limits of detection resulting from moderately separated enantiomers from the biological matrix. This, however, hampers enantiomer determination in complex biological samples. To overcome these limitations, complex matrices like mammalian plasma and urine were subjected to achiral pre-separation steps to isolate target molecules, applying e.g. cation exchangers[35, 40, 122] and two-dimensional thin-layer chromatography[83, 150] before chiral AA analysis. However, such procedures are labor-intensive, time-consuming and not suited for untargeted analysis. That's why chiral metabolomics still requires the implementation of new methods based on innovative separation techniques offering both appropriate enantioselectivity for a broad range of chemically diverse stereoisomers and high overall selectivity.

4.5.2 Derivatization and chiral Selectors

Since established chiral selectors offer enantiomer discrimination based on different interaction types, the choice of the most effective selector/derivative combination is crucial for the baseline separation of a given set of target enantiomers. Despite the great variety of chiral selectors available in particular for LC analysis, the structure/ resolution relation was most frequently investigated for the application of CDs and derivatives thereof. CD selectors were not able to differentiate native AAEs in LC analysis except for aromatic AAEs [151-153]. Thus, the adjustment of selector/derivative structures was often considered. CDs are α-1,4-connected glycopyranose units forming a cyclic tapered cavity accessible for interior hydrophobic interactions for analytes able to enter this small discriminating room[154-156]. The diameter of the broader entrance was gauged to be approximately 6, 8 and 10 Å for α, β or γ–CDs including 6,7 or 8 sugar blocks, respectively[154, 156]. Cavity height was estimated to be 5-9 Å for native α–γ CDs[156]. The external side allows hydrophilic interactions no

matter if unmodified CDs or derivatives carrying polar groups such as acetyl, hydroxyalkyl or thio are used[116, 155].

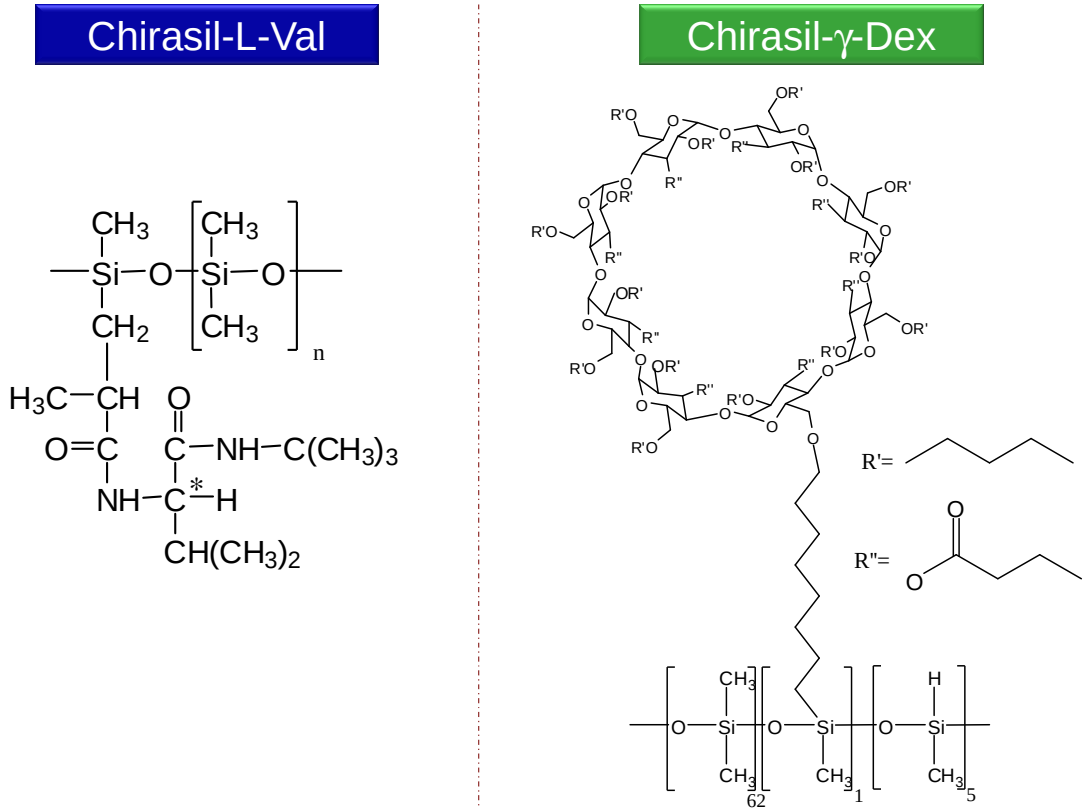

Figure 7. Chiral selector moieties are linked to the polydimethylsiloxane backbone of two enantioselective stationary phases typically employed for GC analysis of AAs.

CD derivatives were introduced to increase solubility in aqueous–organic solvents and therefore selector concentration[116]. Traditionally, CDs were thought to provide enantioselectivity predominantly by formation of inclusion complexes[155] until Sicoli et al. demonstrated that linear acetylated/silylated malto-oligosaccharides were also able to separate a number of chiral aromatic compounds, amines, alcohols and α-AAEs. With their study they pointed out the high impact of hydrophilic interactions on chiral resolution. Nevertheless, CDs provided superior discrimination of enantiomers in most cases[157]. With the restricted dimension of the hydrophobic cavity and polar groups at its opening that further decrease its effective diameter, the stability of inclusion complexes mainly depends on spatial factors, hydrophobic interaction and hydrogen bonding[116, 155]. Thus, matching the chemistry and shape of both the selector host and the analyte guest are highly recommended to adjust their complementarity and thereby enhance binding affinity[156]. This was performed in CE, LC and GC based studies to improve enantioselectivity[19, 151, 153, 155, 158]. Additionally,

for the application of chiral GC the performance of L-Val based stationary phase, providing enantiomer discrimination by hydrogen bonding, was tested for different AAE derivatives, including N-perfluoroacyl-(perfluoro)alkyl esters and N-(perfluoro)-alkyl alkoxy (perfluoro)-carbonyl esters. They resulted from the reaction of anhydrides or chloroformates and alcohols with amino-, hydroxy- and carboxy groups [19, 20, 122, 158]. The Chirasil-L-Val and Chirasil-γ-Dex chiral selector moieties linked to the polydimethylsiloxane backbone are shown in Figure 7. The method employing pentafluoropropyl chloroformate and pentafluoro propionic acid for derivatization and Chirasil-L-Val for separation offered notable enantioselectivity. It resolved 15 pairs of AAEs. The fluorinated chloroformate was synthesized, because it was not commercially available[122]. Derivatization with fluorinated anhydrides in combination with fluorinated alcohols was investigated intensively by Zampolli et al. for the analysis of AAEs on both the L-Val based and a γ-CD derivative (RT-γ-DEXsa) based GC column. The more fluor atoms had been added to the AAEs the higher was the detected response, whereas overall enantioselectivity decreased with increasing derivative size for both column types tested. Furthermore, the derivatives including longer fluorinated chains showed only slightly increased retention on Chirasil-L-Val and even decreased retention on the γ–CD based column [19], possibly due to their bigger size, disabling the formation of inclusion complexes. Limitations of anhydride/alcohol derivatization were the hydrolyzation of Asn and Gln under acidic conditions yielding Asp and Glu, respectively, and the time-consuming two-step procedure[20, 40, 48, 158]. Even though Zampolli et al. realized the less laborious one-step procedure using fluorinated anhydrides and alcohols, this procedure caused high racemization rates during derivatization (10-40% of pure enantiomers isomerize depending on the AAE moiety)[19]. The group considered this phenomenon to be negligible for their application to space analysis[19] but chiral metabolomics aims at the detection of D-AAs in the low percentage range, which is impeded by isomerization. My own attempts to elucidate the nature of racemization during one-step derivatization with pentafluoropropionic acid (PFPA) and heptafluorobutanol (HFB) indicated, that PFPA hydrolyzed to form pentafluoropropionic acid that can catalyze racemization. Reducing applied PFPA volume or keeping PFPA strictly under nitrogen reduced racemization albeit not sufficiently to allow accurate AAE analysis in physiological fluids[158].

The basis of the present doctoral thesis were the experiments of my diploma thesis, in which I had compared the performance of three different chloroformate/alcohol derivatization chemistries and six anhydride/alcohol derivatization strategies for the GC separation of proteinogenic AAEs on a Chirasil-L-Val and an RT-γ-DEXsa column, respectively. Pros of the L-Val based selector were high selectivity for different proteinogenic AA types and short run times, whereas column bleed and the inability to distinguish Pro enantiomers were cons. An important consideration in the selection of an appropriate chiral selector is the preferred elution of the low abundant enantiomer prior to the enantiomer present in excess, to avoid peak masking of small D-AA signals by peak tailing of the nearby L-AA signal. Both chiral selectors provided the favored elution order. RT-γ-DEXsa showed lower column bleed based on its higher temperature limit and, therefore, more reliable analysis. It showed lower selectivity for different AA types and a lower enantioselectivity for AAs treated with fluorinated anhydrides and fluorinated butanol or native isopropanol than the L-Val based selector. Nevertheless, it offered outstanding resolution of the smallest derivatives tested, namely methyl alkoxy methyl esters. The respective derivatization reaction with MCF and MeOH in aqueous solution can be seen in Figure 8. Chromatographic resolution was >2.4 for ten pairs of AAEs after their treatment with MeOH/MCF. No racemization was detected after derivatization of single AAEs[158]. Thus, this selector/derivative combination was chosen for further method optimization and validation to allow its versatile application to physiological matrices. These attempts were the subject of the first part of this thesis.

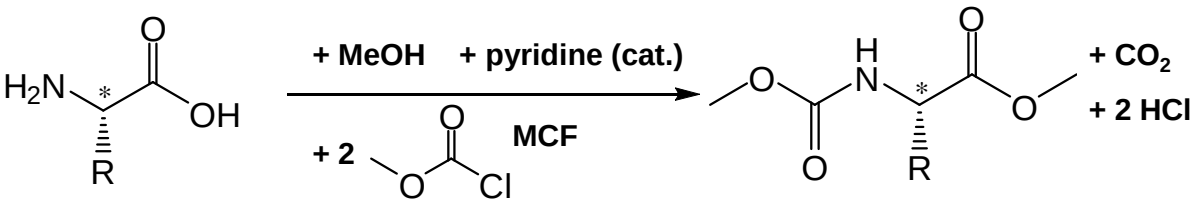

Figure 8. Derivatization reactions for metabolites (here shown for AAEs) with MeOH and MCF in aqueous solution for analysis by enantioselective GC-MS.

4.5.3 Racemization

As already pointed out in the preceding chapter, prevention of accidental racemization is a crucial aspect of chiral metabolomics. Unintended racemization can

occur not only during derivatization but also during sample storage, pre-treatment or during chiral analysis e.g. in the GC injector. Chiral metabolomics, however, is interested in the outcome of enzymatically catalyzed isomerization in organisms and in different metabolism of stereoisomers. Conditions promoting racemization of AAs after sample collection are inter alia high temperature, pressure and low or high pH[23, 159, 160]. AA racemization rates depend on inductive and steric effects of the side chain, on the stability of the planar intermediate but also on structure independent factors like concentration, ionic strength of the medium and the presence of metal traces[159, 160]. Asp and Cys exhibited the highest racemization rate under acidic conditions (4N HCl) and a temperature of 110℃, fol lowed by Pro > Glu > Met > His > Leu > Lys > Phe > Ala > Tyr > Arg > Trp > Val > Ile> Ser and Thr[159]. Two of the most stable presumed planar intermediates of isomerization formed at low pH values are displayed in Figure 9 as well as the one proposed in my diploma thesis for the racemization mechanism caused by derivatization with HFB/PFPA in one step. The most plausible proposition of the underlying reaction mechanism for the creation of these intermediates is the proton catalyzed enolization[23, 159]. Asp racemization rate has been shown to be a function of pH at constant ionic strength of the solvent with a maximum at a pH of three and a pH independent region between pH five and eight at 25 ℃. Interconversion was also favored under alkal ine conditions at pH-values>9 [160]. The planar intermediate under alkaline conditions is formed by elimination of the proton bound to the α-C-atom to form a carbanion[23, 161].

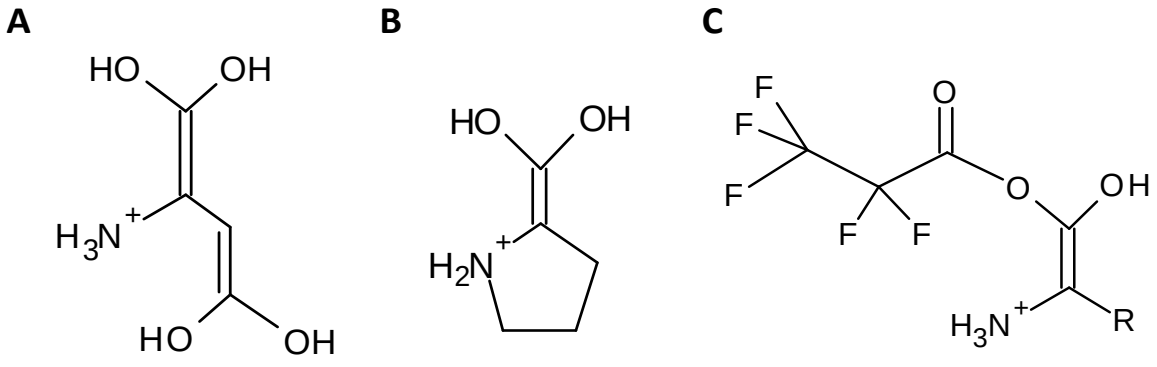

Figure 9. Presumed stable planar intermediate of acid catalyzed interconversion of (A) Asp, (B) Pro or (C) an AA during HFB/PFPA derivatization. Adapted from[159] and[119]

Temperature exerted an even higher impact than pH on racemization velocity[160]. Heating and alkali treatment are often applied in industrial food processing[161, 162]. Caused racemization processes of protein bound AAs affect organoleptic properties

and food quality. Proteins (casein) treated with 1M NaOH at 80℃ for one hour resulted in complete racemization of Asp, Ser, Tyr, and His, while >40% of the D-form was detected for Ala, Met, Phe, Lys and Glu. The least D-AA ratio (<35%) was observed for Val, Leu, Ile and Thr[162]. Racemization of peptide bound AAs is not only influenced by steric and inductive effects of their own moieties, but also by those of chemical groups from nearby AAs. Asn or Asp bound to Gly as part of a protein sequence leads to the formation of an aspartyl succinimide product that is prone to a racemization process based on keto-enol-tautomerism[23, 163].

The different susceptibility of chiral metabolites to isomerization bears the necessity of a racemization check for each stereoisomer of interest to ensure accuracy of chiral metabolomics results. This can be accomplished by preparation and analysis of single enantiomers in the same way as samples have been treated. A lack of readily available enantiopure standards or standards with defined enantiomer excess makes racemization checks often labor-intensive as enantiomer ratios need to be investigated beforehand by direct methods like e.g. optical rotatory dispersion. Furthermore, samples and chiral standards should be kept strictly at low temperatures. Finally, comparison of chiral metabolomics results obtained by techniques employing different preparation and separation strategies is highly recommended to check for racemization at any step of the procedure.

4.5.4 Identification of Enantiomers and Diastereomers

In untargeted metabonomics the identification of unknown metabolite structures is the ultimate goal to clarify how biochemical processes or specific metabolites of interest (e.g. enantiomers) are regulated in response to experimental and/or environmental conditions. To this end, ideally both accurate mass measurements and detection of characteristic fragments are performed to gain information on possible sum formula using algorithms (here 'smart formula' from Bruker) and to exclude or prefer tentative candidates by comparing fragment spectra to respective database entries (here the NIST database was used). Adduct formation in the presence of specific chemical functionalities can assist with structure elucidation[148]. This is useful for identification of chiral and non-chiral metabolites. To confirm a structure and determine the configuration of stereo centers the injection of commercially available standards is

inevitable. However, the presence of chirality can be easily recognized if a pair of enantiomers was detected by either fragmentation or accurate mass measurement without consideration of structure or composition. Enantiomers of small metabolites show identical fragmentation spectra and the same molecular weight. The latter also applies to diastereomers, positional and conformational isomers. Therefore, it is helpful that spectra obtained by means of soft ionization techniques in GC-MS couplings (APCI and CI) include fragments in addition to the (quasi-)molecular ion. Isobars other than enantiomers show the same fragments and molecular masses, while the relative abundance of fragments differs. Thus, computational tools, able to screen chromatograms for equal spectra, can help to identify enantiomers. However, the match of spectra may be low for antipodes, if their abundance differs greatly. Some of the characteristic fragments detected within the high abundant spectrum may occur below the S/N threshold in the low abundant spectrum causing the low match.

4.5.5 Data Analysis and Validation

Internal standards (ISs) are commonly used in metabolic profiling to correct for losses during sample preparation and analysis. ISs may not be part of the original sample but should be similar to target molecules concerning their physico-chemical properties. Stable isotopic labeled IS meet this requirement the best, the more as they do not pose a radiation hazard. Often a single isotopically marked chiral IS is used for the correction of related stereoisomers because of the lack of commercially available racemic IS. This is appropriate if all isomers are affected equally by matrix effects. IS are also suitable to increase precision of semi-quantitative results in fingerprinting approaches. Further normalization of data is required when urine is investigated. Dilution of urine specimens depends on physiological and life style (water consumption) factors. 24h urine volume of rats from different study groups differed up to 15 fold and higher[164]. For normalization, besides 24h urine volume, creatinine concentration, osmolality and the 'MS total useful signal' (MSTUS) have been applied in MS-based metabolomics[164, 165]. The latter two are based on different strategies to estimate the total content of metabolites. To assess osmolality of a sample the freezing-point depression can be measured whereas MSTUS is the total area of peaks common to all samples[164]. Urinary creatinine content was most commonly used for data normalization in clinical chemistry and was employed in this

thesis[164, 166, 167]. It comprises a measure of the glomerular filtration rate in healthy individuals as creatinine is filtered exclusively. The accuracy of this measure can be affected inter alia by acute kidney injury[166]. In contrast, osmolality is the consequence of renal filtration, resorption and secretion.

Computational tools perform peak picking, peak integration and aligne resulting feature areas over all samples. A feature is a peak defined by a single retention time and a single *m/z*. Prior to uni- and multivariate statistical analysis data are often reduced by exclusion of features present below a chosen cut-off. Remaining missing values, if distributed randomly, can be imputed by algorithms that estimate these values. Additionally, data are often transformed to minimize misinterpretation caused by heteroscedasticity. Finally, artifacts like saturated feature or double feature, belonging to the same signal, should be excluded before statistical analysis. There are various statistical testing strategies available for the interpretation of metabolomics data. Distribution, univariate, multivariate, correlation and classification tests can be chosen corresponding to the experimental set up and investigated questions. Often a series of techniques is employed to obtain an appropriate content of information for a valid discussion of the study outcome.

In untargeted metabolomics the number of tested variables usually exceeds the number of analyzed samples. The number of false positives after multiple student-t-testing is nowadays most commonly reduced by the consideration of false discovery rate (FDR). The FDR estimates the ratio of p-values falling below the level of significance by chance. To this end the average frequency of p-values from undifferentiated feature is calculated from the list of probability results. Thus FDRs are list characters. This strategy was introduced by Benjamini and Hochberg[168]. Features with a FDR >0.05 are routinely excluded from the list of significantly regulated features[10]. There are even more conservative approaches for the correction of multiple testing like the Sidak equation and the Bonferroni approximation for the adjustment of the confidence interval. The latter comprises the division of the confidence limit for a single comparison by the number of regarded comparisons to obtain the confidence border that accounts for multiple testing[169, 170]. Particularly such strict rules of sorting out bear the danger of losing significant data and therefore hypothesis-generating trends.

Multivariate analysis assists in the visualization of complex data sets and in the assignment of relationships between samples and variables. To that end unsupervised approaches like principle component analysis (PCA), independent component analysis (ICA) or hierarchical clustering analysis are applied to metabolomics data. Examples for supervised approaches are partial least squares - discriminant analysis, support vector machines or discriminant analysis of principal components[171].

There are many method parameters to be determined in the course of method validation. Lower and upper quantification and detection limits define linear and dynamic ranges. Relative standard deviations of technical and derivatization replicates comprise a measure of method repeatability. Analyte recoveries after spike-in experiments are determined to check accuracy of results. For this objective also a method comparison is recommended, in which the results of the method under investigation are compared to the outcome of an established method after analysis of the same sample set. Hereby Bland-Altman plots help to visualize differences of the data sets or the presence of a systematic bias[172].

5 Experimental Section – Material, Methods and Instrumentation

5.1 Chemicals

Isooctane, pyridine, MCF, 1M NaOH, D-norvaline, racemates of AAs and other chiral metabolites and their respective enantioenriched solids as well as solids of non-chiral metabolites were obtained from Sigma-Aldrich (Taufkirchen, Germany). N-Acetyl-1-methoxy-L-Asp and N-Acetyl-L-Ala were purchased from Bachem (Bubendorf, Switzerland). Methanol (MeOH, LC–MS grade) and chloroform (HPLC grade) were from Fisher Scientific GmbH (Ulm, Germany). The water was purified by a PURELAB Plus system (ELGA LabWater, Celle, Germany). The [U-13C, U-15N] cell free AA mixtures were obtained from Euriso-top (Saint-Aubin Cedex, France).

5.2 Sample Preparation

5.2.1 Precipitation of Proteins

Protein precipitation was performed for the analysis of serum and liver samples. After 20 µL of aqueous internal standard mix were added to the sample, 600 µL of cold MeOH (-20°C) were applied to precipitate proteins and the mixture was vortexed. In case of liver tissues these steps were performed in Precelly-Keramik-Kit 1.4 mm vials (Peqlab Biotechnologie GmbH, Erlangen, Germany) and the mixture was homogenized two times for 15 s at 5500 rpm with a 30 s pause in between before centrifugation. In case of serum 2-mL Eppendorf tubes were used for precipitation and pellet washing. Precipitated serum samples were centrifuged at 1431 x g for 4 min at 5° C. Precipitated and homogenized liver samples were centrifuged at 16658 x g for 5 min at 5° C. The supernatant was transferred to a 1.5-mL glass vial (Macherey-Nagel, Düren, Germany) and the pellet was washed twice either with 250 µL of cold (0°C) MeOH/water (4/1) in case of serum or with 300 µL of the cold (0°C) solvent mixture in case of liver tissues. After each washing step the mixture was centrifuged at 1431 x g for 4 min at 5° C in case of serum or at 16658 x g for 5 min at 5° C in case of liver tissues. Combined supernatants were evaporated in glass vials to complete dryness.

5.2.2 Derivatization with Methanol/ Methyl Chloroformate

Derivatization was performed in 1.5-mL crew cap glass vials (Macherey-Nagel GmbH & Co. KG, Düren, Germany). If available a maximum of 150 µL of the biological specimen or master mixture (MM) (compositions of MM-1 and MM-2 are listed in the next section 5.2.3) were derivatized together with 20 µL of an aqueous IS mixture including U-13C, U-15N labeled proteinogenic D- and L-AAs (IS concentrations of IS mix A, B and C are given in the next section 5.2.3). To allow for identical derivatization reagent concentrations in each reaction vial the mixture was always diluted with water to a constant aqueous start volume of 275 µL. In preliminary experiments 100 µL of a 1N NaOH aqueous solution (according to Villas-Bôas optimized protocol[173]) and 5 µL of a 5.7 µM aqueous D-norvaline standard (useable IS) were added instead of dilution with pure water.

If protein precipitation had been performed, the dry residue of collected supernatants was resolved in 275 µL of water. Subsequently 167 µL MeOH and 34 µL pyridine were added. Finally, MCF was added in two portions of 20 µL each. After every MCF addition the solution was vortexed. Villas-Bôas reported the reaction to be completed within 30 s after the addition of MCF[173]. 300 µL chloroform were added for derivative extraction. The mixture was vortexed for 15 s. All biological samples were centrifuges at 4165 x g for 5 minutes at 5℃ to improve phase separation and subsequently about 100 µL of the lower phase (organic phase) were transferred to a 1.5-mL glass vial with a 100-µL micro-insert (VWR, Cat. No. 548-0006).

For metabolite standard solids dissolved in a MeOH/water mixture or in pure MeOH, the added water and MeOH volumes were adjusted, so that the overall water and MeOH content (275 and 167 µL respectively) were always kept constant for the derivatization reaction.

5.2.3 standards and master mix

MM-I was composed of all proteinogenic AAEs and Gly in concentrations of 0.5 or 1 mM. MM-II consisted of AAE detectable by the here presented chiral methods and Gly at 1mM each except for Phe enantiomers that were present at 0.5 mM, respectively. For preliminary experiments of chapter 6 and 7, 150 µL and 75 µL of MM-I had been derivatized, respectively. The 150-µL aliquot was derivatized using NaOH (according to Villas-Bôas optimized protocol[173]) whereas the 75-µL aliquot

was derivatized without NaOH (according to my derivatization procedure described above). Respectively 150 µL of a MM-I dilution series were derivatized to calibrate the GC-qMS method for spike-in experiments using NaOH. 150 µL each of the dilution series of MM-II were derivatized to calibrate the GC-qMS method for method comparisons and applications and to calibrate the chiral GC×GC-TOFMS method. NaOH was used to derivatize the MM-II calibration series for the first comparison of quantification results from chiral GC-qMS to the results of an established achiral GC-qMS method for AA analysis. In all further calibrations with MM-II no NaOH was applied. AAE concentrations between 1 mM and 31 nM were applied for calibration with MM-II and MM-I. Some AAEs were present in the concentration range between 500 µM and 15 nM in the dilution series of MM-I. 100 µL of MM-II were derivatized for GC×GC-TOFMS parameter optimization.

Originally, the chiral GC-qMS method had been performed with 33 µL of a IS mixture containing U-13C, U-15N labeled AAs in a concentration range of 1.9 - 15.2 mM (IS mix A) in experiments of my diploma thesis. The labeled AAs had been obtained from algae. Thus they were present in the mix at their occurring ratios in algae. D-AA ratios were not determined by the supplier. Dilution of IS mix A to obtain IS mix B was performed in the course of chiral GC-qMS method optimization. IS mix B included labeled D+L-AAs in a concentration range of 0.35 - 2.83 mM. 20 µL of IS mix B were employed for all presented method applications in chapter 6. IS mix C refers to another algae extract that was solved and diluted to the D+L AA concentration range of 0.37-2.58 mM and 20 µL were spiked, respectively, to samples and standards of chapters 7 and 8.

15 µL of aqueous stock solutions (~20 mM) were derivatized together with 20 µL of IS mix C for metabolite identification. Some metabolites solids were solved in MeOH or a MeOH/water mixture (1/4).

5.3 Instrumentation

5.3.1 Quantitative Amino Acid Enantiomer Analysis by GC-qMS

An Agilent model 6890 GC (Agilent Technologies, Palo Alto, CA) equipped with a split/splitless injector, and a quadrupole mass selective detector (MSD) model 5973 A with an EI source was employed. An RT-γDEXsa (2,3-di-acetoxy-6-O-tert-butyl-dimethylsilyl γ-CD doped into 14% cyanopropylphenyl/86% dimethyl polysiloxane)

column (30m×0.25mm ID, 0.25µm film thickness) from Restek GmbH (Bad Homburg, Germany) was used for analyses. It was connected to a fused silica deactivated pre-column (10m×0.25mm ID) from Agilent. Phenomenex AGO 4680 liner was used. The autosampler was equipped with a 10-µL syringe for sample injection. Before and after sample injection the syringe was washed with 5 volumes of isooctane. Samples were kept in a cooled tray at 5 ℃.
The originally used conditions used for AAE analysis, implemented in my diploma thesis, were as follows:

Method I (similar to method D in[158]):
Injection: 1µL; split mode ; split ratio: 1: 10
Injector temperature: 250 ℃
Temperature program: 70℃ (1 min)– 4℃/min to 150℃ (5 min)-3℃/min to 190 ℃ (30 min)
He-flow: 2.0 mL/min
Solvent delay: 10 min
Transfer line temperature: 250 ℃
Detection mode: SIM

They were optimized to the following settings that were used for all quantitative applications of AAE analysis to biological samples described in chapter 6, 7 and 8:

Method II (published as method E in[158]):
Injection: 1µL, splitless mode, splitless time:1 min, purge flow: 20 mL/min
Temperature program: 70℃ (1 min)– 4℃/min to 150℃ (5 min)-3℃/min to 190 ℃ (5 min)
Solvent delay: 19 min
Transfer line temperature: 230 ℃
He-flow, detection mode and injection temperature as in **method I**

In the following course of the thesis, these settings are designated as method I and method II, respectively.

5.3.2 Quantitative Amino Acid Enantiomer Analysis by GC×GC-TOFMS

The following instrumentation and operation information was taken from[174].

The LECO (St. Joseph, MI) Pegasus 4D GC×GC–TOFMS instrument comprised an Agilent Technologies Model 6890 GC, a dual-stage, quad-jet thermal modulator, a secondary oven coupled to a fast acquisition TOFMS providing unit mass resolution, a PTV injector (Gerstel, Muehlheim, Germany), and a MPS-2 Prepstation sample robot (Gerstel). The robot was equipped with a 10-µL syringe for sample injection. Between injections the syringe was washed with 5 volumes of isooctane. Samples were kept in a cooled tray at 5 ℃. An Rt-γDEXsa column (30 m×0.25 mm ID, 0.25 µm film thickness) from Restek (GmbH, Bad Homburg, Germany) protected by a 5 m×0.25 mm ID fused silica deactivated guard column. (Agilent Technologies, Palo Alto, CA, USA) was used as the first-dimension column, while an RTx-1701 (2 m×0.1 mm ID×0.1 µm film thickness, Restek) or a ZB-AAA (2 m×0.25 mm ID, 0.25 µm film thickness, Phenomenex Inc.) column served as the second-dimension column. A sample volume of 1.5 µL was injected in splitless mode with the temperature of the PTV Injector set at 50 ℃ for 0.5 min and then ramped at 12 ℃/s to 250 ℃. A chemically inert Siltek liner from Gerstel was used. The helium flow-rate was set at 1.9 mL/min (constant flow). Modulation was accomplished every 4 s during GC×GC analysis and modulator hot pulse time was 0.6 s. Mass spectra were acquired from 40 to 600 *m/z* at a rate of 200 spectra/s. For 1D GC–TOFMS analysis the modulator was turned off and mass spectra were collected at 50 spectra/s. The solvent delay was kept at 19 min. Transfer-line temperature was held at 260 ℃. The ion source was operated at 200 ℃ and −70 eV. A positive offset of 5 ℃ was used for the second-dimension column and a 15 ℃ offset relative to the first-dimension column for the modulator.

Temperature programs that were considered best for GC×GC based AAE analysis by the two newly tested column combinations are listed in Table 1.

Table 1. Optimized GC temperature programs for the column sets RT-γDEXsa/ RTX-1701 (A) and RT-γDEXsa/ ZB-AAA (B, C), respectively. Taken from[174]

Method	Temperature program
A	70℃ (1 min) –2℃/min – 150℃ (10 min) –2℃/min – 1 80℃ (25 min)
B	70℃ (1 min) – 4℃/min – 150℃ (10 min) - 3 ℃/min – 190℃ (15 min)
C	70℃ (1 min) – 2℃/min – 130℃ (12.5 min) - 8℃/min - 150℃ (4 min) - 4℃/min – 190℃ (6 min)

In the following course of the thesis, these settings are designated as method A, method B and method C, respectively.

5.3.3 Enantioselective Metabolic Fingerprinting

An Agilent model 6890 GC (Agilent Technologies, Palo Alto, CA) equipped with a MSD model 5975 Inert XL, split/splitless injector and a MPS-2 Prepstation sample robot (Gerstel, Muelheim, Germany) was employed. For sample injection, a 10-µL syringe was used. It was washed 5 times with isooctane before and after injection. Prepared samples were kept in a cooled tray at 5 ℃. GC parameters corresponded to those of method II listed in chapter 5.3.1 except for the duration of the last temperature plateau (here 16.5 minutes at 190℃) le ading to a total run time of 55.83 minutes. The solvent delay was decreased to 5 minutes. The qMS was operated in scan mode with an *m/z* range of 60 to 500. The transfer line was kept at 230 ℃. The same chiral GC column, as described in chapter 5.3.1 and 5.3.2, was connected to a fused silica deactivated pre-column (2m×0.25mm ID) from Agilent.

The GC-APCI-TOFMS device consisted of an Agilent model 6890 GC instrument equipped with an Auto Liquid Injector (model 7683B), which was hyphenated to a microTOF orthogonal acceleration TOF mass spectrometer from Bruker Daltonics GmbH (Bremen, Germany) by an APCI source that was operated in positive mode. Published source and MS parameters were applied that had been optimized previously[148]. The acquired *m/z* ranged from 50-1000. Equal GC parameters and GC columns were installed as applied for the measurement of fingerprints by GC-qMS.

5.3.4 Miscellaneous

A Precellys® 24 homogenizer (Peqlab Biotechnologie GmbH, Erlangen, Germany) was employed for the homogenization of liver specimens for quantitative AAE analysis. Solvents were evaporated by a Combi Dancer Infra-Red Vortex-Evaporator (Hettich AG, Baech, Switzerland). For centrifugation a Beckman GS-15R centrifuge (Beckman Coulter GmbH, Brea, CA) was employed. pH indicator paper (pH: 1-14) from MERCK was applied. Creatinine contents of urine samples, discussed in chapter 8, were quantified by Dr. Wentao Zhu using LC-ESI-MS/MS as described previously[175].

5.4 Software and Statistical Tests

Selected ion chromatograms for quantitative AAE analysis by GC-qMS were acquired by G1701DA D.02.00 SP1 MSD Productivity Chemstation from Agilent Technologies. Integration, calibration and quantification were performed using Micromass MassLynx V4.1 software from Waters (Waters Corporation, Milford, MA) with the QuantLynx option. FDRs and p-values based on two-sided students-t-tests for results of biomedical applications of chapter 6 were determined in ‘R’ using the ‘limma’ package.

Raw GC×GC-TOFMS data were acquired and processed with the LECO ChromaTOF software version 3.34. Baseline correction, deconvolution, peak picking, calibration and quantification were performed by this software.

Quantitative results of biomedical applications presented in chapter 7 were tested for normal distribution by the Shapiro-Wilk test in ‘R’. Furtheron, they were analyzed by F-tests and two-sided students-t-tests for unpaired samples and equal or different variances in Microsoft Excel. The diseased group was compared to the corresponding control group.

To record fingerprints the same acquisition software was used as for quantitative AAE analysis by GC-qMS. Quadrupole mass spectra library search was performed with NIST library revision 5.00. GC-APCI-TOFMS data were acquired with the micrOTOFcontrol software embedded into HyStar version 3.2 that was provided by Bruker. ‘Smart formula’ of the Bruker DataAnalysis software version 4.0 was employed to assign tentative sum formula to unknown metabolites.

Raw GC-qMS chromatograms of fingerprints were processed with the Waters Micromass MassLynx V4.1 software using the MarkerLynx option. Peak width at 5% height and peak-to-peak baseline noise were not set to fixed values but appropriate values were determined automatically by the software for each chromatogram. MarkerLynx performed peak picking and assigned a unique retention time and a single *m/z*-value to each feature picked and integrated it on the chosen *m/z*. The software performed data alignment. Further data analysis including exclusion of features that were below the chosen count cut-off and of saturated and double features as well as normalization were performed in Microsoft Excel. For statistical analysis including Shapiro-Wilk test of normality, PCA, ANOVA, as well as two-sided students-t-tests and FDRs for the three comparisons: steatosis *vs*. controls, NASH *vs.* controls, and NASH *vs.* steatosis, the software 'R' and therein the 'limma' package were applied. Reintegration of features, considered to significantly discriminate investigated groups, was performed in Micromass MassLynx V4.1 software using the QuantLynx option.

ANOVA and two-sided students-t-tests were performed in 'R' with the 'limma' package for the three group comparisons with AAE concentrations and thereof calculated D-AA ratios (D/(D+L)-ratio) obtained from quantitative chiral GC-qMS analysis of mouse urine for method validation.

5.5 Validation Methods

5.5.1 LOD and LLOQ

To account for unlabeled AAs present as impurities in the IS mix, blank values were determined by derivatization of 33 µL of IS mix A (U-13C, U-15N labeled AAs in a concentration range of 1.9 - 15.2 mM) in quintuple in the course of my diploma thesis and 20 µL of IS mix B in septuple in the course of this thesis and the following equation was applied to calculate LODs, also known as statistical LODs[176].

$$LOD = mean_{blank} + 3 \cdot SD_{blank} \quad (3)$$

where $mean_{blank}$ and SD_{blank} are the mean AA response and its standard deviation. Calibration curve equations were applied to LOD responses in order to estimate corresponding LOD concentrations[176, 177].

The probability of considering the target analyte as a component of the sample although it is not present in the sample is 5% using this estimation of statistical LODs[177]. In the absence of blank values (S/N<3 for AA peak in all blank value measures), the concentration generating a S/N ≥ 3 was defined as LOD, also known as empirical LOD[176]. The linear range was between the lower (LLOQ) and upper limit of quantification (ULOQ), which define the highest and the lowest point of the calibration curve with an accuracy between 80 and 120%. The LLOQ was additionally required to yield a peak with a S/N of at least ten.

5.5.2 Pearson Correlation Coefficient

The Pearson correlation coefficient is a measure of the linear dependence between two variables X and Y. It is calculated by dividing the covariance of the two variables by the product of their standard deviations. It has no dimension and can vary between -1, indicating a perfect negative linear correlation of X and Y, and +1, which indicates a perfect positive linear correlation. If it is zero, there is no linear relation between X and Y. However, this does not mean the absence of dependence between the two variables, as only the linear dependence was tested. Here the Pearson correlation coefficient was abbreviated by the letter r.

5.5.3 Bland-Altman Plot

A Bland-Altman plot visualizes the concordance and the disagreements of the outcome of two methods under comparison. It is appropriate for the validation of a new approach as it allows the assessment of the grade of agreement of results to those of an established approach in the regarded quantity range. The mean of the two results is plotted on the x-axis and their difference is plotted on the y-axis. Furthermore, the mean of all calculated differences is shown as a horizontal line. The

nearer it is to zero the higher the agreement of the data. There are two further horizontal lines present in a Bland-Altman Plot. They mark the upper and the lower 'limit of agreement' and their positions refer to mean difference ± 1.96 times the SD of the differences. If the differences are normally distributed 95% of the observed differences are expected to lie in between these limits. The closer these limits are to the mean difference the better the concordance of the data. If there is a consistent bias in the data the mean difference is not close to zero but the SD of differences is low so that the three lines lie close to each other. Data of the new approach can be corrected by the mean difference in such a case. If one of the methods or both methods show low repeatability a low agreement of the data is expected[172].

6 Optimization, Validation and Application of quantitative Amino Acid Enantiomer Analysis by GC-qMS

6.1 Introduction

D-AAs are excluded from ribosomal biosynthesis of proteins and, therefore, are believed to fulfill no biological functions. However, they are found in all species ranging from bacteria to humans and some important regulatory functions have been characterized recently. Enzymes involved in the anabolism and catabolism of free D-AAs have been identified in certain tissues. Based on these findings, D-AAs are considered potential diagnostic markers for diseases affecting gut, liver, kidneys or the nervous system. Bacteria release large quantities of D-AAs into their environment and, thus, changes in D-AA serum levels are believed to reflect alterations in the body's microbiota composition and/or permeability of epithelial barrier of the colon, which is home to most commensal bacteria that reside in a human and which exert a significant impact on human metabolism as noted more than 40 years ago by Linus Pauling [178].Hence, there is great interest in methods that allow the sensitive and comprehensive analysis of D-AAs in biofluids such as blood and urine. However, the baseline separation of low abundant D-AAs from their corresponding L-AAs has proven difficult and, as a consequence, most chiral methods have focused on a few AAE types or employed time-consuming pre-separation steps. To find a more efficient chiral GC-qMS based method that allows the sensitive quantification of many proteinogenic AAEs in a single run, a method comparison of various AAE derivatives on two different chiral selectors was performed in the course of my diploma thesis. For two newly investigated derivative /chiral selector combinations that yielded best enantioselectivity and peak abundances, calibration and racemization tests were performed. Since one, namely derivatization by HFB/ PFPA with subsequent analysis on a Chirasil-L-Val selector, yielded high racemization rates that could not be reduced sufficiently, I finally decided to optimize the other, combining MeOH/MCF derivatization with a γ-CD based selector. This section focuses on the optimization, validation and application of the method.

6.2 Material and Methods

6.2.1 Analyzed Samples

Urine from 23 healthy donors and 5 urine specimens from patients collected before and after curative stem cell transplantation (SCT) for non-malignant and malignant disorders of the immunohematopoietic system, and serum from 19 patients with minor liver damage and 19 serum specimens from patients exposed to SCT for the same reasons and a human control serum sample were provided by collaborators from the University Hospital of Regensburg with the approval of the institutional review board. From the 23 human control urine samples a urine pool was prepared. Serum and liver specimens from 20 mice, of which ten were fed a NASH inducing diet and ten were fed a control diet for two or three weeks (N=5 per group), respectively, were provided by Anja Thomas. The composition of the two diets, experimental conditions and characteristics of applied mice as well as the way of sample drawing were reported previously[179]. Also the determination of tumor necrosis factor (TNF) α levels in liver tissues was accomplished by Anja Thomas as it was reported previously [179].

6.2.2 Parameter Optimization

Injection parameters were varied in the course of method optimization. Injection parameter of method II (splitless injection at 250°C; splitless time =1 min) resulted from testing three different splitless (purge) times: 0.5 min, 0.75 min and 1.0 min, respectively. 150 µL of MM I were derivatized and measured under the different injection conditions.

6.2.3 Method Validation and Quantification

Spike-in experiments. In preliminary experiments three aliquots of 100 µL each of control serum were derivatized without protein pre-precipitation together with 20 µL of IS mix B, respectively, to determine AA amounts. Subsequently nine aliquots (100 µL each) of control serum were derivatized without protein pre-precipitation together with 20 µL of IS mix B and either 15 or 30 or 45 µL of the spike-in mix. Thus, three spike-

in levels were added and analyzed in triplicates. The following AAs were included in the spike-in mix: D-Ala, L-Ala, Gly, D-Leu, D-Thr, D-Ser, D-Met, L-Met, L-Asn, DL-Phe. The three spike-in levels corresponded to 0.5, 1.0 and 1.5 fold quantity, added in case of L-AAs and DL-Phe and 2, 4 and 6 times determined quantity, added in case of D-AAs. Method II was employed for all analysis of spike-in experiments. Results were analyzed by calculating percentage recoveries (determined quantity divided by expected quantity and multiplied by 100%).

Method comparison. 150 µL each of 19 serum samples from patients with minor liver damage were prepared as described in chapter 5.2.2 without protein precipitation using 1N NaOH and D-norvaline. They were analyzed using method II. At the same time the samples were analyzed by an established achiral GC-qMS method for AA quantification by a procedure described elsewhere[180]. D- and L- AA amounts found by the chiral method were summed up and relative recoveries were calculated by dividing the D+L-AA concentration obtained by the chiral method by the concentration found by achiral analysis and multiplication by 100%.

Method comparison was repeated with 19 serum samples from patients exposed to SCT applying optimized sample preparation (protein pre-precipitation and dilution with water) to 150 µL aliquots and method II for chiral analysis and the published procedure for the established achiral method[180]. Quantitative results were compared by relative recoveries as explained above.

Method comparison was also performed for the analysis of urine. Five samples from patients exposed to SCT were derivatized using 100 µL 1N NaOH in the reaction mixture and ten samples from patients exposed to SCT were prepared, replacing the NaOH volume by the addition of water. 150 µL aliquots and Method II were applied. The samples were analyzed concurrently by the established achiral GC-qMS approach[180] and quantitative results were compared by relative recoveries as described above.

Comparison of different sample preparation. Each preparation strategy was performed in triplicate and for each experiment 150 µL of control serum were prepared. Four different preparation strategies were tested:

Preparation strategy A: Derivatization with MeOH/MCF as described in chapter 5.2.2 without protein pre-precipitation, using 100 µL 1N NaOH.

Preparation strategy B: MeOH/MCF derivatization without protein pre-precipitation, adding 100 µL water for dilution instead of 1N NaOH.

Preparation strategy C: Protein pre-precipitation with cold MeOH (0℃) and 100 µL 1N NaOH as additive for MeOH/MCF derivatization.

Preparation strategy D: Protein pre-precipitation with cold MeOH (0℃) and derivatization with MeOH/MCF using 100 µL water for dilution instead of 1N NaOH.

Additionally, two 150-µL aliquots of control serum were derivatized in the presence of proteins, one with NaOH and one without addition of NaOH, to estimate the pH in the reaction mixture by pH paper before and after the second addition of MCF.

Calibration. Calibration was performed using a 16-point serial dilution of either MM I for spike-in experiments or of MM II for all other quantitative analysis presented in chapters 6, using method II. The dilution series prepared from MM I included all proteinogenic AAE in a concentration range between 1 mM and 31 nM or between 500 µM and 15 nM. The dilution series prepared from MM II included all AAE detectable by the here presented GC-qMS method in a concentration range between 1 mM and 31 nM. Respectively, 150 µL of the MM dilutions were prepared together with 20 µL of IS mix B. LODs and LLOQs were determined as described in chapter 5.5.1.

Repeatability. Six 150-µL aliquots each of the urine pool and the serum control, respectively, were derivatized using the optimized protocols with protein pre-precipitation in case of serum and without NaOH in the reaction mixture. They were analyzed by method II.

6.2.4 Sample Preparation

Depending on available sample volume 110 -150 µL of urine from patients with renal failure were derivatized. Depending on available sample volume 20 -150 µL of mouse serum and 40.3 -59.4 mg of mouse liver were prepared and analyzed. The samples were prepared as described in chapters 5.2.1 and 5.2.2 with the optimized protocols.

6.3 Results and Discussion

The following results and discussion were published partly[158]. Each section, corresponding to published text, was cited individually.

6.3.1 Optimization of Method Parameters

Figure 10 shows a representative chromatogram of MM II and IS mix B derivatized with MeOH/MCF and recorded by the optimized GC-qMS method performed with the RT-γDEXsa column and method II.

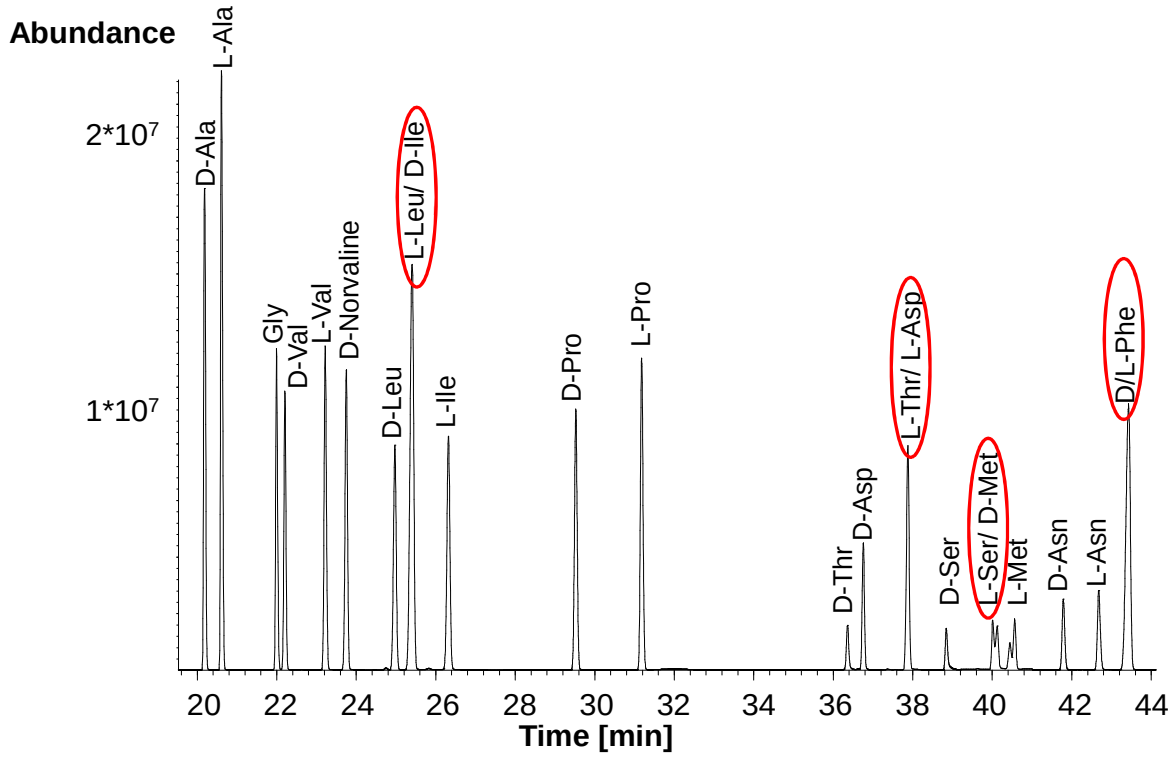

Figure 10. Characteristic chromatogram of 150 µL of MM II with 20 µL of IS mix B, prepared and analyzed using MeOH/MCF derivatization and optimized chiral GC-qMS analysis in SIM mode, the RT-γDEXsa column and method II (temperature program: 70℃ (1 min)– 4℃/min to 150℃ (5 min)-3℃ /min to 190 ℃ (5 min))[158]. Overlapping AAE peaks are encircled.

Four pairs of AAEs coeluted after analysis namely L-Leu/ D-Ile, L-Thr/ L-Asp, L-Ser/ D-Met and D/L-Phe. The signal partially overlapping with the L-Met peak refers most probably to a derivatization byproduct that was not assigned to any AAs. Visible peak intensity differences of antipodes result from distinctly different concentrations of the corresponding labeled enantiomers of the IS mix. No D-AAs were detected upon

derivatization of L-AAs with MeOH/MCF and chromatographic enantiomer resolution ranged between 2.5 for Leu enantiomers and 14.0 for Pro enantiomersRacemization checks and determination of enantiomer resolution had been performed during my diploma thesis[119]. Mass spectra of Ser and Thr enantiomers indicated their occurrence as three-fold MeOH/MCF derivatives. Husek reported that hydroxy groups of hydroxymonocarboxylic acids can be converted into alkoxycarbonyl ether by treatment with MeOH/MCF under certain conditions[181]. Low peak intensities of Ser and Thr enantiomers, when compared to other AAE derivatives, suggest the occurrence of a side product, respectively. They either vanish in the baseline or do not elute from the column with the applied temperature program. No further attempts were made to clarify the structure of yielded Ser and Thr derivatives. Linear ranges including ULOQs and LLOQs, regression coefficients of calibration curves and LODs of the method had been determined in the course of my diploma thesis[119]. However, obtained LLOQs were found to be insufficient to allow quantification of all separated D-AAs in serum and urine of patients suffering from diseases affecting the bowl or the liver[119]. Additionally, high LODs were found due to high blank values detected after the derivatization of 33 µL aliquots of IS mix A because the IS mix, gained from algae, contained up to 2% unlabeled AAs. Thus, my first attempt in the course of this thesis was to decrease LODs and LLOQs. This was achieved by the adjustment of the IS mix concentration. Consequently, the IS mix A containing U-13C, U-15N labeled D+L AAs in a concentration range of 1.9 - 15.2 mM was diluted yielding IS mix B including U-13C, U-15N labeled D+L AA concentration in a range of 0.35 - 2.83 mM. An additional improvement of LLOQs was achieved by the optimization of injection parameters. Derivatization of 20 µL of the diluted IS mix (IS mix B) yielded still appropriate IS intensities with S/N> 50 enabling a valid peak area correction. Blank values and therefore LODs were clearly decreased when compared to those found after derivatization of 33 µL of IS mix A. Thus, 20 µL of IS mix B were spiked to all analyzed samples and standards of this chapter. Besides all proteinogenic L-AA, the labeled IS mix included the corresponding D-AAs at low percentages. The abundance of labeled D-AAs was insufficient to allow their application as ISs. Thus, only labeled L-AA were used as ISs in all analysis of this thesis. Switching from split mode (split ratio 1:10) to splitless mode increased peak intensities. A further increase could be achieved by increasing the splitless time. This is the time period after injection in which analytes are evaporated and transported onto the column. After the

splitless time the injection chamber is purged using a high purge flow (here 20 mL/min). Peak areas of quantifier-ion peaks were approximately doubled when the splitless time was enhanced from 0.5 minutes to 0.75 minute when derivatized MM-I (AAEs concentrations: 1mM or 0.5 mM depending on the AA type) was injected. Peak areas were again approximately doubled after injection of the same derivatized MM-I mixture when the splitless time was enhanced from 0.75 minutes to 1.0 minute. Here the samples were introduced by fast autosampler injection through a cold needle into a split/splitless liner packed with glass wool. Thus the sample enters the vaporization chamber as a band of liquid that is stopped by the glass wool. The boiling points of the solutes (the MeOH/MCF AA derivatives) are higher than the boiling point of the solvent chloroform (61° C) whi ch is the usual situation of liquid samples for GC analysis. The complete solvent must be evaporated until the liquid can reach the boiling points of the analytes as the droplet temperature stays at the solvent boiling point until solvent evaporation is completed. The liner section in which glass wool is holding the sample liquid was reported to be only about 4 mm long. This location of the sample narrows the heat transfer from the liner wall through the gas phase to the sample liquid. Therefore, the time require for complete sample vaporization is higher than for a thermospray moving through a unpacked liner[182]. This approximately four-fold increase of peak areas, achieved by increasing the splitless time, can be seen in the appendix Figure S1. It shows the overlaid chromatogram section of MM I, analyzed with the three different splitless times, showing late eluting AAEs that generally occurred with low peak intensities when compared to early eluting AAEs. Figures of merit for quantitative analysis including linear ranges, square values of the sample correlation coefficients R^2 and LODs before and after method optimization are shown and discussed in the next chapter.

6.3.2 Method Validation and Quantification

Spike-in experiments. The spike-in experiments with control serum yielded good mean recoveries for the three spike levels and for all tested AAEs as well as for D+L-Phe and Gly. Mean recoveries ranged between 90.3 % for L-Met and 98.1 % for D-Thr for the lowest spike level, between 86.8 %for L-Ala and 95.5 % for D+L-Phe for the medium spike level, and between 96.1 % for L-Ala and 104.3 % for D-Thr for the highest spike level (see Figure 11). Lowest standard deviations (SDs) of mean

recoveries were found for the highest spike level (0.5 - 3.1 %), followed by the medium spike level (2.8-10.6%) and the lowest precision was detected for the lowest spike level (SDs: 2.9-13.9%). Thus, spike-in experiments revealed no distinct matrix effect dependent over- or underestimation of AA quantities albeit derivatization was performed in presence of proteins and NaOH. NaOH and therefore a high pH > 10 in the beginning of reaction with MeOH/MCF was reported to increase reaction yields of derivatization as deprotonated carboxy groups react faster with MCF[173]. Nevertheless, high pH-values during the exothermal reaction can promote racemization processes in protein/peptide bound and free AAs as well as proteins/peptides hydrolysis[23, 183]. Matrix dependent overestimation of free AAEs would be the consequence of these unintended but relevant side reactions whereas ion enhancement or ion suppression are no issues in electron impact ionization following GC analysis. Inclusion of AAEs into the proteins that precipitate, due to the significant temperature increase during the highly exothermal reaction, can cause matrix dependent underestimation of free AAEs. Indeed, in general the method tended to slightly underestimate spiked AA concentrations as can be seen in Figure 11.

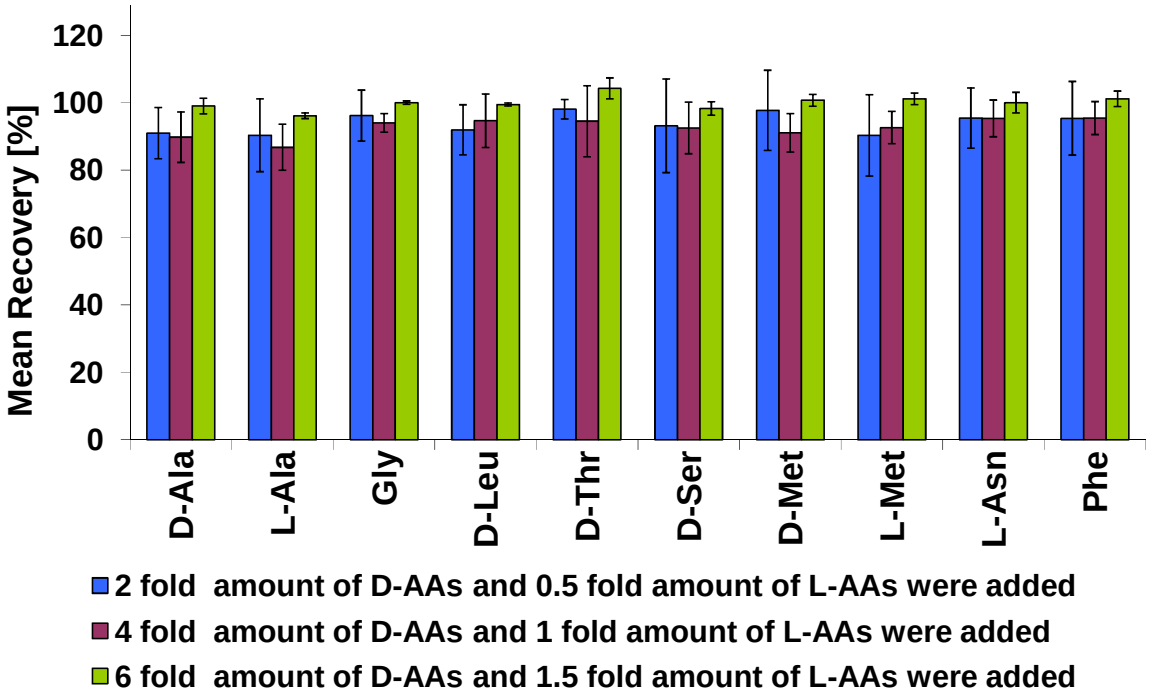

Figure 11. Results of spike-in experiments with ten AAs in control serum.

Method comparison before optimization of sample preparation. To further check method accuracy, 19 serum samples were analyzed both by the enantioselective MeOH/MCF method and an established GC-qMS method for achiral AA analysis[158, 180]. No protein precipitation was performed before MeOH/MCF derivatization in the presence of NaOH. Comparison of results revealed that the enantioselective method overquantified the sum of free AAs (D + L). Averaged recoveries ranged between 116.6% for Asn and 176.1% for Phe using the achiral AA method as a reference[158]. Method comparison was also performed for five urine samples to check method accuracy for the different biological matrix. MeOH/MCF derivatization was performed in the presence of NaOH and the same established method for quantitative AA analysis was used as reference as above. Mean recovery ranged between 105.9% for Ala and 125.8 % for Gly indicating overestimation of AA quantities albeit a less extensive than for serum. In contrast to serum, urine of healthy individuals does not contain any proteins but only peptides. Consequently, I hypothesized that proteins (as ingredients of serum) and peptides (as ingredients of serum and urine) were partly degraded during the highly exothermal MCF derivatization reaction performed under alkaline conditions. To test this hypothesis, derivatization was performed at alkaline or neutral pH, with or without removal of proteins before derivatization[158]. The outcome of these experiments will be discussed in the following section.

Comparison of different sample preparations. As shown in Figure 12 A, the pre-precipitation of proteins with cold MeOH led to a distinct decrease in detected L-AA amounts, whereas replacing the base by water in the reaction mixture in the presence of proteins showed a slight increase in concentrations. Nevertheless, skipping the addition of NaOH after protein precipitation caused a further decrease in the L-AA concentrations determined. This supported the hypothesis that protein and peptide degradation had occurred during derivatization with MeOH/MCF.

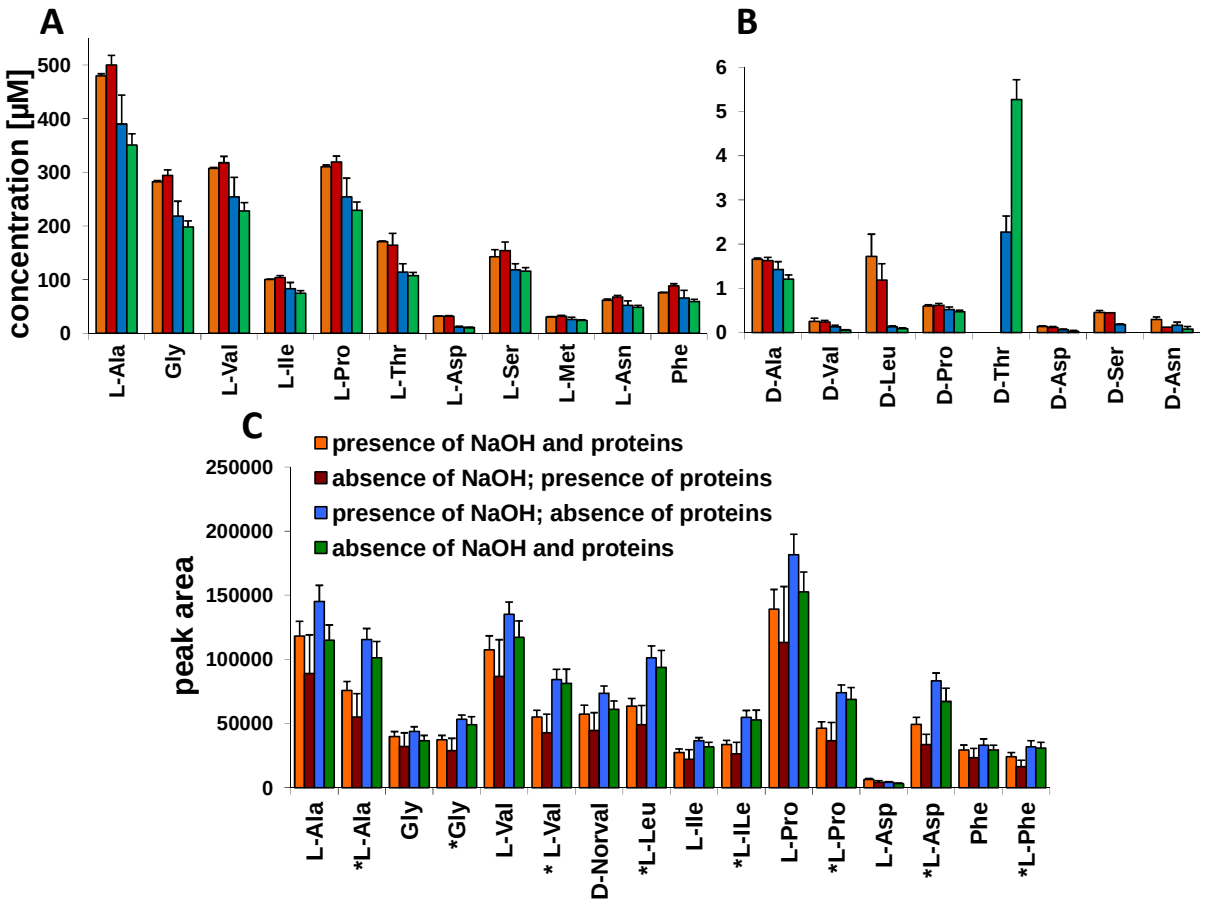

Figure 12. Results from the comparison of different preparation strategies for derivatization of serum with MeOH/ MCF for quantification of (**A**) L-AAs and (**B**) D-AAs by chiral GC-qMS. (**C**) demonstrates preparation dependent reaction yields by peak areas of detected labeled (marked by an asterisk) and unlabeled AAs.

Prior to the second addition of MCF, the solution was slightly basic in the presence of NaOH (pH 8); afterwards, it was slightly acidic (pH 5–6). Replacement of the base with water resulted in a neutral to slightly acidic pH-value (6–7) after the first addition of MCF and acidic conditions after the second addition (pH 1). The relatively low pH-values can be explained by the reaction of MCF with water yielding HCl. Protein degradation seemed to proceed faster at acidic pH, whereas the decomposition of peptides seemed to be faster at pH-values >5. If the underlying mechanism were an acetylation of the N-terminus followed by an alcoholysis, both derivatization reagents (MCF and MeOH) would be protagonists of protein and peptide degradation. Albeit related reactions had been reported, no further efforts were made to ascertain the underlying mechanism[184]. D- and L-AAs showed similar trends for the four different preparation strategies (see Figure 12 A and B). L-AAs contained in proteins were stronger affected by racemization than free AAs[185]. Furthermore, Frank at al. had observed a higher rate of racemization during the initial hydrolysis than several hours

later for AAs such as Asp and Val. They had also described an elevated isomerization rate of protein-bound Leu that was explained by a thiazoline intermediate. In contrast, the racemization rate for Thr was very low[159]. This is consistent with the present results. As can be seen in Figure 12 B, the highest bias was observed for Leu, while D-Thr was the only analyte that did not decrease when proteins were removed[158]. Consequently, it is necessary to perform MeOH/MCF derivatization in the absence of proteins and NaOH in order to determine accurate amounts of free AAEs. Finally, the influence of the omission of NaOH on reaction yield and, therefore, sensitivity was evaluated. Peak areas obtained with the four different preparation strategies were compared (Figure 12 C). Contrary to expectations the sensitivity for serum analytes stayed the same or was even improved by the removal of proteins. This might be caused by reduced AA inclusion into precipitated proteins. In the original procedure proteins precipitated during the first addition of MCF because of high temperatures resulting from reactions with MCF. In the optimized procedure proteins were precipitated before derivatization and the protein pellet was washed two times with a MeOH/ water mixture to release included analytes, which might explain the slightly increased sensitivity that also compensates the effect of omitting NaOH[158]. Thus, improvement of MeOH/MCF derivative yield by pH enhancement, reported to be based on faster esterification of deprotonated carboxylic acid groups[173], was approved with more abundant IS and AA peaks when 100 µL 1N NaOH solution were part of the reaction mixture. However, since a basic pH at high temperature promotes peptide hydrolysis and racemization of peptide bound AAs [160-162] the 100 µL of 1N NaOH solution were replaced by pure water to provide more accurate analysis of free AAEs in body fluids.

Method comparison after optimization of sample preparation. Method comparison was repeated with 19 serum samples from GvHD patients applying the optimized protocol (protein pre-precipitation and dilution with water) and the established achiral AA method as reference method[180]. Analysis yielded mean recoveries between 87.2% and 119.3%. Contrary to serum, which contains proteins at relevant concentrations, urine of healthy people contains no proteins but peptides. Here, the protein precipitation can be skipped, but base hydrolysis of peptides can still occur. The method comparison in 10 urine samples confirmed that accurate concentrations could be obtained by the enantioselective method if the addition of base was replaced by water[158]. Averaged recoveries ranged from 77.2 % to 105.2 %.

Results from all method comparisons are listed for six analytes in Table 2. They confirmed that the altered preparation protocols for serum and urine omitted the release of protein and peptide bound AAEs and therefore allowed the accurate determination of free AAE amounts.

Table 2. Mean recoveries of selected serum and urine amino acids in the presence and absence of protein and/or NaOH, respectively, for the chiral MeOH/MCF method in comparison to an achiral GC-MS method for AA analysis.

Averaged Recovery [%]	Ala	Gly	Val	Pro	Asn	Phe
Serum (N=19) derivatization in presence of proteins and NaOH	144.9	152.5	145.5	138.1	116.6	176.1
Serum (N=19) derivatization in absence of proteins and NaOH	98.3	104.7	87.2	97.8	94.9	119.3
Urine (N=5) derivatization with NaOH	105.9	125.8	117.4	116.4	120.6	110.7
Urine (N=10) derivatization without NaOH	90.4	105.2	92.3	77.2	95.8	92.7

Calibration. Replacing NaOH with water in the derivatization protocol did not affect linear ranges of the chiral GC-qMS method. Quantification parameters like quantifier and qualifier *m/z,* linear ranges and R^2 values as well as LODs before and after method optimization are shown in Table 3. Calibration of L- Asp, L-Thr and L-Ser could be realized for the first time after optimization of the chiral GC-qMS method. High blank values resulting from unlabeled AA impurities of the IS mix A, including the ISs at high concentrations had strongly impeded linear ranges of respective calibration curves. Furthermore, L-Thr coeluted with L-Asp and L-Ser with D-Met. For L-Ser, there was found no characteristic fragment at appropriate abundance that did not appear in the spectrum of D-Met. Thus L-Ser occurred as a double peak, which made reliable integration difficult as reflected by the low regression coefficient of the calibration points and a remarkably high LLOQ (31.25 µM)[158]. To achieve calibration of L-Thr the quantifier *m/z* =132, that referred to its characteristic derivative minus ester moiety fragment, was replaced by *m/z* =147, as the overlaid spectra of Asp and labeled Asp both interfered with *m/z* =132. The *m/z* = 136 of labeled Thr chosen in

my diploma for correction of D- and L-Thr areas was replaced by *m/z*= 149 to correct Thr areas by the corresponding labeled fragment. As a consequence of method optimization, 18 AAEs could be calibrated using the respective labeled L-AA as IS and all LLOQs were improved. However, accurate quantification of L-Ser was hampered by the spectrum of D-Met.

Table 3. Figures of merit for chiral GC-qMS analysis of amino acid enantiomers before (results from my diploma thesis[119]) and after method optimization.

	before method optimization (results from diploma thesis)			after method optimization			
AA	**R^2**	**Linear range [µM]**	**LOD [µM]**	**R^2**	**Linear range [µM]**	**LOD [µM]**	**Ion traces Quantifier + Qualifier**
D-Ala	0.9962	0.061 -1000	0.0512	0.9996	0.031 -500	0.0229	102 + 161
L-Ala	0.9903	1.953 -1000	0.2593	0.9992	0.122* -500	0.0966	102 + 161
Gly	0.9931	31.25 -1000	2.6255	0.9992	0.977* -500	0.0237	88 + 147
D-Val	0.9976	1.953 -1000	1.0236	0.9998	0.244* -500	0.0452	130 + 98
L-Val	0.9930	1.953 -1000	0.6276	0.9998	0.244* -500	0.0178	130 + 98
D-Leu	0.9959	1.953 -1000	1.3791	0.9999	0.244* -500	0.0899	144 + 88
L-Ile	0.9941	0.977 -1000	0.0719	0.9996	0.061* -500	0.0029	144 + 88
D-Pro	0.9914	0.244 -1000	0.0156	0.9997	0.061 -500	0.0032	128 + 187
L-Pro	0.9973	0.244 -1000	0.1933	0.9999	0.061 -500	0.0468	128 + 187
D-Thr	0.9970	62.50 -1000	7.8130	0.9993	0.977* -1000	0.0791	147[a] + 132
L-Thr	-	-	-	0.9975	1.953 -1000	0.7380	147[a] + 132
D-Asp	0.9979	15.63 -1000	4.3459	0.9996	0.122* -500	0.0098	160 + 219
L-Asp	-	-	-	0.9987	0.977 -500	0.2764	160 + 219
D-Ser	0.9985	31.25 -1000	0.5000	0.9997	1.953* -1000	0.4459	118 + 86
L-Ser	-	-	-	0.9912	31.25 -1000	16.4172	118 + 86
D-Met	0.9979	7.81 -1000	0.0313	0.9998	0.488* -1000	0.0402	162 + 221
L-Met	0.9920	15.63 -1000	0.6197	0.9991	0.244* -1000	0.0854	162 + 221
D-Asn	0.9977	0.977 -1000	0.2500	0.9998	0.244 -1000	0.0199	127 + 95
L-Asn	0.9977	1.953 -1000	0.0020	0.9999	0.244* -1000	0.0190	127 + 95
DL-Phe	0.9962	0.244 -1000	0.0303	0.9989	0.061 -1000	0.0415	162 + 178

* at least three additional points were added at the lower end of the calibration curve; [a] the quantifier of Thr was *m/z*= 132 before method optimization; after optimization *m/z*= 147 was used as quantifier for Thr enantiomers.

In case of D-Ala, one calibration point could be added at the lower end of the calibration curve. The calibration curves for D+L-Phe, D-Asn and both Pro enantiomers could be expanded by two calibration points at their lower ends. Calibration curves of the remaining AAEs and Gly included at minimum three additional points at the lower concentration end after method optimization. Summing up, the number of quantifiable D-AAs in physiological fluids was clearly increased (from N=3 to N=4 in human control serum and from N=2 to N=8 in human control

urine) due to optimized injection parameters, decreased IS concentrations and newly selected quantifier *m/z*. Nevertheless, for more reliable quantitative D-AA analysis in matrices like mouse and human serum or mouse liver tissues, that can include D-AAs in the nM range or the low pmol/mg tissue range, further improvement of LLOQs is required. Also LODs and, therefore, the detectable number of D-AAs in physiological fluids and tissues were improved distinctly. Parameter optimization decreased not only LLOQs and LODs but also ULOQs of early eluting AAEs. In these cases the highest concentration point (1 mM) was saturated and had to be excluded. However, measuring this MM-II concentration additionally with a splitless time of 0.5 minutes yielded exclusively unsaturated peaks of which responses fitted into the calibration curves, as IS areas corrected perfectly for the different injection condition. Calibration curves of L-Ala and Gly that were generated using a splitless time of 1.0 min except for the highest concentration point (splitless time = 0.5 min) are displayed in the appendix in Figure S2. Thus, samples including D- and L- AAs at distinctly different concentrations were measured with both splitless times (1.0 and 0.5 min) to realize accurate quantification of both antipodes. Albeit time-consuming, this procedure was applied to samples of this chapter that included L-Ala, L-Val or Gly at concentrations >500µM.

Repeatability. The optimized chiral GC-qMS method showed excellent method repeatability with RSDs between 0.49–11.1% and 0.70–3.87% for the replicate analyses (N= 6) of the urine pool and the serum control, respectively, as shown in Figure 13. The RSD of D-Pro (11.1%) in urine was much higher compared to the other analytes (0.49–4.25%), most likely due to its low level in the analyzed sample, which was close to the LLOQ. In general, for the low-abundant D-AAs higher deviations were observed than for L-AAs. L-AAs benefit from the optimal correction by the structurally very similar labeled L-configured ISs. D-Val, D-Leu, D-Met, D-Ser and D-Asn were not quantified above LLOQ in the serum sample investigated. In the urine sample, only D-Met could not be quantified above its LLOQ[158].

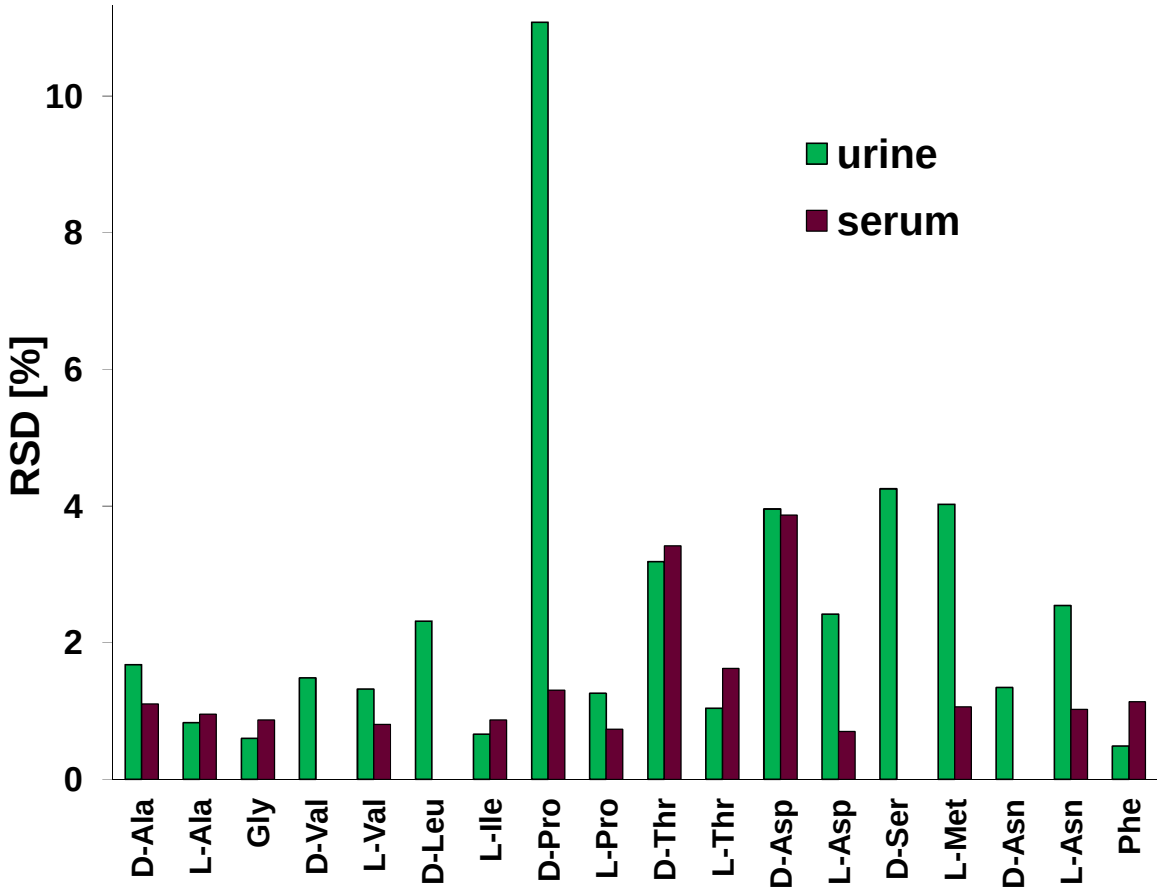

Figure 13. Repeatability of the optimized MeOH/MCF method for the analysis of AAEs in urine and serum. N= 6 replicates were prepared and analyzed, respectively.

6.3.3 Application to the Discovery of Markers of Fatty Liver Disease

Due to the low quality of L-Ser calibration, which was disturbed by coeluting D-Met, L-Ser quantities are neither shown nor discussed in this chiral GC-qMS application.

The progression and physiological effects of non-alcoholic fatty liver disease (NAFLD) were investigated intensively in the last decade due to the increasing incidence of the disease in developed countries[179, 186, 187]. About 95 % of people suffering from obesity are affected by NAFLD. Besides obesity, this chronic liver disease is often accompanied by further characteristic components of the metabolic syndrome like type 2 diabetes, hypertension and dyslipidaemia. Triglyceride accumulation in hepatocytes characterizes the first stage of NAFLD called hepatic steatosis. NAFLD can progress from steatosis over NASH (non-alcoholic steatohepatitis) to fibrosis, cirrhosis and, ultimately, liver cancer. Elevated lipid peroxidation and oxidative stress were reported to be key factors in the development

of NASH from steatosis. Continuous enhanced production and the resulting accumulation of reactive oxygen species promote necroinflammation in the liver, which causes fibrosis[179, 188]. The noninvasive differentiation of the early stages of NAFLD by imaging and molecular means remains difficult and definite diagnosis still requires liver biopsy. Here, the chiral GC-qMS method was applied to learn more about the behavior of AAE levels in the liver and serum of mouse models mimicking the development of NASH. Mice that were fed with the NASH inducing diet for three weeks had increased TNF α levels (data not shown), which indicated a beginning liver inflammation. However, mice fed this diet for two weeks showed no indication of inflammation, yet. However, they already suffered from steatosis.

FDRs were determined for the comparisons of two weeks treated animals (controls versus steatosis) and the comparisons of the three weeks treated animals (controls versus NASH), respectively.

The differences in content between L-AAs and D-AAs in liver tissue were remarkable. It comprised more than three orders of magnitude in case of Ala, Val and Pro. L-Ala, Gly and L-Asp quantities in liver tissues exceeded their ULOQs, whereas most D-AA levels of Ser, Asn, Thr and Met were below LLOQs. Quantities of all remaining AAEs are shown in Figure 14. L-Val and L-Pro yielded only one value below ULOQ in the NASH group after two weeks. For each other AAE displayed, there were found at least three quantifiable concentrations per group and each shown mean D-AA level in Figure 14 was based on five values. As a consequence of method optimization and the up to 16-fold improvement of LLOQs (Table 3), mean liver contents of five D-AAs were determined for the four groups. In contrast, with the original method of my diploma thesis and corresponding LLOQs, only D-Ala amounts would be quantifiable in all of the here investigated liver samples. Therefore, the number of quantifiable D-AAs in mouse liver samples was distinctly increased due to the adjusted IS mix concentration and the optimized injection method. There were observed slightly increased L-AA quantities in mice fed a NASH inducing diet for three weeks when compared to respective controls albeit no significant trend was present considering the FDR. A significant increase in L-AA quantities was observed in liver tissues of mice suffering from steatosis after the two weeks diet for Ile, Met and D+L-Phe (FDR= 0.027-0.033) when compared to respective controls. D-Ala, D-Leu and D-Asp contents were decreased in steatosis and NASH livers when compared to respective

controls. The mean D-Val concentration in mouse liver affected by steatosis was increased when compared to the mean D-Val concentration in respective control mouse livers. However, considering the FDR, these D-AA trends were not significant. Changed D-AA contents cannot be explained by changed DAO activity in the liver as contrary to other mammalian livers, DAO is not expressed in mouse livers[52, 53].

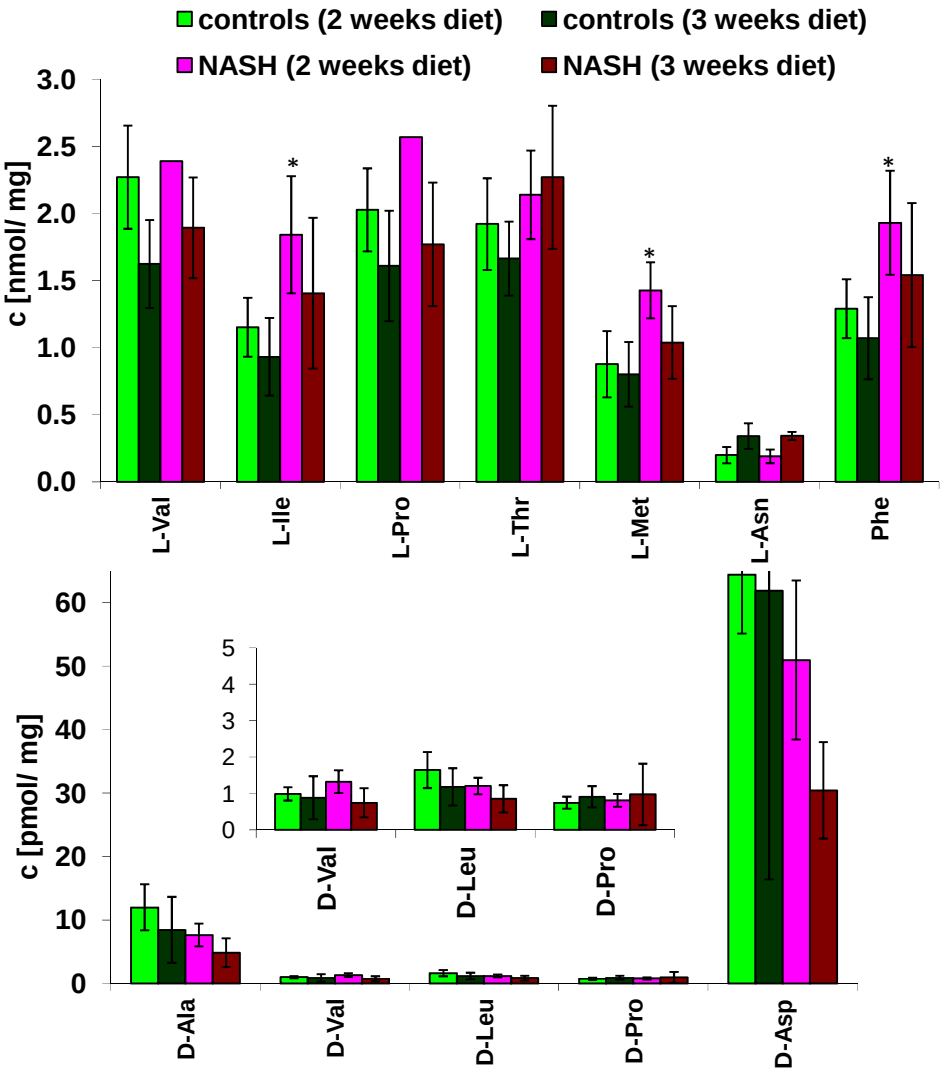

Figure 14. Mean AAE concentrations in liver tissues of a mouse model mimicking the development of NASH and respective control mice (N=5 per group). * 0.001< FDR < 0.05

.AAE trends in the corresponding serum specimens were similar to those in mouse liver with decreased D-AA amounts for some D-AA types and increased L-AA amounts in steatosis and NASH serum when compared to control sera (see Figure 15). The difference in D- and L-AA levels was clearly lower in serum. The highest difference was observed for Val enantiomers comprising approximately three orders

of magnitude. The other quantifiable antipodes differed by more than two orders of magnitude except for Thr enantiomers that differed by only about one order of magnitude. This was comparable to the situation in human serum.

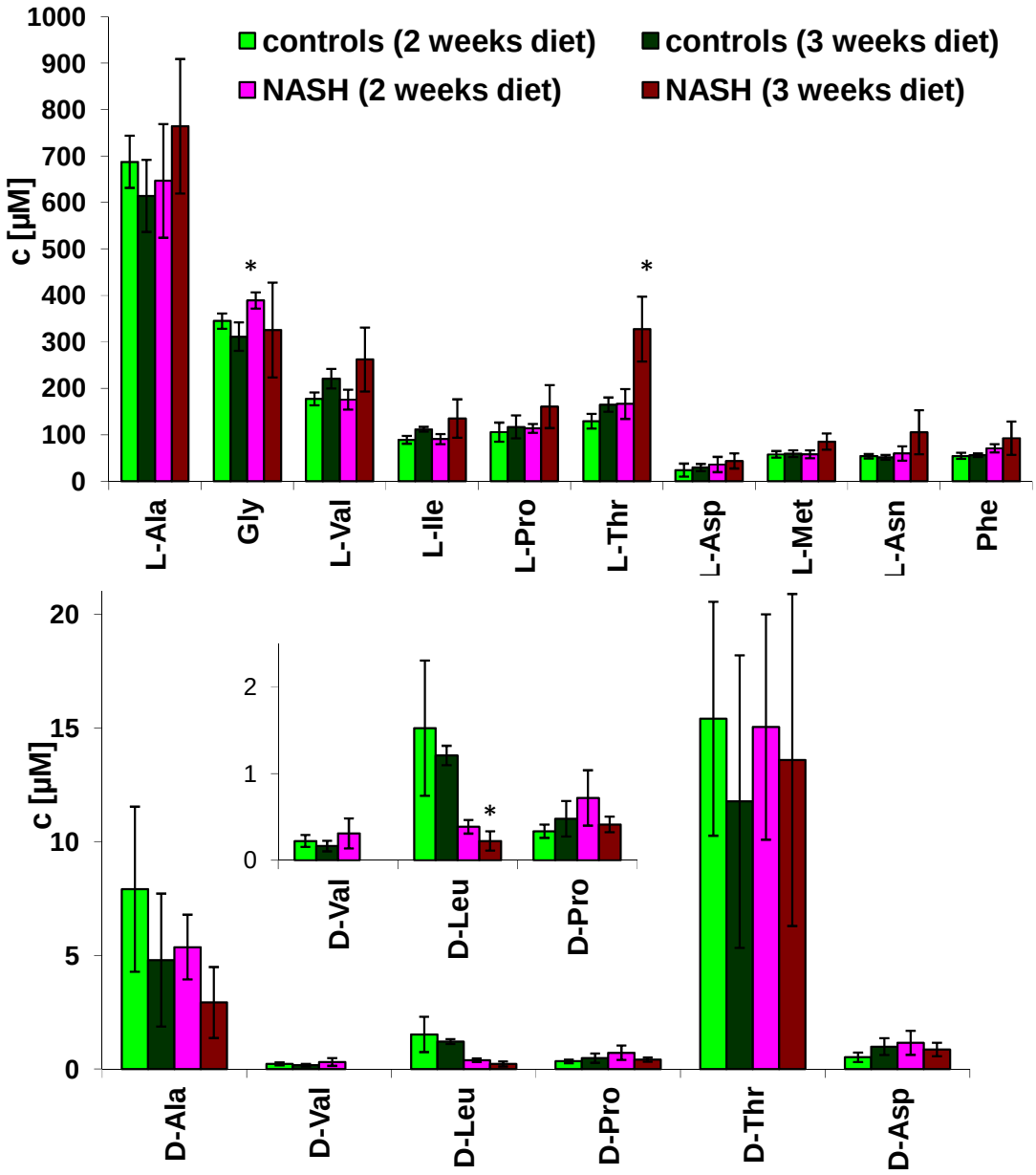

Figure 15. Mean AAE concentrations in serum of mouse models mimicking the development of NASH and of respective control mice. * 0.001< FDR< 0.05.

Consequently, all L-AAs concentrations lay within the linear ranges except for two L-Ala concentrations that exceeded the ULOQ in mice after three weeks on the NASH diet. Significant serum level increases were found for Gly after two weeks of diet (FDR=0.044) and for L-Thr after three weeks of NASH diet (FDR=0.012) when compared to the respective serum levels in the control mouse group. Owing to method optimization and obtained improved LLOQs (Table 3), there could be

determined mean serum quantities of six D-AAs for all investigated groups. Due to the distinctly higher LLOQs, the application of the original chiral GC-qMS method of my diploma thesis would only allow the quantification of D-Ala and D-Pro amounts in all of the here investigated mouse serum samples. Thus, also for mouse serum, method optimization clearly increased the number of quantifiable D-AAs.

A statistically significant D-AA serum level decrease in NASH mice was found exclusively for D-Leu (FDR= 0.023). In contrast the D-Asp, D-Pro and D-Val serum level were enhanced in case of hepatic steatosis albeit not significantly considering the FDR. Accurate quantification of D-Ser, D-Met and D-Asn was not possible in mouse serum because of coeluting matrix compounds that disturbed corresponding quantifier peaks. Reports on elevated gut permeability and prevalent small intestinal bacterial overgrowth (SIBO) in steatosis, and the ability of bacteria to release high D-AA amounts into their environment provide an indication for increased D-AA serum levels [18, 189]. Moreover, decreased D-Asp oxidase activity in the NAFLD livers may be the reason for enhanced D-Asp serum level, however, there was observed no D-Asp level increase in the corresponding liver samples. Therefore, the here found D-AA trends in mouse serum and liver do not support the findings of increased intestinal permeability in NAFLD as it was reported by Miele et al.[189]. However, their conclusions cannot be negated by the here shown results as there is not yet enough known about D-AA metabolism in mammals that most probably influences noticeable D-AA quantities in physiological fluids and tissues. Determined D-AA concentrations in mouse liver and serum were comparable to those, previously reported, for liver and serum of control mice[121, 190, 191].

6.3.4 Comparison with Published Methods

This section was adapted from[158] .

Previously reported GC methods for the separation of anhydride derivatives on a Chirasil-L-Val column had actually not been well suited for D-AA analysis in urine and serum[35, 40, 48]. With 9[35, 48] or 10[40] baseline resolved racemates of proteinogenic AAs, these methods presented suitable enantioselectivity, however, resolution values of the MeOH/MCF method were superior (>2.4). Applying TFAA or PFPA for acetylation, and MeOH, propanol or IPA for esterification, impeded quantification of

several AAs (Asn, Asp, Gln, Glu, Ser, Thr and Tyr)[35, 40, 48]. Asn degraded to form Asp and, analogously, Gln degraded to form Glu. IPA/TFAA derivatives of AA carrying hydroxy groups lacked stability and thus hampered quantification[35]. With the MeOH/MCF method quantification of D-Asn, D-Asp, D-Ser, and D-Thr posed no problem except for the high LLOQs for D-Ser and D-Thr when compared to the other MeOH/MCF D-AAs based on low peak abundances of these hydroxy D-AAs. Another drawback of common methods is a rising baseline caused by strong bleeding of the Chirasil-L-Val column at elevated temperatures >150°C. The here applied γ-CD based chiral column showed no baseline enhancement up to a temperature of 190°C. Albeit the preparation of serum including re moval of proteins was complex, the MeOH/MCF method exceeded formerly reported GC quantification approaches in efficiency. Prior to chiral analysis of anhydride derivatives on Chirasil-L-Val, conventional achiral analysis applying ion exchange chromatography were performed to either determine D+L-AA quantities [35, 48] or to isolate AAs from the biological matrix[40]. Apart from Pätzold et al., who used an IS for quantification[40], D-AA quantities were calculated from D+L amounts using D-ratios estimated from peak areas of the enantiomers[35, 48]. Peak areas are an unreliable measure in case of the Chirasil-L-Val column, because the rising baseline masks later eluting L-AAs more than the corresponding D-AAs. Thus, accuracy of this approach is likely to be inferior to the MeOH/MCF method. Moreover, the latter method is the only technique available to date that has been shown to allow in a single analytical run the direct quantification of D-AAs in several matrices like human and mouse serum and urine and mouse liver. Among the LC methods applied to physiological fluids, the one by Nagata et al. showed the best performance. With 12 D-AAs amenable to quantification, applying Marfey's reagent and a conventional RP-column, the method yielded superior enantioselectivity. Nevertheless, detection limits (4–10 µM) of D-AAs were much higher than those of the MeOH/MCF method (3.2–446 nM). Therefore, only D-Ala, D-Ser and D-Pro were detected in plasma, whereas the MeOH/MCF method enabled accurate quantification of four D-AAs in human control serum and six in mouse serum. Applying two-dimensional thin-layer chromatography for the pre-separation of AAs from the biological matrix rendered the method of Nagata et al. more elaborate, but the pre-separation was required due to the low selectivity of fluorescence detection [83]. Further, several two-dimensional HPLC approaches using chiral columns and fluorescence detection were also not as efficient as the

MeOH/MCF method, because they did not allow to separate more than one racemate per run because of disturbing matrix compounds[121, 192, 193]. Only the multi-loop two-dimensional HPLC system of Hamase et al. enabled resolution of four racemates of branched AAs in one run [51]. LLOQs of two-dimensional LC methods were similar to LLOQs of the MeOH/MCF method[51, 121, 192, 193], but the here presented GC–qMS method excelled in selectivity, robustness and efficiency, as matrix compounds could rarely disturb the analysis of human serum and urine due to mass spectrometric detection in SIM mode. From the other column chromatography methods, presented as outstanding methods for AAE quantification in biological matrices in chapter 4.3.3.1, only the chiral LC-MS/MS method by Barbaro et al. outperformed the chiral MeOH/MCF GC-qMS in sensitivity and efficiency as the resolution of 16 pairs of proteinogenic AAEs was realized in 35 minutes[120]. Nevertheless, the method showed several drawbacks like Leu enantiomers coeluting with Ile enantiomers, inaccurate quantification of D-Ser, D-Orn, L- and D-Trp enantiomers and the unfavorable elution order of D-AAs eluting after L-AAE resulting in distinctly broader peaks for D-AAs than for L-AAs. Therefore LODs and LLOQs of D-AAs were higher than those of L-AAs in most cases in contrast to the here presented GC-qMS method. Finally the chiral LC-MS/MS method was validated for the application to lake water, which is a less complex biological matrix than mammalian physiological fluids and tissues[120]. However, there were three pairs of overlapping peaks in chromatograms of the chiral GC-qMS method, which disturbed quantification of L-Ser, L-Leu and D-Ile. The use of GC×GC-TOFMS should solve this problem and improve resolution from biological matrix compounds. Moreover, it should increase the number of AAEs amenable to quantitative analysis due to improved peak shapes owing to modulation and fast second dimension separation[194].

7 Implementation of enantioselective GC×GC-TOFMS for quantitative Amino Acid Analysis in Urine and Serum

This chapter was adapted from [174]. Each section, corresponding to published text, was cited individually.

7.1 Introduction

The overlapping peak pairs D-Ile/L-Leu, L-Thr/L-Asp, and L-Ser/D-Met impeded the quantification of D-Ile, L-Leu and L-Ser by the chiral GC-qMS method. Further, LLOQs achieved for some D-AAs and resolution of AAEs from other biological matrix components were insufficient for reliable quantitative AAE analysis in serum. Both, the orthogonal separation characteristics and the narrower peaks obtained by cryo-focusing make GC×GC-TOFMS an attractive remedy to overcome the aforementioned limitations of chiral GC-qMS[194].

Junge et al. were the first to apply GC×GC to the separation of AAEs as their ethyl chloroformate derivatives in samples of beer by coupling a Chirasil-L-Val column with a low-polarity column in the second-dimension[195]. The present study expanded the scope of GC×GC-based AAE analysis by applying a combination of an Rt-γDEXsa chiral first-dimension column with an RTx-1701 or a ZB-AAA column as second-dimension column not only to the separation but also the quantitative measurement of AAEs in physiological fluids after derivatization with MeOH/MCF[174].

7.2 Material and Methods

7.2.1 Analyzed Samples

A set of 48 urine and 43 serum specimens, which had been collected from patients before and after curative SCT for non-malignant and malignant disorders of the immunohematopoietic system, was used to validate the GC×GC-TOFMS method with the Rt-γDEXsa/ZB-AAA column set by comparing determined AAE amounts with the results obtained by the chiral GC-qMS method. Urine specimens were not treated with preservatives but were frozen at −20 °C as quickly as possible after sampling to avoid bacterial growth. Further, 25 serum specimens from patients with liver cirrhosis

and 16 control sera were analyzed by the validated GC×GC-TOFMS method to demonstrate relevance for medical diagnostics. At the time of blood drawing, none of the patients had been treated with peptide antibiotics or other drugs that might affect D-AA serum levels. For the evaluation of method repeatability a human serum control was obtained. Serum specimens were stored at −80 ℃. Specimens were provided by collaborators at the University Hospital of Regensburg with approval from the institutional review board[174].

7.2.2 Sample Preparation

Serum samples were prepared with the optimized procedures including protein pre-precipitation with 600 µL of cold MeOH (-20℃) and two washing steps of the pellet with MeOH-water (80% MeOH; 0℃) with subsequent derivatization of the dried residue of the collected MeOH-water phases. The following volumes were added for derivatization: 275 µL of water, 167µL of MeOH, 34 µL of pyridine and 40 µL of MCF that was added in two portions to the reaction mixture. Derivatives were extracted into 300 µL of chloroform. The optimized procedure for the derivatization of urine included the addition of water to a constant start volume of 275 µL and the subsequent addition of the above listed derivatization reagent volumes. Sample aliquots of 150 µL and 20 µL of IS mix C were used for quantitative analysis by GC×GC-TOFMS and GC-qMS. Prepared MM aliquots for preliminary experiments were noted in chapter 5.2.3.

7.2.3 Instrumental Set-up and Applied Methods

The LECO (St. Joseph, MI) Pegasus 4D GC×GC–TOFMS instrument included the following components: an Agilent Technologies Model 6890 GC with a PTV injector, a dual-stage, quad-jet thermal modulator and a secondary oven coupled to a fast acquisition TOFMS providing unit mass resolution (Gerstel, Muehlheim, Germany). An Rt-γDEXsa column (30 m×0.25 mm ID, 0.25 µm film thickness) from Restek (GmbH, Bad Homburg, Germany) protected by a 5 m×0.25 mm ID fused silica deactivated guard column (Agilent Technologies, Palo Alto, CA, USA) was used as the first-dimension column and an RTx-1701 (2 m×0.1 mm ID×0.1 µm film thickness, Restek) or a ZB-AAA (2 m×0.25 mm ID, 0.25 µm film thickness, Phenomenex Inc.)

column were employed as second-dimension columns, respectively. A sample volume of 1.5 µL was injected in splitless mode with the temperature of the PTV Injector set at 50 ℃ for 0.5 min and then ramped at 12 ℃/s to 250 ℃. A chemically inert Siltek liner from Gerstel was used. The helium flow-rate was set at 1.9 mL/min (constant flow). Modulation was accomplished every 4 s. Mass spectra were acquired from 40 to 600 *m/z*. For 1D GC–TOFMS analysis the modulator was turned off. The solvent delay was 19 min. Transfer-line temperature was held at 260 ℃. The ion source was operated at 200 ℃ and −70 eV. A positive offset of 5 ℃ was used for the second-dimension column and a 15 ℃ offset relative to the first-dimension column for the modulator. Applied temperature programs for the first column oven are given in Table 1.

7.2.4 Quantification and Method Validation

Calibration. For AA identification, EI spectra were compared to the EI spectra of the validated GC-qMS method. Calibration was performed with the Rtγ-DEXsa/ZB-AAA column set using a 16 point-serial dilution of MM II. It contained all AAs, whose elution from the RTγ-DEXsa column as MeOH/MCF-derivatives could be detected, over a concentration range of 31 nM to 1 mM each. Applied IS concentrations of IS mix C are given in chapter 5.2.3. As the labeled AAs had been gained from algae, they were present in the mix at their naturally occurring ratios in algae. Most D-AAs were detected in the labeled mix but their abundance was too low (< 3.4% of the respective L-AA area) to be suitable as ISs. Thus, the stable isotope-labeled L-AAs were used to correct areas of the corresponding D- and L-AA in quantitative measurements. Correspondingly, stable isotope-labeled Gly, the only natural nonchiral AA, was used for correcting Gly area integrals[174]. LLOQ was defined as described in chapter 5.5.1. Data analysis of calibration measurements was performed by Dr. Martin Almstetter.

Repeatability. Eight aliquots of the human control serum were prepared and analyzed to test method repeatability[174].

Method comparison. Accuracy was checked by comparing results with those obtained by the validated chiral GC-qMS method for AAE analysis. Relative recoveries were determined for urine (N = 48) and serum (N = 43) by dividing the

enantiomer amount determined by GC×GC-TOFMS by the respective amount measured by chiral GC-qMS and multiplying by 100. Mean recoveries and Pearson correlation coefficients were calculated. Additionally, Bland-Altman plots were generated, which display for each specimen analyzed the difference in concentration versus the mean of the concentrations determined by the two methods and, therewith, assesses agreement between methods[172, 196, 197] as explained in chapter 5.5.3. Since it takes too much space to show all Bland-Altman plots, the mean difference was divided by the averaged mean of all couples and multiplied by 100. These values were named 'mean deviation'[174].

7.3 Results and Discussion

Initial experiments focused on the evaluation of two different column combinations for the GC×GC separation of MeOH/MCF derivatives of AAEs. In GC×GC the length of the second-dimension is kept short to allow the elution of analytes within one modulation period. Length of the first-dimension column, in contrast, is not limited.

Therefore, the chiral Rt-γDEXsa column was always chosen as first-dimension stationary phase, as the resolution of enantiomers improves with increasing length of the chiral column. Secondly, the Rt-γDEXsa phase reacted sensitive to high temperatures >190 °C, yielding reduced enantioselec tivity and accelerated column degradation (data not shown). Therefore, a fast second-dimension enantioselective separation at high elution temperatures of AAEs, eluting late from the non-chiral columns would be unfavorable for AAE resolution[174].

7.3.1 Rt®-γDEXsa/Rtx®-1701 Column Set

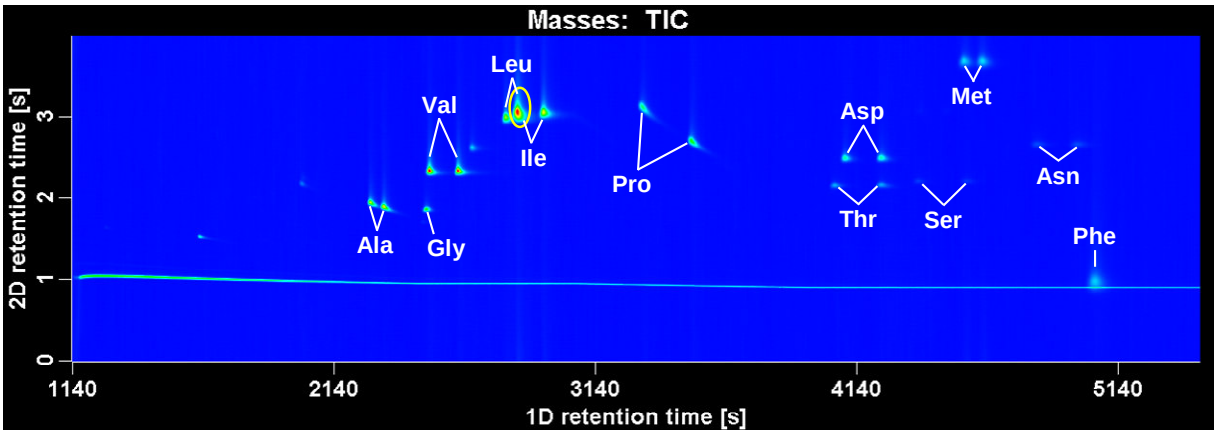

Figure 16. Characteristic GC×GC-TOFMS chromatogram of the AAE MM II using the Rt-γDEXsa (30m x 250 µm x 0.25 µm)/Rtx-1701 (2m x 100 µm x 0.1 µm) column combination and the optimized temperature program (method A) : 70℃ (1 min) – 2℃/min – 150℃ (10 min) –2℃/min – 180℃ (25 min), a constant He flow of 1.9 mL/min, a modulation rate of 4s and a positive offset of 5℃ for the Rtx-1701 column. Coeluting D-Ile and L-Leu isomers were encircled.

Initially, a 2-m midpolarity 14% cyanopropylphenyl/86% dimethyl polysiloxane RTx-1701 capillary column with an inner diameter of 100 µm served as the second-dimension column. This narrow bore column and the intended high He-flow limited applied temperature programs to flat temperature ramps and generally low temperatures. During fast temperature ramps and temperatures >180℃ the GC x GC device was not able to continuously provide the required pressure to maintain the high constant He-flow of the enantioselective method. Consequently, a method comparable to the chiral GC-qMS method could not be tested. Nevertheless, low temperatures were favorable for enantiomer resolution in the first-dimension. A characteristic chromatogram of MM II obtained under optimized temperature program (method A, Table 1) is shown in Figure 16. The RTx-1701 column compensated for the lack of selectivity of the Rt-γDEXsa for L-Thr/L-Asp and L-Ser/D-Met, respectively, and allowed their baseline resolution in the second-dimension. However, L-Leu and D-Ile still coeluted. MeOH/MCF-Phe enantiomers were not resolved at all by the chiral Rt-γDEXsa column and, therefore, could not be separated by the RTx-1701 column either[174].

7.3.2 RT®-γDEXsa/ZB-AAA Column Set

Previously, Kaspar et al. had demonstrated the successful separation of Leu and Ile as their propyl chloroformate (PCF) derivatives on a 15-m ZB-AAA capillary column that reportedly consists of 50% phenyl/50% dimethyl polysiloxane[180, 198]. Therefore, the ZB-AAA column was tested next as second-dimension column.

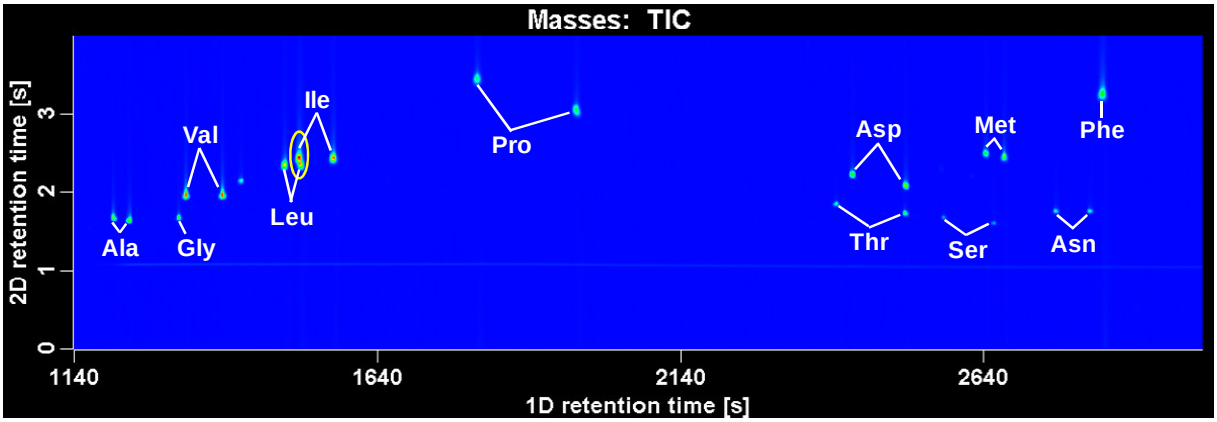

Figure 17. Characteristic GC×GC-TOFMS chromatogram of the AAE MM II using the Rt-γDEXsa (30m x 250 µm x 0.25 µm)/ ZB-AAA (2 m×250 µm x 0.25 µm) column combination and a comparable temperature program to the optimized GC-qMS method (method B): 70℃ (1 min) – 4℃/min – 150℃ (10 min) - 3 ℃/min – 190℃ (15 min). A constant He flow of 1.9 mL/min, a modulation rate of 4s and a positive offset of 5℃ for the Rtx-1701 column were applied. Overla pping D-Ile and L-Leu isomer peaks were encircled.

A representative chromatogram of MM II obtained with a temperature program (method B, Table 1) comparable to the previously optimized GC-qMS method II is pictured in Figure 17. Again L-Thr/L-Asp and L-Ser/D-Met, which coeluted from the chiral column, were resolved completely in the second-dimension. In addition, partial resolution of D-Ile and L-Leu was observed. Following optimization of the temperature program (method C, Table 1), baseline separation was achieved for all analytes except for the Phe enantiomers. This is demonstrated by first and second-dimension retention times in Table 4 and by a 2D chromatogram of MM II in Figure 18 A as compared to a respective measurement in 1D mode (Figure 18 B).

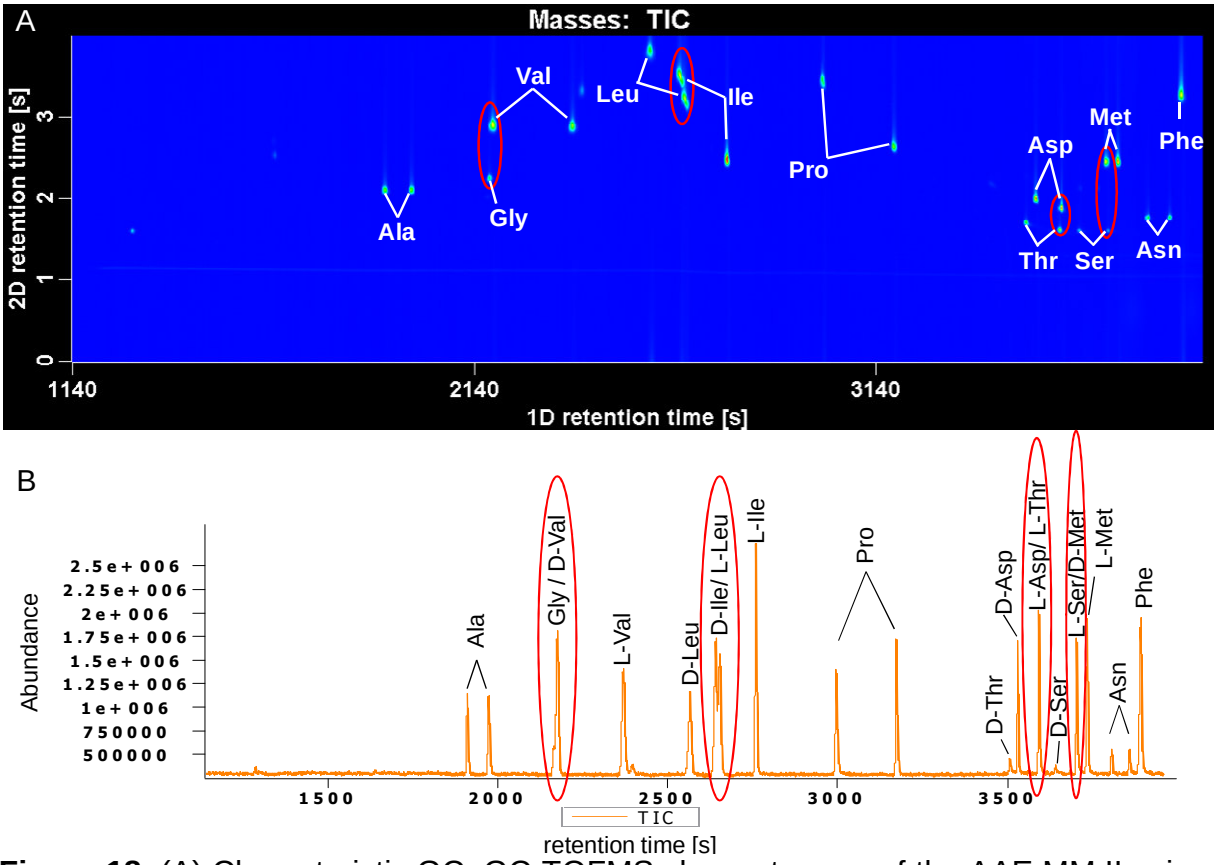

Figure 18. (A) Characteristic GC×GC-TOFMS chromatogram of the AAE MM II using the Rt-γDEXsa/ZB-AAA column combination and the optimized temperature program (method C): 70℃ (1 min) – 2℃/min – 130℃ (12.5 mi n) - 8℃/min- 150℃ (4 min) - 4℃/min – 190℃ (6 min) in 2D mode and in (B) 1D mo de after modulation was turned off. Each peak pair, that was not baseline separated after 1D separation but was baseline separated by the second dimension was encircled, respectively.

The 1D GC-TOFMS measurement yielded 3 coeluting peak pairs and the D-Ile/L-Leu peak pair that was partly separated using GC method C (Table 1), reflecting the insufficient selectivity of the Rt-γDEXsa column. Selectivity was improved by using thermal modulation and the different separation properties of the second-dimension ZB-AAA column. Enhanced resolution of enantiomers that were separated by a temperature program on the chiral first-dimension column was achieved due to the fast and therewith approximately isothermal separation on the second-dimension column. It allows additional separation of enantiomers even though the second-dimension selector provides no stereo-specific retardation. This can be seen for the enantiomers of Leu, Ile, and Pro in Figure 18 A[174].

Table 4. First and second-dimension retention times and fragment ion masses used for quantification of MeOH/MCF AAE-derivatives by GC×GC-TOFMS employing the column sequence: Rt-γDEXsa (30m x 250 µm x 0.25 µm)/ ZB-AAA (2 m×250 µm x 0.25 µm) and method C: 70℃ (1 min) – 2℃/min – 130 ℃ (12.5 min) - 8℃/min-150℃ (4 min) - 4℃/min – 190℃ (6 min).

AA	1st retention time (s)	2nd retention time (s)	Quantifier analyte + U-^{13}C,^{15}N-labeled IS
D-Ala	1916	2.105	102 + 105
L-Ala	1976	2.110	102 + 105
Gly	2172	2.250	88 + 90
D-Val	2180	2.895	130 + 135
L-Val	2372	2.890	130 + 135
D-Leu	2572	3.810	144 + 150
L-Leu	2660	3.255	144 + 150
D-Ile	2648	3.530	144 + 150
L-Ile	2764	2.480	144 + 150
D-Pro	3004	3.445	128 + 133
L-Pro	3176	2.660	128 + 133
D-Thr	3512	1.705	147 + 149
L-Thr	3592	1.620	147 + 149
D-Asp	3536	1.995	160 + 164
L-Asp	3596	1.890	160 + 164
D-Ser	3644	1.605	118 + 121
L-Ser	3712	1.610	118 + 121
D-Met	3708	2.455	162 +167
L-Met	3740	2.455	162 + 167
D-Asn	3812	1.770	127 + 132
L-Asn	3864	1.770	127 +132
Phe	3900	3.280	162 + 171

7.3.3 Quantification and Method Validation

Calibration. Calibration curves were generated for absolute quantification of AAEs. Table 4 lists fragment ion masses chosen for quantification. Values for linear range, R^2 and repeatability are shown in Table 5. For direct comparison, Table 5 also includes the values obtained for 1D-GC-qMS. GC×GC-TOFMS calibration curves were linear with the square values of the Pearson correlation coefficient r ranging between 0.9938 and 0.9992, which is comparable, albeit inferior to the 1D GC-qMS method, whose R^2 values ranged from 0.9956 to 1.0000. LLOQs were in the range of 0.03–2 µM[174]. While those for GC-qMS ranged from 0.03 to 31.25 µM. The most

striking improvement was achieved for L-Ser, whose LLOQ could be reduced by three orders of magnitude from 31.25 µM to 0.031 µM due to the baseline separation of L-Ser from D-Met by the second-dimension column. In the GC-qMS method the mass spectrum of coeluting D-Met had interfered with the calibration of L-Ser leading to a flat calibration curve and a remarkably high LLOQ. In contrast, LLOQs for D-Met and L-Met deteriorated from 0.488 µM and 0.244 µM for GC-qMS to 1.953 µM and 0.977 µM, respectively, for GC×GC-TOFMS as their lowest calibration points did not fit, with an accuracy between 80 and 120%, into the calibration curves. This was possibly a consequence of the lower repeatability of the method when compared to the chiral GC-qMS method (see Table 5).

Table 5. Comparison of linear ranges, R^2 values and relative standard deviations (RSDs) for AAE analysis in serum by GC×GC–TOFMS and GC–qMS.

	GC×GC-TOF-MS			GC-qMS		
AA	**Linear range (µM)**	**R^2**	**RSD (%; N=8)**	**Linear range (µM)**	**R^2**	**RSD (%; N=6)**
D-Ala	**0.031 -1000**	**0.9971**	**12.15**	**0.031 -500**	**0.9998**	**1.10**
L-Ala	**0.061 -1000**	**0.9974**	**2.16**	**0.122 -500**	**0.9996**	**0.95**
Gly	**0.031* -1000**	**0.9979**	**3.78**	**0.977 -500**	**0.9996**	**0.87**
D-Val	**0.244 -500**	**0.9971**	**-**	**0.244 -500**	**0.9999**	**-**
L-Val	**0.061* -500**	**0.9961**	**3.81**	**0.244 -500**	**0.9999**	**0.81**
D-Leu	**0.244 -1000**	**0.9974**	**-**	**0.244 -500**	**1.0000**	**-**
L-Leu	**0.061 -1000**	**0.9954**	**1.28**	**-**	**-**	**-**
D-Ile	**0.061 -1000**	**0.9970**	**-**	**-**	**-**	**-**
L-Ile	**0.061 -1000**	**0.9973**	**3.07**	**0.061 -500**	**0.9998**	**0.87**
D-Pro	**0.031 -500**	**0.9988**	**4.52**	**0.061 -500**	**0.9998**	**1.31**
L-Pro	**0.061 -500**	**0.9970**	**3.38**	**0.061 -500**	**0.9999**	**0.73**
D-Thr	**0.122* -500**	**0.9986**	**-**	**0.977 -1000**	**0.9996**	**-**
L-Thr	**0.061* -500**	**0.9980**	**3.53**	**1.953 -1000**	**0.9988**	**1.62**
D-Asp	**0.031* -1000**	**0.9938**	**16.64**	**0.122 -500**	**0.9998**	**3.87**
L-Asp	**0.061* -1000**	**0.9990**	**3.18**	**0.977 -500**	**0.9994**	**0.70**
D-Ser	**0.244* -1000**	**0.9987**	**-**	**1.953 -1000**	**0.9999**	**-**
L-Ser	**0.031* -1000**	**0.9991**	**2.37**	**31.25 -1000**	**0.9956**	**-**
D-Met	**1.953 -1000**	**0.9988**	**-**	**0.488 -1000**	**0.9999**	**-**
L-Met	**0.977 -1000**	**0.9992**	**2.56**	**0.244 -1000**	**0.9996**	**1.06**
D-Asn	**0.061* -1000**	**0.9973**	**9.93**	**0.244 -1000**	**0.9999**	**-**
L-Asn	**0.031* -1000**	**0.9983**	**3.43**	**0.244 -1000**	**0.9999**	**1.02**
DL-Phe	**0.061 -1000**	**0.9978**	**3.41**	**0.061 -1000**	**0.9995**	**1.13**

RSD of analytes that were <LLOQ in the investigated serum were not listed. * At least two additional calibration points were included at the lower end of the GC×GC calibration curve compared to the GC–qMS calibration curve[174].

Repeatability. Octaplicate analysis of a serum specimen yielded relative standard deviations (RSDs) below 5% except for D-Ala (12.2%), D-Asp (16.6%), and D-Asn (9.9%), whereas hexaplicate 1D-GC–qMS analysis yielded in general RSDs < 4%[174] that are shown in Table 5. The SDs of octaplicate serum analysis by GC×GC were significantly different (P-Value <0.05) based on the result of the F-Test when compared to the replicate serum analysis (N=6) by GC-qMS for D-Ala, Gly, L-Val, L-Ile, L-Pro, L-Asp, L-Met, L-Asn and DL-Phe.

Method comparison. For evaluation of method accuracy, 48 urine and 43 serum specimens were analyzed by both GC×GC-TOFMS and the 1D-GC-qMS method that had been validated by comparison to an established non-chiral GC-qMS method for quantitative AA analysis. Determined D+L amounts of free AAs had been compared by averaged recoveries.

Table 6. Comparison of quantitative AAE data obtained by the chiral GC–qMS method and the GC×GC–TOFMS method. Mean recoveries, mean deviations, and Pearson correlation coefficients (r) were listed for all analytes whose urine and serum concentrations, respectively, fell within the linear ranges of both methods for N≥20 specimens.

	Urine				Serum			
AA	N	Mean Recovery (%)	Mean deviation (%)	r	N	Mean Recovery (%)	Mean deviation (%)	r
D-Ala	48	93.9	-3.8	0.9892	43	90.3	-12.0	0.9752
L-Ala	48	101.3	1.8	0.9935	43	104.4	4.2	0.9067
Gly	47	101.9	1.1	0.9983	41	104.8	4.5	0.9964
D-Val	<20	-	-	-	<20	-	-	-
L-Val	48	105.6	5.6	0.9937	43	111.1	10.6	0.9159
D-Leu	47	78.4	-17.6	0.9704	<20	-	-	-
L-Ile	48	114.5	18.5	0.9955	43	129.4	25.4	0.9909
D-Pro	25	116.4	22.1	0.8186	34	91.3	-11.2	0.9873
L-Pro	48	101.7	5.9	0.9931	42	114.8	12.6	0.9571
D-Thr	-*	-*	-*	-*	<20	-	-	-
L-Thr	48	93.3	-21.1	0.9823	43	72.2	-44.1	0.3691
D-Asp	45	81.6	-21.4	0.9185	<20	-	-	-
L-Asp	45	84.2	-10.6	0.9888	43	115.6	15.0	0.9938
D-Ser	48	89.8	-5.2	0.9773	-*	-*	-*	-*
L-Ser	34	81.5	-8.8	0.9911	42	74.7	-29.1	0.8725
D-Met	<20	-	-	-	<20	-	-	-
L-Met	44	111.9	0.2	0.9125	42	101.2	0.2	0.9697
D-Asn	48	85.8	-10.3	0.9881	-*	-*	-*	-*
L-Asn	48	100.9	4.9	0.9990	43	103.1	3.4	0.9841
Phe	48	105.1	8.0	0.9978	43	103.3	2.9	0.9665

*Analyte was affected by matrix overlaps that impeded accurate quantification.

Here, mean recoveries were calculated using the data generated by chiral 1D-GC-qMS as reference. Mean recoveries, mean deviations as results of the Bland-Altman plots, and Pearson correlation coefficients are shown in Table 6. Only analytes detected in N ≥20 urine and serum specimens, respectively, were evaluated. Mean recoveries between 80% and 120% and absolute values of mean deviations below 15% were defined as quality criteria for the accuracy. These criteria were fulfilled for both enantiomers of Ala, Ser, and Asn, as well as for Gly, L-Val, L-Pro, L-Asp, L-Met, and D+L-Phe in the analysis of urine. Urinary concentrations of D-Val and D-Met were below the LLOQ for either method in most of the investigated specimens. GC×GC-TOFMS yielded slightly higher (mean deviation of 18.5%) urinary L-Ile concentrations. Nevertheless, both mean recovery (114.5%) and the correlation coefficient (R = 0.996) between the methods were excellent. Compared to 1D-GC–qMS, GC×GC-TOFMS gave slightly lower urinary concentrations for L-Thr and D-Asp with mean deviations of -21.1% and -21.4%, respectively, whereas mean recoveries were 93.3% and 81.6%. Note that superior concordance was observed for L-Met (mean deviation of 0.2%) despite a low correlation coefficient of 0.913.

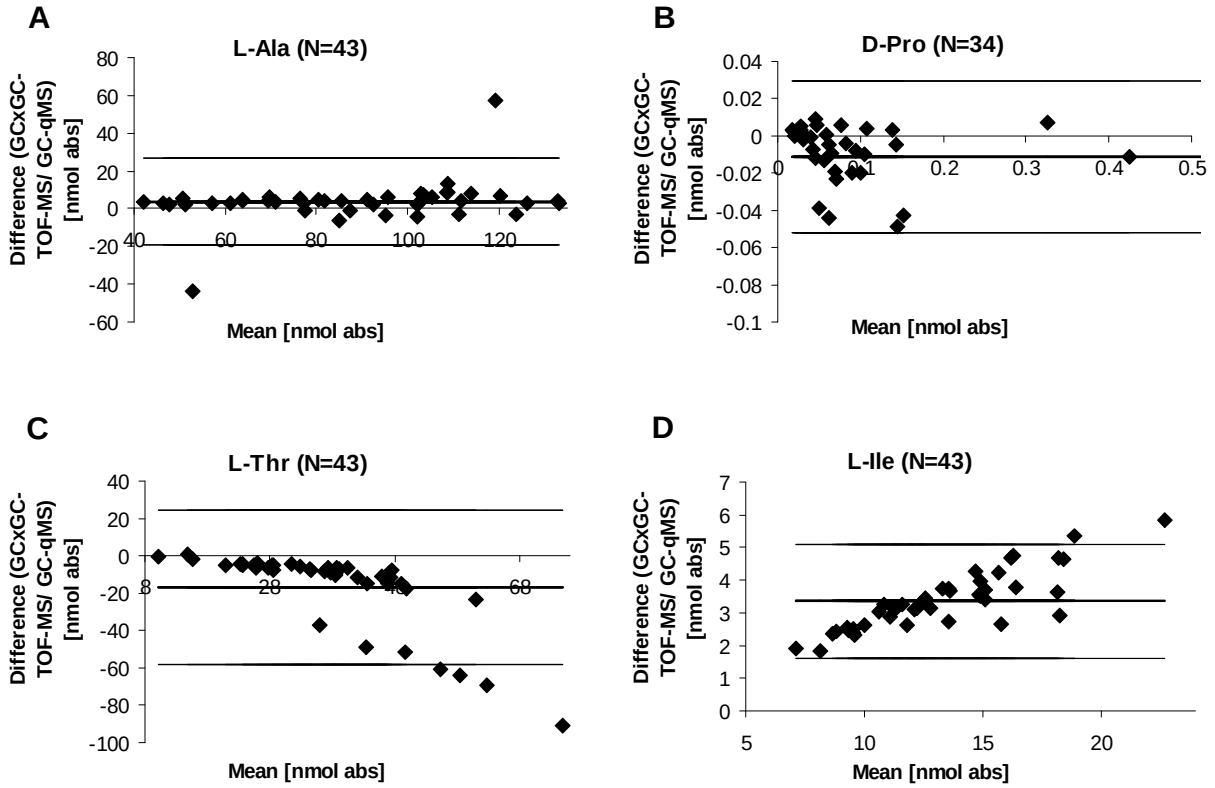

Figure 19. Bland–Altman plots for the analysis of (A) L-Ala and (B) D-Pro in serum show good agreement between GC–qMS and GC×GC, while the Bland–Altman plots for (C) L-Thr and (D) L-Ile show proportional error in agreement between the two methods[174].

For D-Thr, a method comparison was not possible, because a highly abundant urinary matrix compound had interfered with its 1D-GC-qMS analysis. The low values of concordance observed for D-Leu, D-Pro, and D-Asp resulted from urinary levels close to the respective LLOQs of either method, and in the case of D-Pro and D-Asp due to insufficient LLOQs for the GC-qMS method. Similar results were obtained for the analysis of serum. Accuracy was high for both enantiomers of Ala and Pro, and for Gly, L-Val, L-Asp, L-Met, L-Asn, and D+L-Phe. In Figure 19 A and B, Bland-Altman plots demonstrate good agreement between GC-qMS and GC×GC-TOFMS for the serum levels of L-Ala and D-Pro. Serum levels of D-Val, D-Leu, D-Thr, D-Asp, and D-Met in most of the analyzed specimens were below LLOQ for either method. Again a slight overestimation of L-Ile (129.4%) by GC×GC-TOFMS was observed. Bland-Altman plots of L-Thr and L-Ile serum analysis displayed in Figure 19 C and D picture exemplary low concordances with the reference GC-qMS method. The plots show a proportional error and in case of L-Ile also a systematic error and can be classified as Bland-Altman plot types E and D, respectively, as recently defined by Kaspar et al.[196]. Type D describes increasingly positive differences at high concentrations whereas type E describes increasingly negative differences. Apparently lower L-Thr amounts determined by GC×GC-TOFMS result from L-Thr overquantification by GC-qMS analysis that was affected by a coeluting serum compound, which appeared at elevated levels in serum specimens of one patient and resulted in the 7 outliers visible in Figure 19 C. Systematically lower L-Ser concentrations were found by GC×GC–TOFMS for concentrations below 330 µM for both urine and serum, whereas concentrations above 330 µM determined in urine were systematically increased. A flat calibration curve of the GC-qMS method with a high y-axis interception caused by overlapping D-Met, and a serum matrix peak are responsible for this trend. The GC×GC approach provides more reliable L-Thr and L-Ser results as matrix compounds were separated from targets in the second-dimension. However, their accuracy could not be ascertained because of the lack of both a validated reference method and a certified standard for Ser and Thr enantiomers. Furthermore, a serum matrix peak interfered with the quantification of D-Ser using both 1D and 2D GC. Finally, a coeluting serum matrix compound impeded GC-qMS analysis of D-Asn, but the adequately resolved GC×GC peak and accurate urine analysis indicate accuracy of D-Asn serum analysis[174].

7.3.4 Application to Serum Specimens from Patients with Liver Cirrhosis

An exemplary application of GC×GC-TOFMS to diagnostics was performed by analyzing serum specimens from N= 16 healthy probands and N= 25 patients with liver cirrhosis. The clear trend of increased serum levels of D-AAs in liver cirrhosis patients is visible in Figure 20.

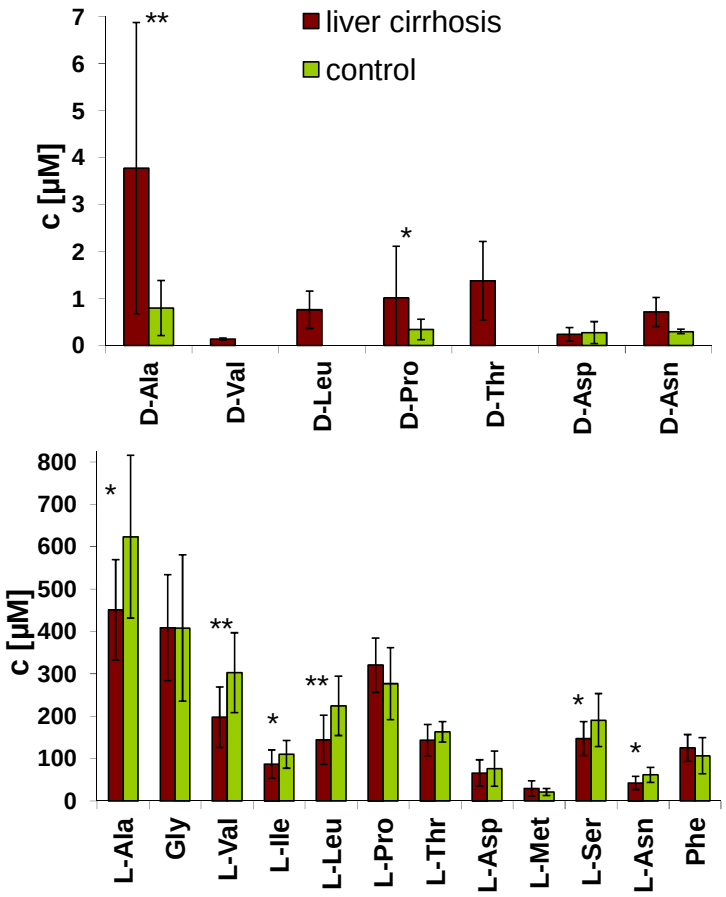

Figure 20. Mean concentrations of AAEs in serum specimens of patients suffering from liver cirrhosis and of healthy probands. 0.001 <*P-value < 0.05, **P-value< 0.001.

Only D-Asp concentrations were not increased when compared to the respective mean concentration of the control group. D-Val, D-Leu, and D-Thr were found above the LLOQ only in some of the serum specimens of cirrhosis patients. D-Ile and D-Met were detected in none of the samples, and D-Ser could not be measured because of the interference by a unknown serum matrix component as mentioned above. The null hypothesis comprising that the data are normally distributed, could not be rejected according to the p-values (>0.05) resulting from the Shapiro-Wilk test. Compared to the controls, significantly elevated serum concentrations of D-Pro (P = 0.013) and D-Ala (P = 0.00008) were observed as determined by a two-tailed

student's t-test. Mean D-Asn concentrations were not tested because of an insufficient number (N = 2) of values above LLOQ in the control group. Determined concentrations of D-Ala, D-Pro and D-Asn + D-Asp in control sera were in good agreement with respective serum levels reported previously for healthy volunteers[48] [199]. L-AA serum levels were significantly decreased in liver cirrhosis specimens as shown in Figure 20: L-Ala (P = 0.0051), L-Ile (P = 0.036), L-Ser (P = 0.0099), L-Asn (P = 0.0011), L-Val (P = 0.00028), and L-Leu (P = 0.0003). The increased D-AA serum levels observed for liver cirrhosis reflect the loss of intact liver parenchyma and, hence, a reduced enzymatic capacity to catalyze D-AA decomposition[174].

7.3.5 Comparison of Enantioselective GC×GC-TOFMS with GC-qMS

The quantification parameters determined for GC×GC-TOFMS and GC-qMS are shown in Table 5. Linear ranges, square values of the sample correlation coefficient R^2, and RSDs for replicate AAE analysis of a serum sample (N = 8) were compared. LODs are not given, because the IS mix contained up to 2% unlabeled AAs that appeared as blank values in the chromatograms as reported in chapter 6. Since blank values affect LODs, this parameter was not considered for method comparison. GC×GC-TOFMS yielded distinctly lower LLOQs for Gly, L-Val, and both enantiomers of Thr, Asp, Ser, and Asn. Chromatographic band focusing in the thermal modulator and fast second-dimension separation yield narrow peaks and, thus, enhance detection sensitivity[194]. Analytes eluting late from the chiral column showed an improved LLOQ in GC×GC-TOFMS, because column bleed in contrast to GC-qMS was separated from all analytes in the second-dimension. Linearity of calibration curves was good for both methods. Peak resolution was improved by coupling two columns with orthogonal separation characteristics. All target analytes were resolved adequately from matrix peaks except for D-Ser in serum, whereas D-Asn and both enantiomers of Thr and Ser were disturbed by matrix compounds in GC-qMS analysis. Separation of D-Met/L-Ser and L-Thr/L-Asp, respectively, which had coeluted from the chiral column, was accomplished with the GC×GC approach. Separation of D-Ile/L-Leu was possible but required decreased operation temperatures for both columns and, as a consequence, increased analysis time from 44 to 66 minutes. Analysis time of 2D data took also longer. Automatic peak

assignment by comparison of found mass spectra with given standard spectra was sometimes incorrect, such as for D-Val and Gly that dissociated into similar ions and featured almost identical first-dimension retention times. Another problem resulted from the slightly earlier elution of ISs compared to the respective analytes as shown in Figure 21. Since the base fraction peak of the labeled AA appeared one modulation before the analyte maximum, the analyte-to-standard area ratio was different for each fraction. Thus, peaks from all modulations had to be integrated to determine the response.

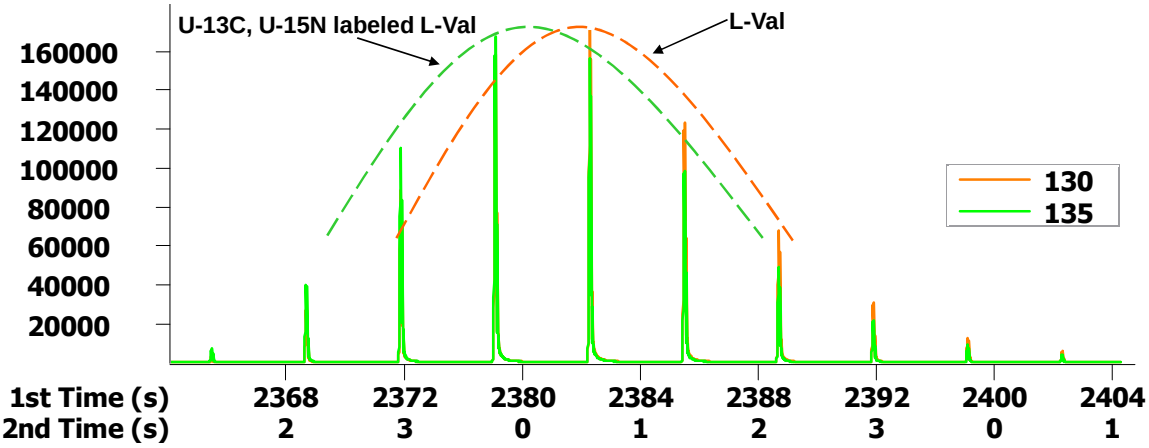

Figure 21. Extracted ion chromatogram of L-Val quantification masses. Peak envelopes (dashed lines) of L-Val and U-13C, U-15N labeled L-Val are indicated to demonstrate their position shift and the varying analyte-to-internal standard area ratio for each fraction[174].

As the software mostly integrated the major analyte fractions, the remaining fractions had to be integrated manually and summed up, leading to a significant increase in data analysis time, as highly abundant L-AAs and ISs may yield ten and more modulations (visible in Figure 21). These problems reflect the complexity of GC×GC-TOFMS data handling, because more parameters including a mass spectral match factor need to be considered in combining all modulated peaks. Due to the impact of noise, low abundant modulated peaks suffer from an insufficient spectral match and, therefore, are not integrated automatically. Reproducible manual inclusion of a great number of sub-fraction integrals is a challenging task and contributes to higher RSDs for GC×GC-TOFMS quantitative data as compared to the excellent repeatability of chiral GC-qMS analysis (RSDs < 4%). In this study, a large sample volume (150 µL) was derivatized and extracted and splitless injection was used to increase intentionally peak intensities in an effort to facilitate detection of D-AAs. As a

consequence, we observed broad peaks, peak tailing, and in turn a great number of modulations for L-AAs and stable isotope-labeled ISs. Optimally, each first-dimension peak should be sampled three to five times, which was the case for D-AAs. The correction of the area integral of a D-AA with a stable isotope-labeled L-AA that generates ten or more modulations is not optimal and, consequently, lowers repeatability of D-AA quantification results as reflected in comparatively great RSDs for D-Asp (16.6%), D-Ala (12.2%), and D-Asn (9.9%), whereas RSDs for the other target analytes were <5%. Comparable peak tailing was observed for L-AAs and ISs, whereas it was barely visible for D-AAs. This also indicates that correction of area integrals of D-AAs by labeled L-AAs is unfavorable as the differences in concentration may be as great as three orders of magnitude. A set of stable isotope labeled D-AAs for D-AA area integral correction would probably improve precision of quantification results, but is not available at present.

The same number of proteinogenic AA types eluted from the Rt-γ-DEXsa column in GC×GC analysis as in GC–qMS analysis. Reasons for the failure to detect the proteinogenic AAs Glu, Gln, Cys, Lys, His, Arg, Tyr, and Trp remain to be elucidated, but may be due to chemical or thermal derivative instability as reported for propyl chloroformate derivatized Arg [180], or strong interactions with the CD core leading to strong retardation and broad peaks that vanish into the baseline. Anyway, the presented GC×GC approach bears the potential to be expanded to enantiomers of other small organic acids due to higher peak capacity compared to 1D GC separation. Enantiomers of lactic acid and 3-methyl-2-oxo-valeric acid were found to be perfectly resolved in the chromatogram of a serum sample (data not shown). They were identified by searching for equal mass spectra and their comparison to fragmentation spectra of analyzed standards[174]. There were found even more peak pairs with identical mass spectra in serum but their structural identity was not clarified. Even though GC×GC offered better sensitivity and resolution of AAEs, I decided to apply GC-qMS for the first chiral fingerprinting approach because high repeatability of responses is inevitable for a good group separation.

7.3.6 Comparison of Chiral GC×GC–TOFMS to Published Methods

In chapter 6.3.4 there was discussed the superior performance of the chiral GC-qMS method over other published methods for the quantitative analysis of AAEs in physiological fluids. No other 1D GC method had been reported to quantify more than 5 D-AAs in serum and urine without pre-separation of AAs from biological matrix compounds[174]. To date, Barbaro et al. had presented the most effective quantitative 1D-LC method that allowed the baseline resolution of 16 pairs of proteinogenic AAEs in 35 minutes; however, accurate quantification could be realized for only 12 D-AAs in lake water samples. The applicability of this highly sensitive LC-MS/MS method to more complex biological matrices like mammalian physiological fluids was not demonstrated[120]. Nagata et al. had demonstrated the applicability of their LC method to plasma samples. The method was able to baseline separate 12 pairs of AAEs, however, due to poor sensitivity (LODs ranged from 4 to 10 µM), only 3 D-AAs were detected in blood plasma[83]. Two-dimensional HPLC performed by Hamase et al. yielded comparable LLOQs to GC-qMS and GC×GC-TOFMS analysis, namely 0.25 µM for all investigated AAEs, comprising branched aliphatic AAs. The method enabled direct quantification of 4 D-AAs in physiological fluids [51]. Consequently, the optimized GC×GC-TOFMS method presented here for the determination of AAEs in physiological fluids is at present to the best of my knowledge the most effective technique for AAE analysis of mammalian physiological fluids, enabling quantification of eight D-AAs in serum or urine in a single chromatographic run[174].

8 CHIRALOMICS: ADDING A NEW DIMENSION TO METABOLOMICS

8.1 INTRODUCTION

Metabolic fingerprinting aims at the detection of metabolite patterns in tissues or biofluids that distinguish two or more experimental groups. The ideal fingerprinting method should be capable of detecting and resolving the constituents of metabolomes in their entirety. However, due to the great chemical variety between metabolite classes, the structural similarity within metabolite classes and the broad range of metabolite abundance, no analytical method has succeeded in attaining this objective to date.

Among the most powerful tools in metabolomics are GC-MS based techniques[1, 200]. Thus far, however, untargeted GC-MS methods treat enantiomers as single features despite the fact that stereoisomers of chiral metabolites do not only differ in abundance, as shown in the preceding chapters for AAEs, but also possess different biological functions[51, 116, 158, 174, 201]. That makes the separation of stereoisomers a necessity in the correct interpretation of abundance changes of chiral metabolites. Chirality is not a rare phenomenon in the metabolome, as all sugars, most AAs and related amines, many organic acids and some lipids feature one or more asymmetrical C atoms.

The progression and physiological effects of NAFLD were investigated intensively in the last decade[186, 187]. NAFLD can progress from steatosis to NASH (non-alcoholic steatohepatitis), fibrosis, cirrhosis and, ultimately, liver cancer. The noninvasive distinction of the early stages of NAFLD by both imaging and molecular means remains challenging and definite diagnosis requires liver biopsy and histopathological examination. To learn more about metabolic changes and, in particular, those affecting chiral metabolites that potentially distinguish steatosis from NASH, I applied chiral fingerprinting using enantioselective GC-qMS to detect MeOH/MCF derivatized features in urine specimens of mouse models mimicking both diseases, followed by GC-APCI-TOFMS for the assignment of significant features to known metabolites.

8.2 Material and Methods

8.2.1 Mouse Models and analyzed Samples

Urine specimens were obtained from 3 groups of female C57BL/6 mice (N=6 each) that had been fed one of three diets, respectively, for 14 weeks starting in week 13: The standard diet #V1534-0 of Ssniff (ssniff R/M-H), a hepatic steatosis inducing high-fat diet (similar composition as the Ssniff standard diet, but containing 30% fat), and a NASH initiating western-type diet (containing 16.1 % (w/w %) protein, 38 % fat, 0.2 % cholesterol, 30.9 % sugar, 5.5 % starch, 3.3 % ash, and 2.7 % fibre). Urine specimens were stored at -20℃.

8.2.2 Sample Preparation

Urine volumes of 50-100 µL were derivatized depending on the volume available. Urine available in excess of 100 µL for four and two mice on standard and high-fat diet, respectively, were combined to yield a total volume of 475 µL of a urine pool. Samples were prepared with the optimized protocol including the dilution of the sample together with 20 µL of IS mix C, applying pure water, to a constant start volume of 275 µL and the successive addition of 167 µL MeOH, 34 µL pyridine, two portions of 20 µL MCF and 300 µL of chloroform as extracting agent. After the addition of each MCF portion the reaction mixture was vortexed. MeOH/MCF derivatives were extracted into chloroform by vortexing the extraction mixture for 15 s. Subsequently the extraction mixtures were centrifuged at 4165 x g for 5 minutes at 5℃ to improve phase separation and about 100 µL of the lower phase (organic phase) were transferred to an insert. Samples were randomized for sample preparation and sample analysis.

8.2.3 Analysis of Samples

Derivatized and randomized samples were analyzed by three different GC-MS devices, namely the GC-qMS that was applied for fingerprinting analysis in scan mode, the GC-qMS used for quantitative AAE analysis in SIM mode and the GC-APCI-TOFMS to enable identification of unknown features. The Rt-γDexsa column, was employed, respectively. Between fingerprint analyses by GC-qMS and GC-APCI-TOFMS, respectively, chloroform blanks were run to avoid baseline

disturbances by late eluting compounds. In addition, an MM II aliquot was analyzed before and after the analysis of mouse urine by GC-APCI-TOFMS to check if the M+H ions of AAEs were the most abundant ions in respective mass spectra as their formation strongly depended on moisture in and around the ion source[149]. As the $M+H^+$ *m/z* was the most abundant *m/z* for AAEs, injection of water into the ion source was omitted. Finally, creatinine contents of the 18 urine samples, were quantified by Dr. Wentao Zhu using LC-ESI-MS/MS as described previously[175].

8.2.4 Data Analysis

The whole data analysis procedure, including the identification of significantly differentiating features, is visualized in Figure 22.

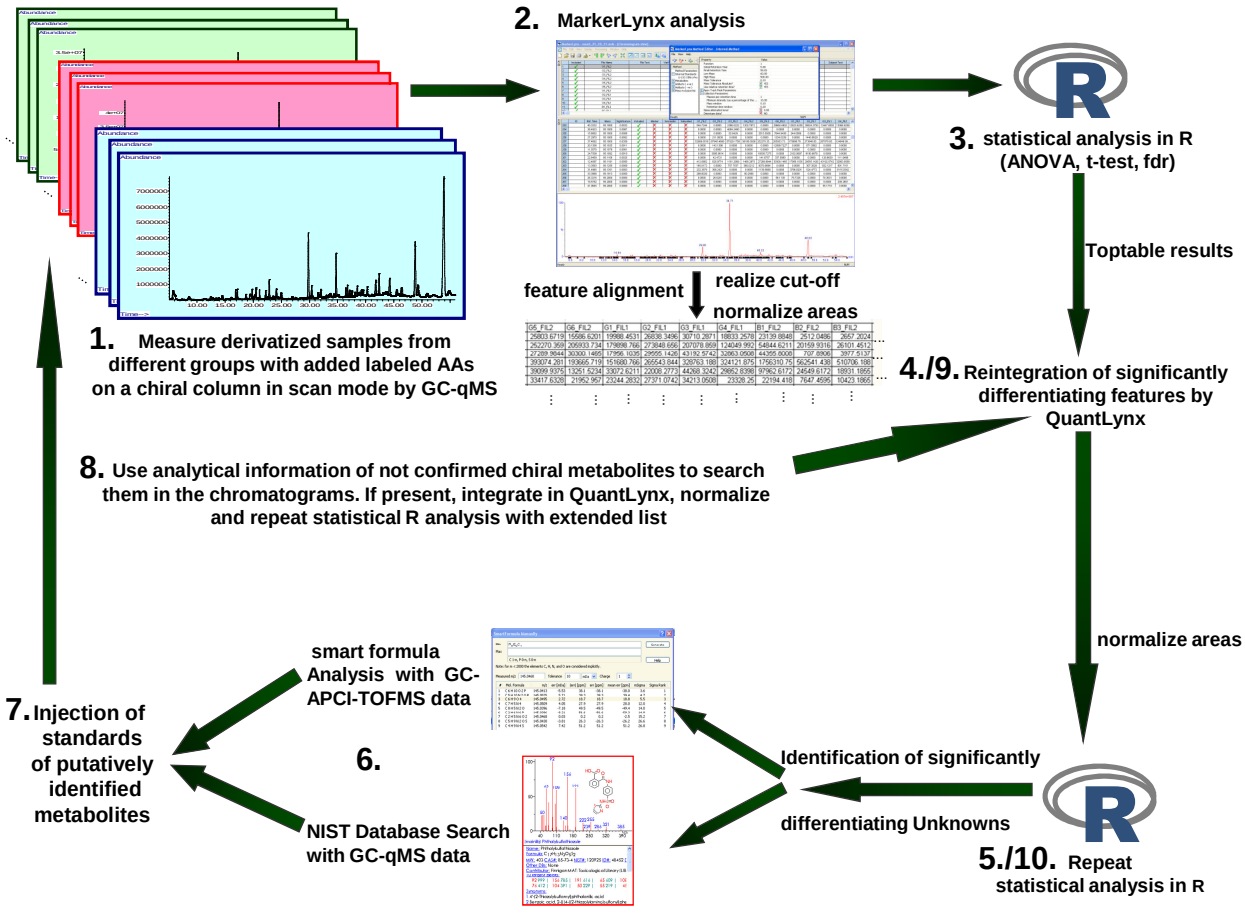

Figure 22. Scheme of the pipeline implemented for the identification of significantly differentiating metabolites in enantioselective fingerprints.

Fingerprinting data resulting from the measurement of 18 urine samples from three groups (steatosis, NASH and controls; N=6 per group) by chiral GC-qMS (see 1.,

Figure 22) were subjected to MarkerLynx analysis. MarkerLynx performed peak picking and assigned a unique retention time and a single *m/z*-value to each picked feature and integrated it. Furthermore, the software performed data alignment (see 2., Figure 22). Exclusively, features detected in at least four out of 18 samples were applied for data analysis with the additionally prerequisite that the feature was found in at least three samples of one of the groups. This filter refers to the detection of a feature in at least half of the group members in contrast to its failed detection in another group, which I considered to indicate a tentative biomarker. Furthermore, the cut-off four out of 18 possible counts was chosen in order to fulfill the criterion for imputation of missing values for PCA by 'R'. The used 'R' algorithme was able to impute at maximum 80% of missing values. Additionally, saturated signals were excluded. Peak areas were normalized to the area of the internal standard (U-13C-15N-L-Pro, *m/z*=133), the used sample volume and the urinary creatinine concentration. The resulting feature list was subjected to statistical analysis in 'R' (see 3., Figure 22). Features that yielded a FDR <0.05 for ANOVA and at least one of the three comparisons: steatosis *vs*. controls, NASH *vs.* controls, and NASH *vs.* steatosis and those that were found at least in three samples of one group but were missing in another group were considered to be significantly discriminating. These features were reintegrated together with the IS in QuantLynx (see 4., Figure 22), except for double feature. Double features belong to the same metabolite and were accidently appointed by MarkerLynx. The double feature with the lower abundant ion was excluded from further analysis. Additionally, all picked AAEs were reintegrated for method validation. For some AAEs, the picked *m/z*-values belonged to the coeluting labeled AAE. These AAEs were reintegrated on the corresponding fragment of the unlabeled AAE. All reintegrated peak areas of peaks with a S/N >8 were normalized by IS area, used sample volume and creatinine content and subjected to R for statistical reanalysis (see 5., Figure 22). Significantly differentiating features were assigned on the basis of the same criteria as listed above for preliminary statistical results.

8.2.5 Identification Strategies

The sixth step in data analysis as depicted in Figure 22 was the identification of significantly differentiating features. For this purpose, a Visual Basic script was used

to recalibrate the *m/z*-values obtained by GC-APCI-TOFMS analysis employing the known *m/z*-values of eight U-13-C,15-N labeled AAs. After recalibration, the *m/z* shift was <5 mDa. Due to the presence of retention time shifts between the chromatograms recorded by GC-qMS and GC-APCI-TOFMS, the linear function of retention times of the uniformly 13-C and 15-N labeled AAs was used to find the respective peak in the GC-APCI-TOFMS chromatogram. The 'smart formula' option of the Bruker software was applied to $M+H^+$ ion (refers to the most abundant *m/z*) to assign tentative sum formula. Sum formulas that fulfilled the criteria of *m/z* bias <5 mDa and mSigma value <50 in case of separated peaks and <100 in case of overlapping and low abundant peaks (S/N <50), which accounts for a good match of theoretical and detected isotope pattern, were further considered for identification. Metabolites that corresponded to the obtained sum formulas after deletion of the proton and possible derivatization groups were searched in the Pubchem compound database and in the Human Metabolome Database (HMDB). The MeOH/MCF derivatization modifies carboxylic acids, amino groups and partly hydroxy groups. Thus, a sum formula was mostly assigned to more than one metabolite since different chemical groups and different isomers can be assumed. A further indication for the actual structure was obtained by NIST database search based on the spectrum recorded by qMS in scan mode. Finally, tentative identifications were confirmed by analysis of corresponding standards (see 7., Figure 22). Relative retention times, normalized to the retention time of the IS and the mass spectrum were compared. I focused primarily on the identification of small organic acids (e.g. TCA cycle metabolites), non-proteinogenic AAs and AA derivatives, with a special emphasis on chiral candidates. When the injection of a racemate confirmed the identification of one antipode and the other was also found with a S/N>8 above the cut-off in the chromatograms of the urine specimens, the peaks were integrated in QuantLynx, normalized and added to the list of reintegrated features. When the confirmation of chiral metabolites failed after standard injection, the gained information on retention times and mass spectrum was used to search the enantiomers in the chromatograms (see 8., Figure 22). Peaks passing the cut-off were integrated by QuantLynx, normalized and added to the list of reintegrated features (see 9., Figure 22). This should avoid that low abundant stereoisomers that were not picked sufficiently or that were integrated incorrectly remain undiscovered.

8.2.6 Treatment of Lactones, Hydroxy Acids, Diacids and allo*-Ile*

Furthermore, area integrals of two derivatives or a derivative and its lactone, originating from the same hydroxy acid, respectively, were summed up, normalized and added to the list of reintegrated features. D-*allo*-Ile, which had been identified as one of the differentiating features, was initially integrated on *m/z*=88. This *m/z* was present in the mass spectrum of *allo*-Ile. However, the ratio of *m/z*=88 to the more characteristic fragment with *m/z*=144 (molecule minus ester moiety) was not constant in the urine specimens, indicating a coeluting compound. Therefore, D-*allo*-Ile was additionally reintegrated on *m/z*=144, which was the highest *m/z* in its spectrum. Finally, I searched in the chromatograms for saturated medium-chain dicarboxylic acids, as their urinary levels have been reported to be highly elevated in disordered fatty acid (FA) metabolism[202, 203]. If characteristic fragments were found in the qMS data, the M+H mass was found with a Δm< 5mDa in the microTOF data and identified peaks were present above the cut-off, the respective standards were injected. Confirmed diacids were integrated, normalized and added to the extended list of features. This final enlarged list of (re)integrated features was subjected to repeated statistical reanalysis in R (see 10. Figure 22).

8.2.7 PCA Analysis

For principal component analysis (PCA), missing values were imputed with the help of the R package “missMDA”. PCA was performed in R with normalized, log2 transformed areas of all significantly differentiating features after univariate statistical analysis of the final extended feature list. Double features were excluded. In case of two- and three-fold derivatized malic acid only the summed areas were used as it was done for 2-HG lactone and 2-HG three-fold derivative.

8.2.8 Method validation

Quantitative AAE analysis of mouse urine was performed in the way it was described in chapter 5.3.1 and 5.4 in order to compare quantitative with semi-quantitative AAE results for method validation.

From the 475 µL of prepared urine pool six 75-µL aliquots were derivatized according to the same procedure as applied to the urine samples, to assess repeatability of the

fingerprinting method. Eight chosen peaks of the pool measures were integrated in QuantLynx on the *m/z* picked by MarkerLynx. Additionally the IS (U-13C-15-N labeled L-Pro) was integrated in the same way and RSDs of response values were calculated.

8.3 Results and Discussions

8.3.1 Data Analysis and Zero Values

Automatic peak picking in the total ion chromatograms acquired for the 18 investigated urine specimens yielded 1077 features. However, 31.3 %, 23.3 % and 10.9% of the features were picked in only one, two or three chromatograms, respectively. Nevertheless, plotting mean areas, in group and count sorted boxplots, of all features that were picked at least three times in a group, showed that peak picking and automatic integration by MarkerLynx were not arbitrary as the minimum value, the first quartile and the median decreased continuously with decreasing counts, indicating that the likelihood of being picked decreased as a function of signal intensity (see Figure 23). Implementing the cut-off of four out of 18 possible values with at least three in one group, 258 features remained. Following exclusion of four saturated, albeit redundant signals, 254 features remained for statistical analysis. FDRs <0.05 for ANOVA and at least one of the three group comparisons were obtained for 22 features, while 85 features were deemed significantly differentiating as they had no values in one group and ≥ three values in another group and the overall count number was ≥ four. Thus, as a result of the third step of data analysis (Figure 22) 107 features were considered to differentiate the groups. After the exclusion of seven ‘double features’ 100 differentiating features were reintegrated. Additionally seven AAEs that were not found to differentiate the groups, however, that were present above the count cut-off were reintegrated for method validation and to provide closer insights into AAE trends in steatosis and NASH.

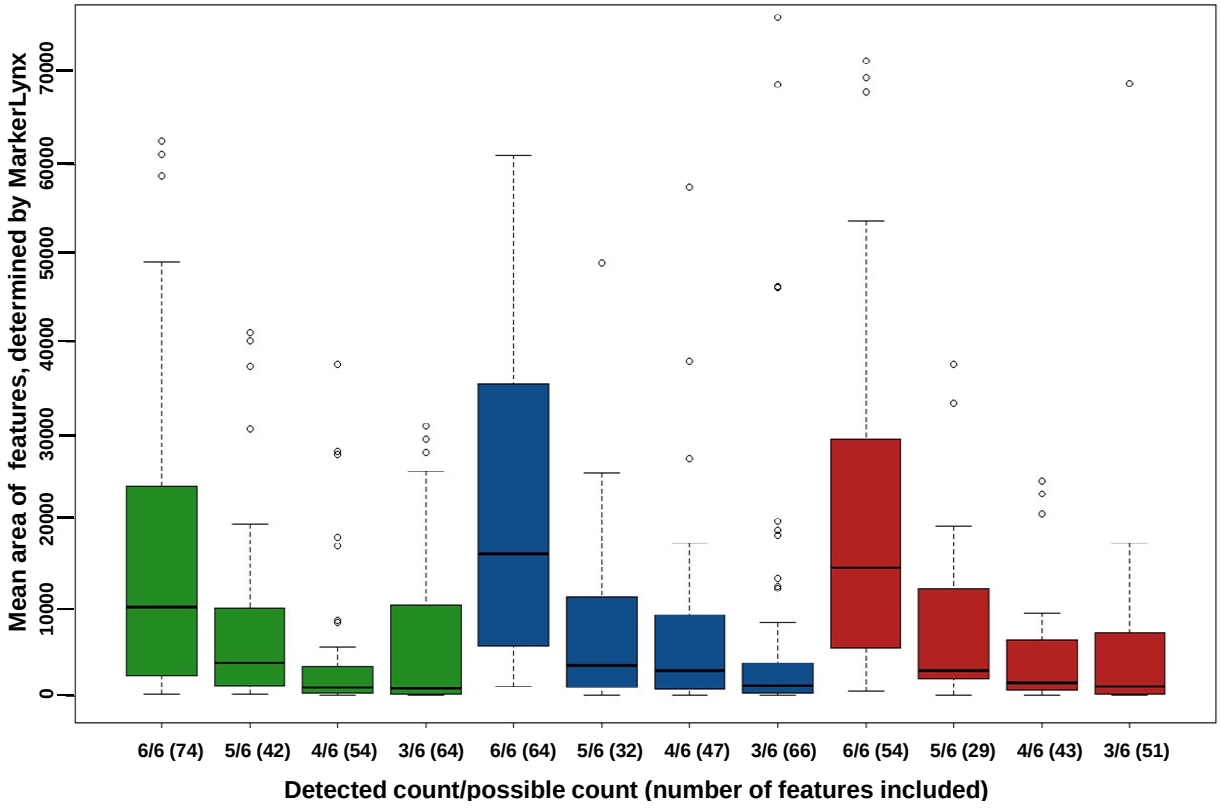

Figure 23. Group and group count sorted boxplots of mean areas of features that were picked and integrated by MarkerLynx above the cut-off for controls (green), steatosis (blue) and NASH (red). Not all outliers were displayed as the shown range of mean areas was restricted to the range of boxplots, to make trends of quartiles visible. The number of features included in each boxplot was given in brackets.

In Figure 23 the outliers and the increased third quartiles and maximum values of the 'three counts boxplot' of the control and the NASH group indicated inaccurately picked and/or integrated features and were the reason why manual reintegration was sought. Reintegration clearly reduced the number of zero values from 975 to 233 corresponding to 50.6% and 12.1% zero value percentages, respectively, of 1926 possible values for 107 reanalyzed features. Consequently, the resulting matrix provided more testable features for statistical analysis. 96 features were considered as significantly discriminating features after reintegration either due to FDR<0.05 for ANOVA and at least one of the three group comparisons (85 features) or because ≥three values were present in one group in contrast to zero values in another group (eleven features) being the result of the fifth step of data analysis of Figure 22. Thus, from 107 reintegrated features eleven were not considered to significantly discriminate the groups. Four of these eleven features belong to AAEs that were not significantly discriminating already after initial statistical analysis. Consequently

seven initially discriminating features were excluded following reintegration. Three AAEs that had been picked on the *m/z* of their labeled counterpart were finally shown to significantly differentiate the groups, owing to reintegration on the respective unlabeled *m/z*. After addition of eleven additional features of interest to the list (summed areas of metabolites yielding 2 derivatization products, low abundant stereoisomers, lactones and medium-chain diacids) and repeated statistical reanalysis (10. in Figure 22), 106 features were finally considered as significantly differentiating features: 92 according to the FDR<0.05 obtained for ANOVA and at least one the three group comparisons and 14 features because they were missing in one group while ≥three values were detected in another group or in case of the D-malic acid derivatives because of one count in the steatosis group and six counts in the control group which I also considered a tentative biomarker. Only one of the additional features of interest, namely L-*threo*-isocitric acid γ-lactone, did not discriminate the groups significantly.

8.3.2 Group Separation and Significant Differences

One characteristic fingerprint each is displayed in Figure 24 for control, steatosis and NASH, respectively. The shown chromatograms correspond to the analysis of 100 µL of derivatized urine and the displayed abundance range was adjusted to the creatinine content found in the samples. It is obvious, that the intensity of many peaks was decreased in steatosis and NASH as compared to the control group. Identified metabolites, confirmed by the injection of standards, with a S/N>8 are labeled in the chromatogram of the steatosis group.

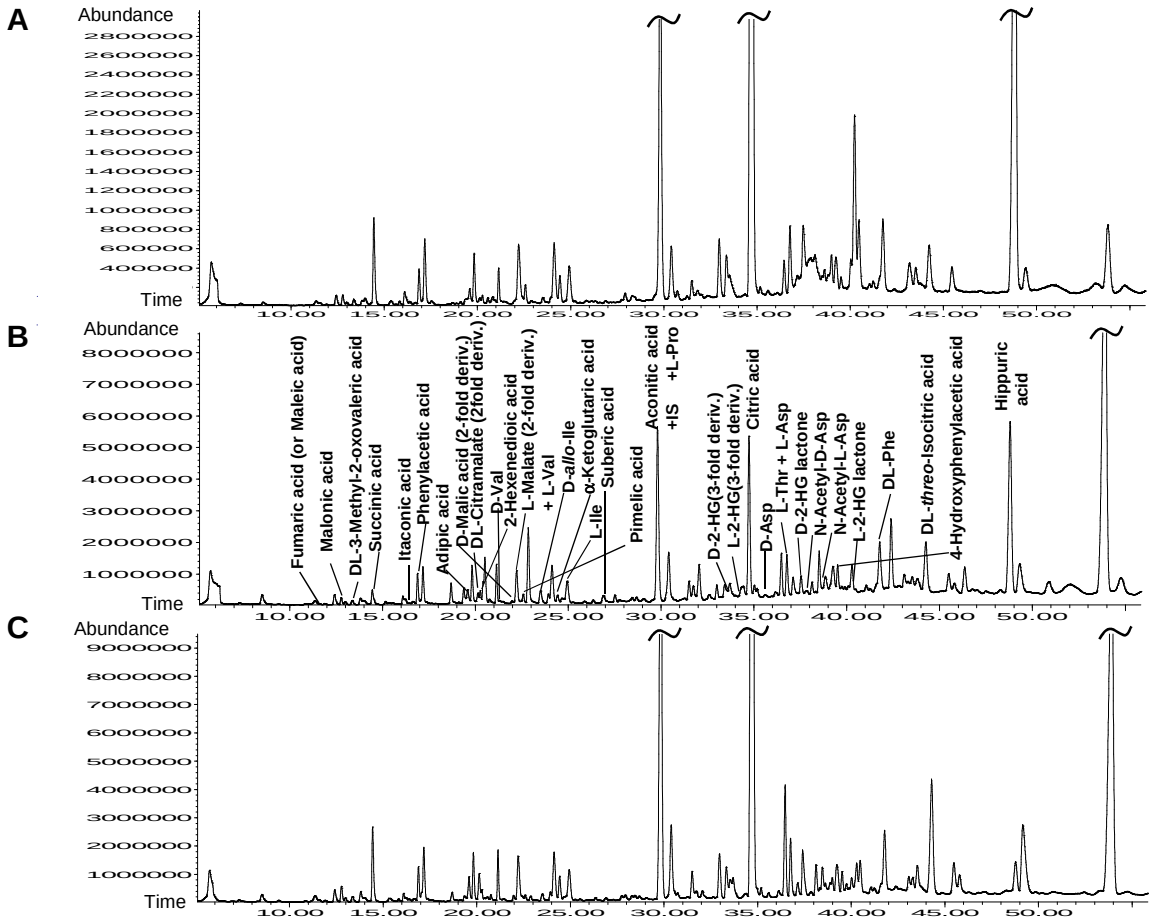

Figure 24. Characteristic GC-qMS TIC chromatograms obtained by derivatization of 100 µL each of representative urine samples from the (A) control, (B) steatosis and (C) NASH group, respectively. Intensity ranges that were displayed were adjusted to the creatinine content in the respective urine specimen. The IS and identified metabolites with a S/N>8 in the chromatogram of the steatosis group were labeled.

Of the 92 features that significantly differentiating the groups according to statistical analysis, 81 yielded a FDR <0.05 for the comparison steatosis vs. controls. Normalized area integrals of 72 from the 92 features were decreased (fold changes(fcs)<1) for the steatosis group when compared to controls. For the NASH vs. controls comparison, 69 of the 92 features yielded a FDR <0.05. Again, the majority of mean area integrals namely 74 of 92 features were decreased in the NASH group according to the fcs. Sixty-one features significantly differentiated both the steatosis and the NASH group from controls. Finally, the NASH vs. steatosis comparison revealed 35 features with FDRs<0.05. Normalized peak areas in the NASH group were mostly decreased when compared to those of the steatosis group. Table 7 lists fcs and FDRs of metabolites that were confirmed by standard injection. Table S2 lists fcs and FDRs of all feature that differentiated the groups and that were

subjected to sf analysis. Table S3 lists fc and FDRs of additionally identified metabolites of particular interest. A clear group separation as a result of PCA of significantly differentiating features is visible in Figure 25.

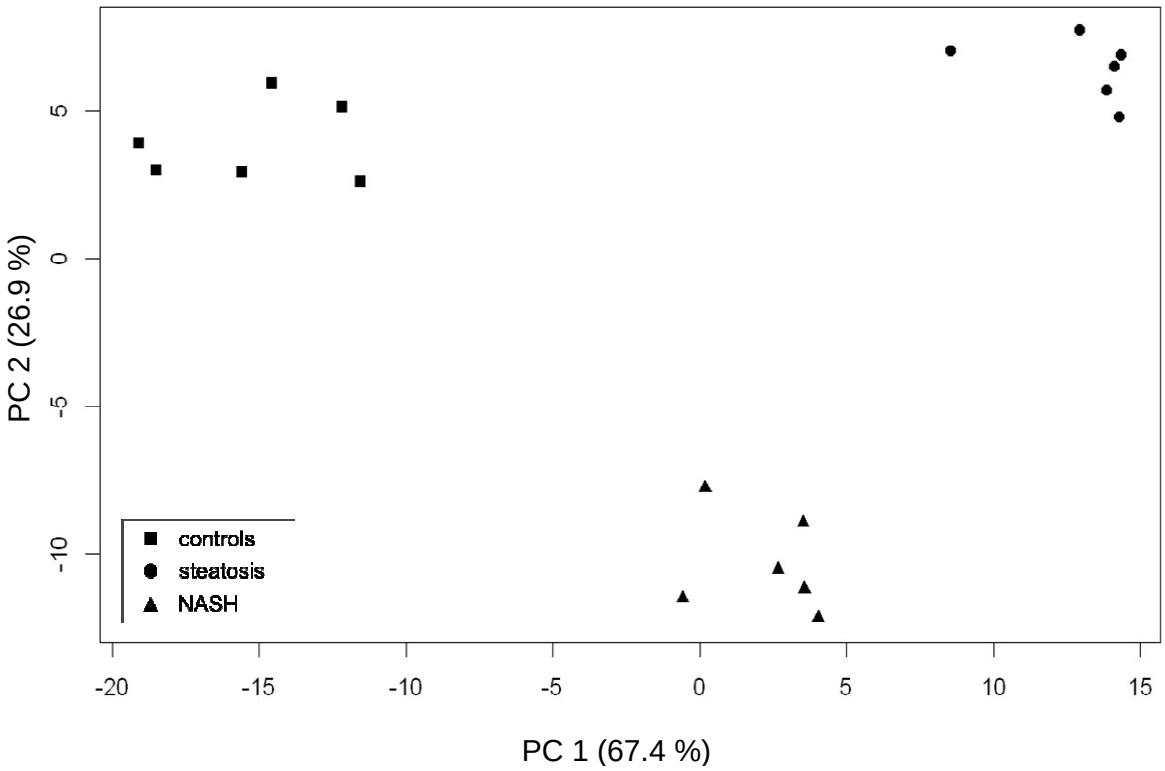

Figure 25. PCA based on log2 transformed normalized areas of all integrated features that differentiated significantly the groups, based on univariate statistical analysis. In case of two- and three-fold derivatized malate only the summed area values were used as it was done for 2-HG lactone and three-fold derivative. Missing values were estimated with the R package “missMDA”. The variance explained by PC 1 and PC 2, respectively, is given in brackets.

The three groups formed tight clusters and were separated along PC 1, which accounted for 67.4% of the total variance. The NASH group was further separated from the steatosis and the control group along PC 2, which accounted for 26.9% of the total variance. Combined, PC1 and PC2 accounted for 94.3% of the total variance.

Table 7. Standard confirmed differentiating metabolites, their retention times, integrated *m/z*, FDRs and fold changes (fc). For analytes with less than three quantifiable values (S/N>8) in at least one group the counts of compared groups were noted in brackets. The number of functional groups derivatized in metabolites that carry hydroxy groups was noted in brackets next to the metabolite name.

					steatosis / controls		NASH / controls		NASH / steatosis	
Nr	identified metabolite	identified by	ret.t [min]	m/z	fc (counts)	FDR	fc (counts)	FDR	fc (counts)	FDR
2	Fumarate(or Maleic acid)	NIST; sf; std	11.55	113	0.04	2.94E-02	0.13	3.21E-02	3.45	>0.05
4	Malonic acid	NIST; sf; std	12.77	101	0.55	2.97E-06	0.67	1.41E-04	1.21	>0.05
5	DL-3-Methyl-2-oxovaleric acid	std	13.36	85	0.92	>0.05	0.66	8.05E-03	0.71	>0.05
7	Succinic acid	NIST; sf; std	14.44	115	0.14	1.62E-06	0.41	1.62E-04	2.93	4.63E-02
11	Itaconic acid	NIST; sf; std	16.37	127	0.16 (1/ 6)	1.69E-02	0.33 (6/ 6)	2.60E-03	2.12 (6/ 1)	>0.05
14	Phenylacetic acid	NIST; sf; std	16.88	91	1.72	8.54E-04	0.80	>0.05	0.46	2.56E-04
20	Adipic acid	std	19.59	114	0.52	1.67E-02	0.74	>0.05	1.43	>0.05
22	DL-Citramalate(2-fold)	NIST; sf; std	20.13	117	1.38	1.24E-02	1.92	1.84E-05	1.39	3.93E-03
23	trans-2-Hexenedioic acid	NIST; sf; std	20.25	74	10.52	1.59E-07	1.52	>0.05	0.14	2.27E-07
26	D-Val	std	21.29	130	1.15	>0.05	0.31	9.78E-03	0.27	6.04E-03
28	L-Val	std	22.21	130	0.56	3.07E-05	0.66	7.09E-04	1.18	>0.05
-	L-Malate (2-fold)	NIST; sf; std	22.26	71	0.04	1.06E-02	0.11	2.01E-02	2.87	>0.05
30	Pimelic acid	NIST; sf; std	22.57	125	0.44	9.82E-06	0.16	5.85E-07	0.38	1.45E-02
33	D-*allo*-Ile	sf; std	23.53	144	0.86	>0.05	0.22	1.78E-03	0.26	1.42E-02
34	α-Ketoglutaric acid	NIST; sf; std	24.42	115	0.05	2.67E-03	0.16	8.05E-03	3.25	>0.05
35	L-Ile	std	24.93	144	0.49	1.45E-04	0.63	3.48E-03	1.29	>0.05
39	N-Acetyl-L-Ala	std	26.58	86	0.21 (1/ 4)	n. av.	n. av. (0/ 4)	n. av.	n. av. (0/ 1)	n. av.
40	Suberic acid	std	26.87	129	1.40	>0.05	0.63	>0.05	0.45	3.47E-02
41	N-Acetyl-D-Ala	std	27.06	86	0.28 (4/ 5)	n. av.	n. av. (0/ 5)	n. av.	n. av. (0/ 4)	n. av.
48	cis (/trans) -Aconitate	NIST; sf; std	29.80	153	0.33	9.82E-06	0.57	1.19E-03	1.75	>0.05
49	L-Pro	std	29.86	128	0.63	8.01E-05	0.76	4.87E-03	1.22	>0.05
59	Citric acid (3-fold)	NIST; sf; std	34.73	175	0.05	1.12E-06	0.33	8.97E-05	6.67	>0.05
61	D-Asp	std	35.59	160	0.45	9.45E-03	0.48	2.88E-02	1.08	>0.05
64	L-Thr	std	36.76	147	1.23	>0.05	1.57	2.18E-03	1.27	>0.05
65	L-Asp	std	36.77	160	0.52	1.83E-04	0.57	8.53E-04	1.09	>0.05
-	D-2-HG-γ-lactone	sf; std	37.47	85	0.22	1.61E-05	0.57	4.31E-03	2.61	3.09E-02
67	N-Acetyl-D-Asp	NIST; std	37.85	102	0.18	8.40E-06	0.25	5.06E-05	1.34	>0.05
69	N-Acetyl-L-Asp	NIST; sf; std	38.62	102	0.10	5.00E-06	0.25	7.79E-05	2.39	>0.05
75	4-Hydroxyphenylacetate(1-fold)	NIST; sf, std	39.50	107	2.89	7.10E-05	1.83	3.38E-02	0.63	2.15E-02
-	L-2-HG-γ-lactone	std	40.33	85	0.08	5.42E-04	0.31	6.55E-03	3.93	>0.05
85	DL-Phe	std	41.77	162	0.69	1.38E-03	0.69	2.30E-03	1.01	>0.05
89	DL-*threo*-Isocitrate(4-fold)	sf; std	44.25	129	0.88	>0.05	1.46	8.20E-03	1.66	4.09E-03
94	Hippuric acid	NIST; sf; std	48.81	77	0.21	7.89E-08	0.02	1.46E-08	0.11	4.63E-02
97	D-Malate (2-fold+3-fold)	std + std	22.00; 29.30	103; 75	0.06 (1/ 6)	>0.05	0.12 (4/ 6)	>0.05	1.93 (4/ 1)	>0.05
98	L-Malate (2-fold+3-fold)	NIST; sf; std + std	22.20; 30.73	103; 75	0.09	4.78E-03	0.22	1.41E-02	2.30	>0.05
99	D-2-HG (3-fold+lactone)	std + std	33.52; 37.47	71; 85	0.21	1.27E-05	0.56	3.48E-03	2.62	2.92E-02
100	L-2-HG (3-fold+lactone)	std + std	34.24; 40.34	71; 85	0.10	6.07E-04	0.33	7.27E-03	3.22	>0.05

n. av. refers to not available for the calculation of fcs due to <three quantifiable values in one of the compared groups. The R 'limma' package can determine adjusted p-values (FDRs) if ≥ one value was available as it estimates a SD from the SDs of the other features.

The loadings plot of the PCA with numbered significantly differentiating features is shown in the appendix (Figure S3; corresponding discriminating features are listed with respective numbers in Table 7, Table S1, Table S2 and Table S3). Thus, stereoselective fingerprints of mouse urine specimens allowed the differentiation of steatosis from NASH in a non-invasive way. This had been also reported by Klein et al., who had observed a less clear but visible separation by ICA of NMR spectra signals[204]. From the identified and standard confirmed enantiomers, all stereoisomers of hydroxy dicarboxylic acids clearly contributed to the separation along PC 1, while D-Val and D-*allo*-Ile contributed to the separation along PC 2. Isomers of medium chain (C6) unsaturated dicarboxylic acids and hippuric acid contributed to the separation along both PC 1 and PC 2.

8.3.3 Identification Results

From 96 features that were considered to be significantly differentiating after reintegration and statistical reanalysis (5. in Figure 22) seven were proteinogenic AAEs and another feature represented D+L-Phe. Retention times and mass spectra of proteinogenic AAEs were known from the quantitative GC-qMS method. The remaining 88 discriminating peaks, recorded by GC-APCI-TOFMS, were subjected to sf analysis (see sf results in Table S1). This proved to be an effective tool for metabolite identification in complex biological matrices[148]. For 77, a sum formula was obtained that could be assigned to one or more metabolites found in mammals or bacteria after deletion of the proton and possible derivatization groups. For the remaining eleven features the respective peaks were low abundant in the chromatograms recorded by APCI-TOFMS and obtained formula did not fit with molecules that were known as endogenous metabolites of mammals or bacteria. The different abundances of some features after APCI-TOFMS analysis when compared to EI-qMS analysis can be explained by different ionization efficiency in APCI which depends on metabolite structure. Another three features were finally assessed as ‘double features’ following their identification by standard injection (see Table S1). For 39 of the 74 remaining elemental formulas a stereoisomeric metabolite could fit (namely enantiomers, diastereomers, cis/trans-isomers). For 25 of these stereoisomers a standard was commercially available.

Table 8. Mean reintegrated normalized areas, SDs, resolution, elution order and results of racemization checks for standard confirmed chiral metabolites. In case of hydroxy acids the number of derivatized functional groups is given in brackets.

		controls		steatosis		NASH				
chiral metabolite	**config**	**mean**	**SD**	**mean**	**SD**	**mean**	**SD**	**resolution**	**elution order**	**racemization**
3-Methyl-2-oxovalerate	**D+L**	**0.0283**	**0.0052**	**0.0261**	**0.0068**	**0.0187**	**0.0021**	**0.2**	**unk.**	**-**
Citramalic acid (2-fold)	**D+L**	**0.0261**	**0.0018**	**0.0361**	**0.0073**	**0.0502**	**0.0064**	**0.4**	**unk.**	**-**
Citramalic acid (3-fold)	**D**	**n.d.**	**n.d.**	**n.d.**	**n.d.**	**n.d.**	**n.d.**	**3.3**	**unk.**	**-**
	L	**n.d.**	**n.d.**	**n.d.**	**n.d.**	**n.d.**	**n.d.**			
Malic acid (2-fold)	**D**	**0.0091**	**0.0065**	**0.0012**	**0.0005**	**0.0011**	**0.0003**	**1.9**	**D,L**	**n.d.**
	L	**0.1259**	**0.1201**	**0.0050**	**0.0017**	**0.0144**	**0.0044**			
Malic acid (3-fold)	**D**	**0.0041**	**0.0012**	**n.d.**	**n.d.**	**n.d.**	**n.d.**	**10.2**	**D,L**	**n.d.**
	L	**0.0432**	**0.0420**	**0.0010**	**0.0004**	**0.0052**	**0.0023**			
***allo*-Ile**	**D**	**0.0089**	**0.0023**	**0.0077**	**0.0043**	**0.0020**	**0.0009**	**7.1**	**D,L**	**n.d.**
	L	**n.d.**	**n.d.**	**n.d.**	**n.d.**	**n.d.**	**n.d.**			
N-Acetyl-Ala	**D**	**0.0027**	**0.0012**	**0.0008**	**n.d.**	**n.d.**	**n.d.**	**2.7**	**L,D**	**16%** [a]
	L	**0.0042**	**0.0027**	**0.0009**	**0.0002**	**n.d.**	**n.d.**			
2- HG-γ-lactone	**D**	**0.3873**	**0.1213**	**0.0842**	**0.0327**	**0.2195**	**0.0566**	**17.2**	**D,L**	**0.95%** [b]
	L	**0.0388**	**0.0231**	**0.0031**	**0.0011**	**0.0120**	**0.0045**			
2-HG (3-fold)	**D**	**0.0526**	**0.0149**	**0.0107**	**0.0038**	**0.0306**	**0.0077**	**5.9**	**D,L**	**0.38%** [b]
	L	**0.0056**	**0.0028**	**0.0015**	**0.0002**	**0.0027**	**0.0006**			
N-Acetyl-Asp	**D**	**0.0098**	**0.0032**	**0.0018**	**0.0005**	**0.0024**	**0.0006**	**6.7**	**D,L**	**n.d.**
	L	**0.0727**	**0.0257**	**0.0075**	**0.0028**	**0.0179**	**0.0041**			
***threo*-ICA-γ-lactone**	**D**	**n.d.**	**n.d.**	**n.d.**	**n.d.**	**n.d.**	**n.d.**	**2.1**	**L,D**	**n.d.**
	L	**0.1401**	**0.0080**	**0.1714**	**0.0319**	**0.1729**	**0.0582**			
***threo*-ICA (4-fold)**	**(D+)L**	**0.1174**	**0.0219**	**0.1034**	**0.0196**	**0.1715**	**0.0407**	**0.1**	**unk.**	**-**

n.d. refers to 'not detected';

unk. refers to unknown;

[a] the L-enantiomer standard (>99.9%) was derivatized four times and yielded a mean D-enantiomer area ratio (D/(D+L-area)) of 16%;

[b] derivatization of the L-enantiomer standard (enantiomer excess was not determined by the supplier) yielded a D-enantiomer area ratio of 0.95% for the 2-HG lactone peaks and 0.38% for the 2-HG three-fold derivatives ($S/N_{D\text{-}form}$ <8)

After standard injection and the proceedings used for confirmed and rejected stereoisomers (8. in Figure 22) in sum 18 features were found to describe stereoisomers that were no proteinogenic AAEs. These features corresponded to 3 cis/trans isomers and 12 chiral metabolites (see Table 7). The discrepancy between the number of features and the respective number of assigned metabolites resulted from the formation of two derivatives or lactones from hydroxy acids by partial derivatization of hydroxy groups or internal esterification. Eight of the 12 chiral metabolites namely two-fold derivatized L-malic acid, D-*allo*-Ile, both enantiomers of N-Acetyl-Asp (NAA) and one-fold derivatized 2-HG-γ-lactone enantiomers as well as unseparated two-fold derivatized DL- citramalate and DL-*threo*-ICA were identified and confirmed due to sf analysis of 88 features. The other four stereoisomers namely D-malic acid (two derivatives), both N-acetyl-Ala enantiomers and DL-3-methyl-2-oxovaleric acid as well as three-fold derivatized L-malic acid were identified due to racemate injection of tentatively identified chiral metabolites. The identity of features that were initially assigned to N-acetyl-Ala enantiomers and DL-3-methyl-2-oxovaleric acid could not be confirmed. Anyway they were present in the chromatograms at other retention times and were added as additional features to the list of reintegrated features for second statistical reanalysis (10., Figure 22). The peak of DL-3-methyl-2-oxovaleric acid had been integrated inaccurately by MarkerLynx and was therefore not under the significantly differentiating features after first statistical analysis and low abundant N-Acetyl-Ala enantiomers had not been picked above the cut-off. This applied also for D-malic acid. Injection of racemic malic acid recovered the appearance of two-fold and three-fold derivatives. Standard injection of racemic *threo*-ICA and 2-HG yielded four peaks, respectively, as lactonization had occurred. Additionally, standards of 2-HG-γ-lactone and *threo*-ICA-γ-lactone enantiomers were injected to confirm lactone identification. Averaged normalized area integrals, standard deviations, elution order, resolution, and the outcome of racemization checks of identified enantiomer pairs other than proteinogenic AAs were summarized in Table 8. Quantitative and semi-quantitative AAE results are visualized in Figure 26. Configuration of two-fold derivatized citramalate and 3-methyl-2-oxovaleric acid could not be specified due to failed enantiomer separation. Injection of MeOH/MCF citramalate racemate showed that the three-fold derivatized stereoisomers were baseline separated, however, they were not detected in urine samples. Albeit *threo*-ICA enantiomers were not separated, the detection of exclusively the L-configured

threo-ICA γ-lactone in urine indicated that the open form occurred mainly in L-configuration as stereo centers were not affected by lactonization that occurred inter alia as an artifact of MCF derivatization. There were two baseline-separated features under the significantly differentiating (see Table S1, feature Nr 72 and 77) with similar mass spectra belonging most probably to two stereoisomers that remained unconfirmed. Eleven non-stereoisomeric organic acids could be confirmed by the injection of standards (Table 7). Two of them were adipic and suberic acid. Their features were not under the significantly regulated features after first statistical analysis but were additionally searched in the chromatograms for the following reason. We found four features that were distinctly elevated in the steatosis group when compared to the other groups that were identified as unsaturated medium-chain dicarboxylic acids (feature Nr. 16, 23, 24, 42 in Table 7, S1 and Table S2). Increased urinary excretion of saturated and unsaturated medium-chain dicarboxylic acids had been reported at enhanced or inhibited fatty acid metabolism[202, 203]. Hence we were interested in the identification and behavior of related saturated diacids. Three of the four mentioned features were identified as hexenedioic acid isomers. However the confirmation of identification and the detection of the position and configuration of the double bond could be accomplished only for the commercially available trans-2-hexenedioic acid. The remaining of the four features was tentatively identified as an isomer of octenedioic acid.

8.3.4 Artifacts of MCF Derivatization

As already mentioned in the preceding section lactonization of hydroxy acids occurred inter alia as an artifact of MCF derivatization. Nevertheless, lactones exist in equilibrium with their open form in aqueous solutions. On which side the equilibrium lies is pH-dependent with the lactone being favored at acidic conditions. Furthermore, the position of the equilibrium highly depends on structural features such as lactone ring size, side groups, etc.[205-208]. An equilibrium between the two forms is reached faster in mammalian organisms with the help of serum paraoxonases. These enzymes can catalyze both the hydrolysis of the cyclic esters and lactonization[208] . However, lactonization was reported previously as an artifact of derivatization at acidic conditions[209, 210]. Area integrals of the open form and the lactone of 2-HG enantiomers were added up, respectively, as they were highly correlated (r= 0.97 for

the D-forms ; r= 0.96 for the L-forms) . It was not clear, if the slightly higher lactone to open form ratios in the samples when compared to respective enantiomer ratios after standard derivatization occurred due to spontaneous lactonization during sample storage or due to endogenous occurrence of lactone enantiomers. In contrast the ratio of L-*threo*-ICA γ-lactone to its open form was distinctly higher in mouse urine than in the chromatograms of *threo*-ICA enantiomer standards. Moreover the L-lactone levels showed no linear correlation to the levels of the corresponding open form in the urine samples (r= -0.1). Consequently L-*threo*-ICA-γ-lactone was treated as an individual feature of interest in statistical analysis (Table S3).

The injection of fumaric acid and trans-aconitic acid resulted in the detection of two peaks with similar mass spectra, which indicated that MCF derivatization had induced the conversion of trans- into cis-isomers and vice versa as similar observations were made after the injection of the respective cis-isomers. The purity of the standard solutions had been checked by non-chiral GC-qMS analysis of the MSTFA silylated standards (data not shown). Because of the different biological functions and sources of the cis- and trans-isomers, the abundance changes of these metabolites were not considered for interpretation. Cis- or trans-aconitic acid coeluted with the IS but its mass spectrum did not interfere with the *m/z*=133 used for area integral correction. There was detected a single peak for trans-2-hexenedioic acid during the analysis of the derivatized standard solution. Thus, MCF derivatization induced cis-trans conversion was most probably structure dependent and did not proceed in the medium-chain diacid. However, the possibility of cis- and trans-isomer coelution could not be excluded in case of 2-hexenedioic acid as the cis-isomer was not commercially available.

A further drawback of MCF derivatization can be concluded from the observation of hydroxy groups being not derivatized in all molecules of malic acid and citramalic acid. In both cases the two-fold derivative with the unmodified hydroxy group was the predominant one and eluted first. There was observed only a minor abundance difference for the two malic acid derivatives (two-fold/(two-fold+three-fold derivative)-ratio=0.56; N=7 standard injections) whereas in case of citramalic acid the two-fold derivative was much more abundant than the three-fold derivative (two-fold/(two-fold+three-fold derivative)-ratio=0.98; N=5 standard injections). Even though mass spectra obtained from the injection of derivatized Ser and Thr standards indicate a

three-fold derivatization, the low abundances of these AAEs after standard derivatization, suggest the existence of the two-fold derivatized forms that, however, were not detected within the used run time. Thus, the incomplete derivatization of hydroxy groups by MCF limited peak intensities. This impeded the detection of biologically low abundant D-malic acid. In case of citrmalic acid it hampered the determination of its predominant configuration in mouse urine.

Finally, racemization of N-acetyl-Ala enantiomers was observed. It was most probably promoted by high temperatures and low pH during derivatization with MCF and MeOH. This phenomenon will be discussed in more detail in the following section. A minor racemization of 2-HG enantiomers could not be excluded (see Table 8).

8.3.5 Method Validation

The pooled urine was applied to investigate the repeatability of the fingerprinting method, including preparation and GC-qMS analysis (N=6) as well as the technical repeatability (N=6) using uniformly 13-C,15-N-labeled L-Pro as IS. This IS was chosen for integral area correction as it eluted approximately after half of the analysis time. A total of eight peaks were chosen to cover a broad scope of *m/z*-values, retention times, and peak intensities. The RSDs (displayed in Figure 27) were always below five percent for the derivatization replicates except for one early and one late eluting metabolite, which were identified as succinic acid (RSD= 9.3) and hippuric acid (RSD= 7.5), respectively. The response of the chosen eight peaks showed RSD below three percent after repeated injection of one derivatized pool aliquot, except for one early eluting compound (RSD=3.3) that remained unidentified. These results attested to the ability of the IS to correct for losses during sample preparation and for fluctuations of injected volume and other technical conditions.

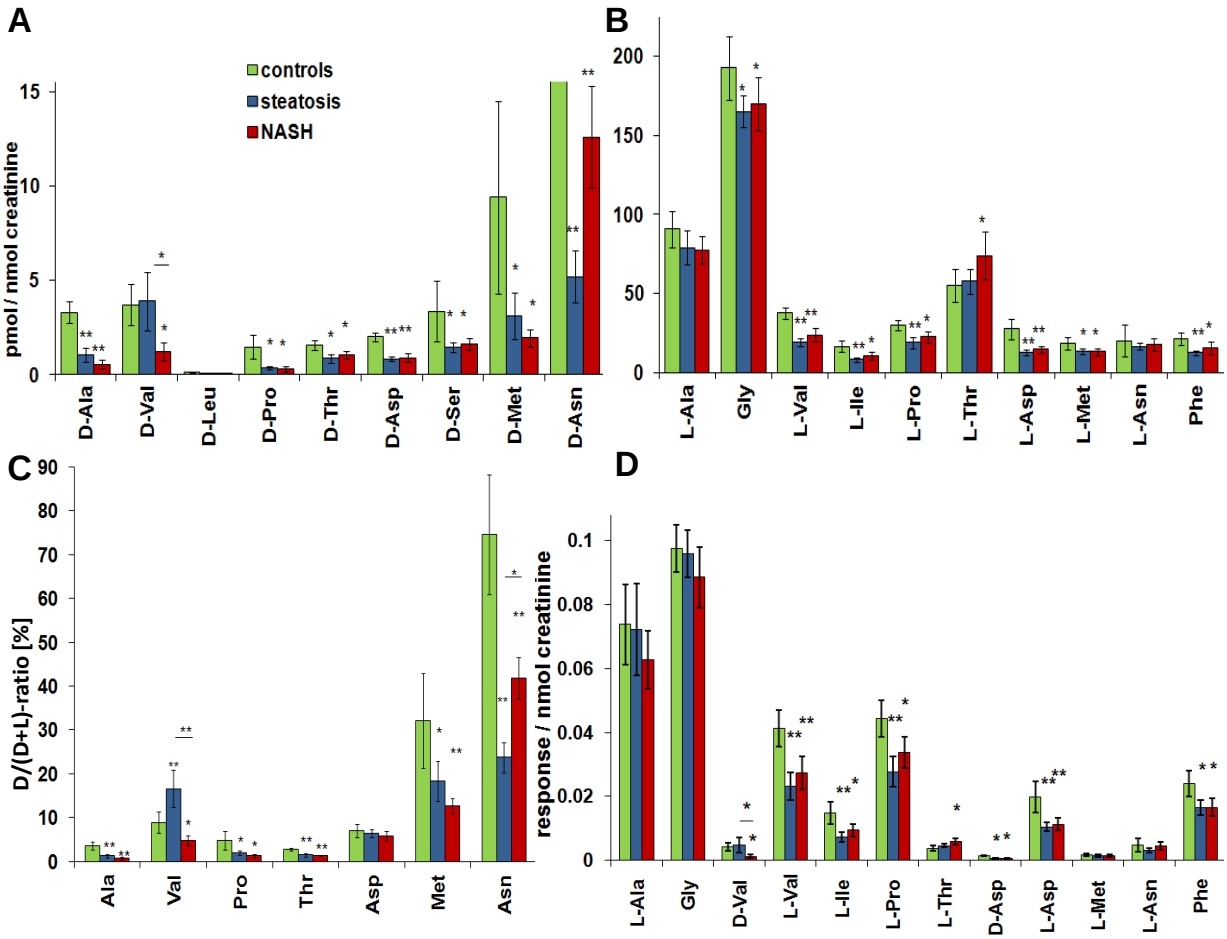

Figure 26. Mean concentrations of (A) D-AAs and (B) L-AAs, relative to creatinine contents, respectively, in the control group (N=5), the steatosis group (N=6), and the NASH group (N=6), determined by the quantitative GC-qMS method of chapter 6. (C) D-AA ratios were calculated from AAE quantities. (D) Shows semi-quantitative results for the three groups (N=6 respectively) of 12 AAE that were picked above the cut-off. They were reintegrated and areas were corrected by isotopically labeled L-Pro. *0.001 <FDR < 0.05, **FDR< 0.001 and FDR_{ANOVA}< 0.05, respectively, for quantitative data and for semi-quantitative data after third statistical analysis.

For identified stereoisomers, pure enantiomer standard solutions were measured to ensure that the appearance of their antipode in urine is of biological nature and not the result of racemization during MCF derivatization. The exact enantiomer excess of the applied L-HG standard has not been determined by the supplier (Sigma). An area percentage of 0.95% and 0.39% were found for the D-enantiomer (relative to the D+L area) of the 2-HG-γ-lactone and the three-fold derivatized open form, respectively.

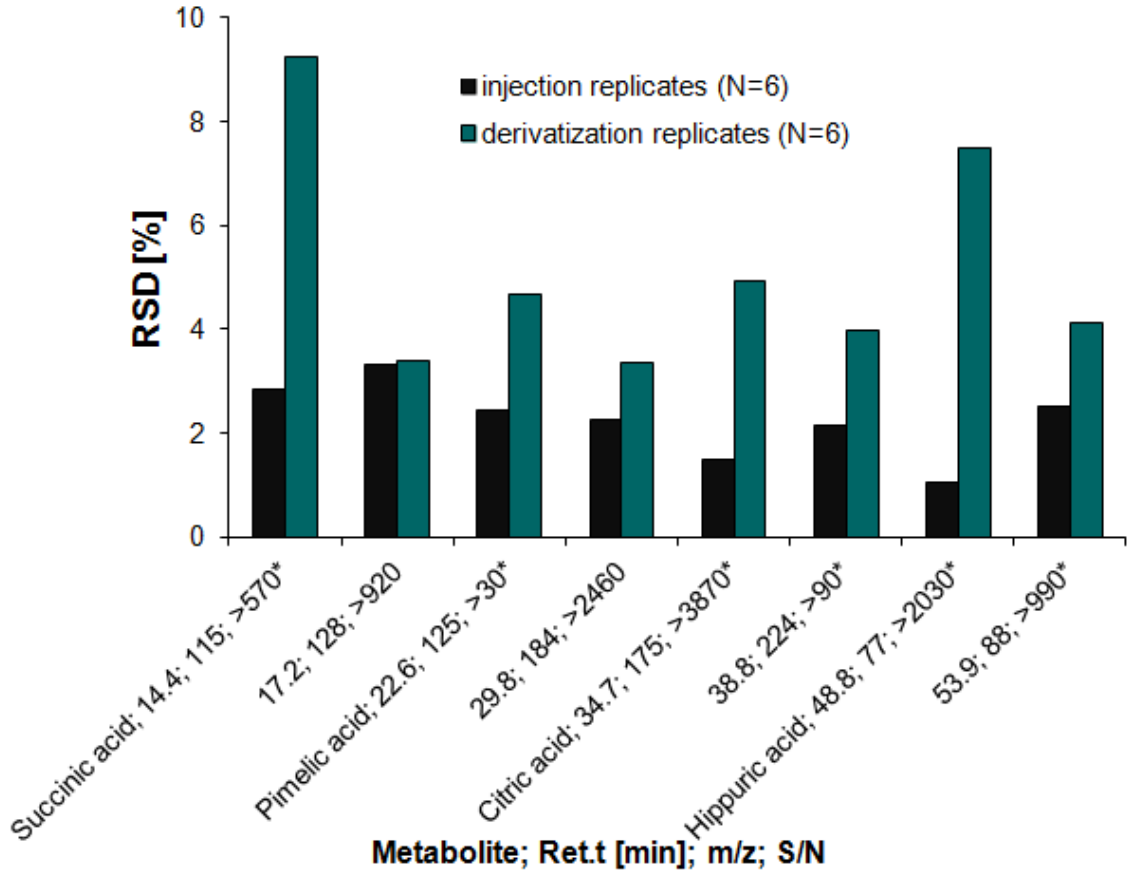

Figure 27. RSDs of response values of 8 peaks in the chromatograms generated by GC-qMS in scan mode of six MeOH/MCF derivatized aliquots of the urine pool. Injection replicates refer to six injections of one MeOH/MCF derivatized aliquot of the urine pool. Identified and standard confirmed metabolites were marked. * peak that significantly differentiated groups**.**

For the open form the signal of the D-enantiomer had a S/N<8 so that the determined area may be inaccurate. The appearance of the D-signals indicated either a slight racemization during derivatization or a minor impurity of the standard. No racemization was detected for the other enantiomers identified except for N-Acetyl-L-Ala. This racemization was most probably catalyzed by pyridine as the mean area percentage of the D-enantiomer decreased from 16% to 0.1% when the pyridine amount was decreased in the reaction mixture from 34 µL to 4 µL (data not shown). However, reducing the applied pyridine amount decreased the derivative yield distinctly. The reduction of reaction yield was dependent on the metabolite structure (data not shown). Finally, the AAE trends between the groups revealed by semi-quantitative chiral GC-qMS analysis were in good agreement with the results obtained by the validated quantitative GC-qMS method for AAE analysis, visualized in Figure 26. MarkerLynx had failed to pick above the cut-off seven of the low

abundant D-AAs as well as L-Ser. The S/N in scan mode was distinctly lower than in the more sensitive selected ion monitoring, performed for quantitative AAE analysis. L-Ser coeluted with D-Met and the software picked an *m/z* of the D-Met spectrum in some chromatograms (below the cut-off) but no *m/z* of the Ser spectrum probably because of the similar retention time. Nevertheless, the fingerprinting method proved suitable for the semi-quantitative analysis of chiral and non-chiral metabolites in urine.

8.3.6 Biological Interpretation

Urinary metabolite profiles represent the summed metabolite trends of all organs and tissues and, therefore, a concrete assignment of observed differences between the groups to changes in specific tissues or pathways is difficult. Moreover, decreased urinary metabolite levels, can either indicate decreased metabolite contents in all tissues or a higher requirement of the metabolite as a substrate of activated pathways and vice versa. Therefore decreased urinary amounts of L-malic acid, citric acid, 2-ketoglutarate (2-KG) and succinic acid in the steatosis group (see Table 7) could indicate the activation of the TCA cycle in tissues which is consistent with the findings of An et al. who observed increased TCA cycle intermediate levels in the liver of obese rats whereas their urinary excretion was decreased[211]. In contrast Thomas et al. observed reduced expression level of three enzymes associated with the TCA cycle at earlier time points of the NASH inducing diet (10-30 days)[212]. Also other pathways can contribute to the reduction of urinary citric acid and 2-KG amounts. 2-KG is a product of AA transamination and L-AA intake was lower with the steatosis and NASH inducing diets than with the standard diet. The distinct decrease in citrate excretion can be further supported by an elevated expression of ATP-citrate lyase (ACL) found in relation to the development of NAFLD. ACL metabolizes citrate to acetyl-CoA and links therewith glucose catabolism with lipogenesis[213]. In the NASH mouse model, fed a high sugar content, the citrate levels were decreased more moderately than in the steatosis group when compared to controls, respectively. This was also observed for the other TCA cycle metabolites and *threo*-ICA was even elevated in the NASH group when compared to controls. This suggests metabolic changes in mitochondria when inflammation progresses, which was supported by the report on mitochondrial abnormality observed in some NASH

patients[214]. The elevated *threo*-ICA amounts could be a protective response on inflammation. Inflammation can inhibit the production of red cells. ICA was shown to reduce chronic inflammation caused anemia by lessening the erythroid iron restriction response[215]. Indeed Thomas et al. found ICA dehydrogenase to be down regulated in the first 30 days of a NASH inducing diet[212]. The lack of a linear relation between L-*threo*-ICA γ-lactone and *threo*-ICA (r= -0.1) responses suggested either a biological source of the lactone, which is independent from the open form, or a concentration dependent lactonization. In contrast baseline separated 2-HG enantiomers showed high linear correlation with the related lactone enantiomers, respectively ($r_{D\text{-}form}$=0.97; $r_{L\text{-}form}$=0.96). This correlation was based on a high, concentration independent and therefore constant, lactonization rate (65 %) during derivatization and either spontaneous lactonization during sample storage or enzyme catalyzed lactonization in mouse organisms. D- and L-2-HG enantiomer (lactone+open form) abundances behaved similar with lower levels in the diseased groups than in controls while their amounts in NASH were respectively higher than in the steatosis group. D-2-HG was the predominant form in mouse urine. It was reported that both D- and L-2-HG can be converted to 2-KG by two different stereo specific enzymes namely D- and L-2-HG dehydrogenase that were found to be active in rat tissues such as liver, kidney, heart and brain[97, 99].The relation of 2-HG enantiomers to 2-KG is visible in comparable trends between the groups. Similar trends were detected also for the baseline separated NAA enantiomers. Many reports on NAA do not account for its chiral character. It was found to serve as an important source for acetate in the brain and the liver, that is required e.g. for lipid synthesis[216]. My data showed reduced urinary excretion of D- and L-NAA, which could indicate a higher requirement of the acetyl moiety of NAA in tissues during NAFLD, and suggests that both enantiomers could serve as acetyl donors. However, a decreased synthesis of NAA enantiomers in NAFLD mice could not be excluded. I found for the low abundant baseline separated D-Malate similar trends than for its antipode. A comparable metabolism for administrated labeled D- and L-Malate in rats was observed already in 1969[96]. For proteinogenic L-AAs that can be catabolized to Krebs cycle intermediates or their precursors, comparable trends were observed as for TCA metabolites with lower amount found in the NAFLD groups than in controls. A study investigating the early development of NASH in mice, revealed moderately elevated expression levels of proteins involved in the degradation of L-AAs[179].The reduced protein ratios in the

here applied steatosis (18.5%) and NASH (16.1%) inducing diets when compared to the standard diet (33%) contributed to reduced L-AA excretion in the NAFLD mice albeit could not explain the increased urinary levels of most detected L-AAs in NASH when compared to steatosis. Reduced urinary D-AA excretion was not a dietary effect as proteins typically do not contain D-AAs. The interpretation of D-AAs trends remains difficult, as their metabolism and functions in mammals are not completely understood. So far two enzymes are known to synthesize D-AAs in mammals namely Ser and Asp racemase and two enzymes were found to catalyze D-AA degradation being D-AA oxidase (DAO) and D-Asp oxidase[52-54, 56, 57]. The findings of elevated gut permeability and prevalent small intestinal bacterial overgrowth (SIBO) in steatosis [189] and a high release of D-AAs by bacteria at stationary phase conditions[18] as well as increased D-AA serum level found in patients with liver cirrhosis (chapter 7.3.4) encourage the expectation of increased urinary D-AA excretion. However, only D-Val levels were slightly albeit not significantly increased in the steatosis group. These observations cannot be explained by changed DAO activity in the liver as contrary to other mammals, mice do not express DAO in the liver. Nevertheless, DAO expression might be regulated in the kidney and the brain of NAFLD mice[52, 53]. Citramalate is a bacterial metabolite and showed significantly elevated levels in steatosis and NASH, probably due to SIBO and changed permeability of the gut[189]. Phenylacetylglycine (PAG), phenylacetic acid and 4-hydroxyphenylacetic acid (4-HPA) are also gut flora related metabolites that were significantly increased in the steatosis *vs.* controls comparison (Table 7, S1 and S2). The most distinct increase was observed for PAG that was also found to be grossly elevated in long term treated obese rats. An et al also found slightly increased 4-HPA levels after 80 days of the steatosis inducing diet[211]. I found phenylacetic acid to be slightly decreased in the NASH *vs*. controls comparison whereas PAG and HPA were significantly increased.

Contrary to reports on elevated urinary excretion of saturated and unsaturated medium-chain dicarboxylic acids at disordered FA metabolism[202, 203] adipic acid amounts were decreased in both diseased groups and suberic acid was only increased in the steatosis group albeit not significantly when compared to controls. Nevertheless, the three features identified as hexenedioic acid isomers were grossly increased in the steatosis *vs*. controls comparison with fc >10.5. They were more moderately increased in the NASH *vs*. controls comparison (fc >1.5, see Table 7, Table S1and Table S2). Therefore, they were distinctly decreased in the NASH mice

when compared to steatosis. Finally an octendioic acid isomer was tentatively identified. It was detected exclusively in urine of all six members of the steatosis group at quantifiable levels. These results can denote a selective activation of FA metabolism. Furthermore, my results did not support the reported supposition that trans-2-Hexenedioic acid originates from dehydrogenation of adipic acid[203, 217]. Most of the here discussed small organic acids and the 2-HG γ-lactone had already been identified previously as urinary metabolites of healthy individuals as methyl ester derivatives after non-chiral GC-MS analysis[218].

8.3.7 Relevance of the Chiral Dimension

The combination of MeOH/MCF derivatization and a γ-cyclodextrin derivative chiral GC column yielded generally excellent enantioselectivity with resolution values between 1.9 and 17.2 for baseline-separated enantiomers. Besides ten proteinogenic AAE pairs, the method allowed the baseline separation of nine identified enantiomer pairs including two- and three-fold derivatized malic acid enantiomers and 2-HG latcone and open form enantiomers (Table 8). An obverse trend was found for D-Val in the steatosis vs control comparison when compared to its antipode L-Val, which underlines the importance of enantiomer resolution. Also D-Thr showed converse trends to its antipode in both diseased groups when compared to controls (see quantitative data in Figure 26). The discriminating *allo*-Ile was further specified as the D-enantiomer whereas the L- *allo*-Ile was not detected in any of the urine specimens. Hamase et al. also found high urinary amounts of D-*allo*-Ile in rats, mice and dogs whereas only traces of L-*allo*-Ile were detected in urine of rats[51]. In sum, 16 separated enantiomers of chiral metabolites, including nine newly identified enantiomers and seven AAEs, significantly discriminated the groups in at least one group comparison. D-Val, D-*allo*-Ile and D-2-HG (lactone+open form) were baseline-separated enantiomers that significantly differentiated NASH from steatosis (FDRs were 5.55E-03, 1.32E-02, and 2.92E-02, respectively), which demonstrated the relevance of the chiral dimension for the classification of NAFLD stages in this murine model. Whether these metabolites are also suited for the differential diagnosis of steatosis and NASH in human patients needs to be evaluated.

9 CONCLUSIONS AND PERSPECTIVES

Quantitative GC-qMS and GC×GC-TOFMS for AAE analysis using MeOH/MCF derivatization and a γ-CD derivative as chiral selector were implemented, optimized, validated and finally applied to mammalian urine, serum and liver. Quantitative AAE analysis by GC-qMS offered superior repeatability, shorter run times and less time-consuming data analysis compared to GC×GC-TOFMS. It allowed accurate quantification of four D-AAs in human control serum, six in mouse serum and eight in human control urine as well as five in mouse liver. GC×GC-TOFMS, on the other hand, showed improved enantiomer resolution and resolution from serum and urine matrix molecules as well as lower LLOQs when compared to the GC-qMS method. The chiral GC×GC method allowed the accurate quantitation of up to seven D-AAs in human urine and serum. Therefore, the application of GC×GC-TOFMS clearly increased the number of quantifiable D-AAs in human serum. However, it slightly decreased the number of quantifiable D-AAs in urine. Therefore, the chiral GC×GC method for AAE analysis is recommended for the analysis of serum whereas the related GC-qMS method for AAEs quantitation is recommended for urinary metabolome analysis due to its superior repeatability as well as faster analysis. Chiral GC-qMS analysis of AAEs in mouse liver revealed distinctly differing concentrations when D-AA levels were compared to L-AA levels. Thus, the GC×GC method will most probably provide more quantifiable AAE peaks due its broader linear ranges compared to GC-qMS. However, AAE analysis of liver tissues by GC×GC was not tested and therefore a definite recommendation is not possible as the disturbance by liver matrix compounds was not assessed for the two-dimensional method. Though chiral GC-qMS enabled the quantification of nine D-AAs in some analyzed human and mouse urine specimens, both methods had insufficiently low LLOQs and a lack of selectivity to allow quantification of all (in respect of the antipode) baseline separated D-AAs in all specimens of interest. Thus, further improvement of LLOQs and selectivity is required to provide more efficient AAE analysis in physiological fluids. This can be achieved by the application of an IS mix that does not impede sensitive AAE analysis by the generation of blank values. Here blank values limited LODs of both methods, LLOQs of both methods for early eluting (high abundant) AAEs and LLOQs of GC×GC analysis for all detected AAEs. Another drawback of the here applied IS mix, gained from algae, was that AA abundance varied widely, with labeled Ser and Met being the least abundant. Since these two amino acids also

yielded low peak abundances after MeOH/MCF derivatization and chiral analysis, dilution of the IS mix was limited by the abundance of these AA types. Therefore, a synthetic equimolar mixture of labeled racemic AAs would help to improve LLOQs and repeatability of the here presented GC-MS based methods. Furthermore, the here established methods were not able to baseline separate all proteinogenic AAEs in a single chromatographic run as Phe enantiomers were not separated by the γ-CD derivative and nine proteinogenic AA types did not elute from the chiral column. However, the final goal of chiral AA analysis in metabolomics is to establish a method that allows the monitoring of all proteinigenic D-AAs in physiological fluids and tissues to investigate their potential as biomarkers efficiently and to learn more about their biological relevance. Therefore, direct or indirect chiral LC-MS approaches, and thereby in particular the application of LC-MS/MS because of its excellent sensitivity[120], should be considered to enlarge the quantifiable analyte spectrum for the analysis of physiological fluids and tissues.

The here presented chiralomics approach demonstrates the relevance of the chiral dimension in the differentiation of experimental groups. Eighteen of the N=106 significantly differentiating features detected could be assigned to stereoisomers in addition to the known AAEs, of which seven and D+L-Phe discriminated the study groups significantly. From the 18, three corresponded to cis/trans isomers and 12 corresponded to enantiomers of small hydroxy diacids, non-proteinogenic AAs and AA derivatives as well as lactones. Principal component analyses separated murine hepatic steatosis from NASH along both PC1 and PC2 (Figure 25). Additionally, both diseased groups were perfectly separated from controls along PC1. The loadings plot (Figure S3) showed that from the identified and standard confirmed enantiomers, all stereoisomers of hydroxy dicarboxylic acids clearly contributed to the separation by PC 1 and D-Val and D-*allo*-Ile contributed to the separation by PC 2. This was reflected by p-values and FDRs obtained from statistical analysis for the steatosis *vs*. NASH comparison. D-Val, D-*allo*-Ile and D-2HG significantly differentiated NASH from steatosis (FDRs were 5.55E-03, 1.32E-02, and 2.92E-02 respectively), which further depicted the relevance of the chiral dimension for the classification of NAFLD stages in mouse models. Next, the application of chiralomics to human urine in the differentiation of NASH from hepatic steatosis needs to be explored in patients, for whom definite diagnosis based on liver biopsies is available. Such an approach will reveal if the aforementioned D-enantiomers are also diagnostic in human.

There were assigned 15 stereoisomers to 18 differentiating feature. This was a consequence of MeOH/MCF derivatization artifacts, specifically the incomplete modification of hydroxy moieties and the promotion of lactonization. Moreover, the highly exothermal reaction with MeOH/MCF, under acidic conditions, promoted racemization of N-Acetyl-Ala enantiomers as well as cis-trans-conversion in case of aconitate and fumaric acid/maleic acid. Thus, alternative, more gentle derivatization protocols or chiral LC- based methods requiring no derivatization at all should be investigated.

10 REFERENCES

1. Dettmer, K.; Aronov, P. A.; Hammock, B. D., Mass spectrometry-based metabolomics. *Mass Spectrom Rev* **2007,** *26* (1), 51-78.

2. Dettmer, K.; Hammock, B. D., Metabolomics-a new exciting field within the" omics" sciences. *Environ Health Perspect* **2004,** *112* (7), A396-A397.

3. Oliver, S. G.; Winson, M. K.; Kell, D. B.; Baganz, F., Systematic functional analysis of the yeast genome. *Trends Biotechnol* **1998,** *16* (9), 373-378.

4. Urbanczyk-Wochniak, E.; Luedemann, A.; Kopka, J.; Selbig, J.; Roessner-Tunali, U.; Willmitzer, L.; Fernie, A. R., Parallel analysis of transcript and metabolic profiles: a new approach in systems biology. *EMBO Rep* **2003,** *4* (10), 989-993.

5. Nicholson, J. K.; Lindon, J. C., Systems biology: metabonomics. *Nature* **2008,** *455* (7216), 1054-1056.

6. Gowda, G. N.; Zhang, S.; Gu, H.; Asiago, V.; Shanaiah, N.; Raftery, D., Metabolomics-based methods for early disease diagnostics. *Expert Rev Mol Diagn* **2008,** *8* (5), 617-633.

7. Nobeli, I.; Ponstingl, H.; Krissinel, E. B.; Thornton, J. M., A structure-based anatomy of the E. coli metabolome. *J Mol Biol* **2003,** *334* (4), 697-719.

8. Aharoni, A.; Ric de Vos, C.; Verhoeven, H. A.; Maliepaard, C. A.; Kruppa, G.; Bino, R.; Goodenowe, D. B., Nontargeted metabolome analysis by use of Fourier transform ion cyclotron mass spectrometry. *OMICS* **2002,** *6* (3), 217-234.

9. Fiehn, O., Metabolomics - the link between genotypes and phenotypes. *Plant Mol Biol* **2002,** *48* (1-2), 155-171.

10. Almstetter, M. F. Tools and Applications for One- and Two-dimensional Gas Chromatography - Time-of-Flight Mass Spectrometry-based Metabolomics. Ph.D. Thesis, University of Regensburg, **2011**.

11. Kaderbhai, N. N.; Broadhurst, D. I.; Ellis, D. I.; Goodacre, R.; Kell, D. B., Functional genomics via metabolic footprinting: monitoring metabolite secretion by Escherichia coli tryptophan metabolism mutants using FT - IR and direct injection electrospray mass spectrometry. *Comp Funct Genomics* **2003,** *4* (4), 376-391.

12. Nagao, R.; Tsutsui, H.; Mochizuki, T.; Takayama, T.; Kuwabara, T.; Min, J. Z.; Inoue, K.; Todoroki, K.; Toyo'oka, T., Novel chiral derivatization reagents possessing a pyridylthiourea structure for enantiospecific determination of amines and carboxylic acids in high-throughput liquid chromatography and electrospray-ionization mass spectrometry for chiral metabolomics identification. *J Chromatogr A* **2013,** *1296*, 111-118.

13. Heil, M.; Podebrad, F.; Beck, T.; Mosandl, A.; Sewell, A. C.; Böhles, H., Enantioselective multidimensional gas chromatography-mass spectrometry in the analysis of urinary organic acids. *J Chromatogr B Biomed Sci Appl* **1998,** *714* (2), 119-126.

14. Oh, S. F.; Pillai, P. S.; Recchiuti, A.; Yang, R.; Serhan, C. N., Pro-resolving actions and stereoselective biosynthesis of 18S E-series resolvins in human leukocytes and murine inflammation. *J Clin Invest* **2011,** *121* (2), 569-581.

15. Pérez-Trujillo, M. R.; Lindon, J. C.; Parella, T.; Keun, H. C.; Nicholson, J. K.; Athersuch, T. J., Chiral metabonomics: 1H NMR-based enantiospecific differentiation of metabolites in human urine via direct cosolvation with β-cyclodextrin. *Anal Chem* **2012,** *84* (6), 2868-2874.

16. Nakanishi, K.; Katagi, M.; Zaitsu, K.; Shima, N.; Kamata, H.; Miki, A.; Kato, H.; Harada, K.-I.; Tsuchihashi, H.; Suzuki, K., Simultaneous enantiomeric determination of MDMA and its phase I and phase II metabolites in urine by liquid chromatography-tandem mass spectrometry with chiral derivatization. *Anal Bioanal Chem* **2012,** *404* (8), 2427-2435.

17. Cava, F.; Lam, H.; de Pedro, M. A.; Waldor, M. K., Emerging knowledge of regulatory roles of D-amino acids in bacteria. *Cell Mol Life Sci* **2011,** *68* (5), 817-831.

18. Lam, H.; Oh, D. C.; Cava, F.; Takacs, C. N.; Clardy, J.; de Pedro, M. A.; Waldor, M. K., D-Amino acids govern stationary phase cell wall remodeling in bacteria. *Science* **2009,** *325* (5947), 1552-1555.

19. Zampolli, M.; Meunier, D.; Sternberg, R.; Raulin, F.; Szopa, C.; Pietrogrande, M. C.; Dondi, F., GC-MS analysis of amino acid enantiomers as their N(O,S)-perfluoroacyl perfluoroalkyl esters: application to space analysis. *Chirality* **2006,** *18* (4), 279-295.

20. Zampolli, M.; Basaglia, G.; Dondi, F.; Sternberg, R.; Szopa, C.; Pietrogrande, M., Gas chromatography–mass spectrometry analysis of amino acid enantiomers as methyl chloroformate derivatives: Application to space analysis. *J Chromatogr A* **2007,** *1150* (1-2), 162-172.

21. Griffin, R.; Moody, H.; Penkman, K.; Collins, M., The application of amino acid racemization in the acid soluble fraction of enamel to the estimation of the age of human teeth. *Forensic Sci Int* **2008,** *175* (1), 11-16.

22. Eliot, A. C.; Kirsch, J. F., Pyridoxal phosphate enzymes: mechanistic, structural, and evolutionary considerations. *Annu Rev Biochem* **2004,** *73* (1), 383-415.

23. Erbe, T. Die Quantifizierung von Aminosäurenisomeren in Lebensmitteln mittels chiraler Gaschromatographie-Massenspektrometrie im Hinblick auf die Relevanz und die Entstehungsmechanismen von D-Aminosäuren. Ph.D. Thesis, University of Gießen, **1999**.

24. Höltje, J.-V., Growth of the stress-bearing and shape-maintaining murein sacculus of Escherichia coli. *Microbiology and Molecular Biology Reviews* **1998,** *62* (1), 181-203.

25. del Pozo, A. M.; Merola, M.; Ueno, H.; Manning, J. M.; Tanizawa, K.; Nishimura, K.; Soda, K.; Ringe, D., Stereospecificity of reactions catalyzed by bacterial D-amino acid transaminase. *J Biol Chem* **1989,** *264* (30), 17784-17789.

26. Bellais, S.; Arthur, M.; Dubost, L.; Hugonnet, J.-E.; Gutmann, L.; Van Heijenoort, J.; Legrand, R.; Brouard, J.-P.; Rice, L.; Mainardi, J.-L., Aslfm, the D-aspartate ligase responsible for the addition of D-aspartic acid onto the peptidoglycan precursor of Enterococcus faecium. *J Biol Chem* **2006,** *281* (17), 11586-11594.

27. Veiga, P.; Piquet, S.; Maisons, A.; Furlan, S.; Courtin, P.; Chapot-Chartier, M.-P.; Kulakauskas, S., Identification of an essential gene responsible for D-Asp incorporation in the Lactococcus lactis peptidoglycan crossbridge. *Mol Microbiol* **2006,** *62* (6), 1713-1724.

28. Pioli, D.; Venables, W.; Franklin, F., D-Alanine dehydrogenase. *Arch Microbiol* **1976,** *110* (2-3), 287-293.

29. Hills, G., Chemical factors in the germination of spore-bearing aerobes. The effects of amino-acids on the germination of Bacillus anthracis, with some observations on the relation of optical form to biological activity. *Biochem J* **1949,** *45* (3), 363-370.

30. Hu, H.; Emerson, J.; Aronson, A. I., Factors involved in the germination and inactivation of Bacillus anthracis spores in murine primary macrophages. *FEMS Microbiol Lett* **2007,** *272* (2), 245-250.

31. O'Connor, K. A.; Zusman, D. R., Starvation-independent sporulation in Myxococcus xanthus involves the pathway for β–lactamase induction and provides a mechanism for competitive cell survival. *Mol Microbiol* **1997,** *24* (4), 839-850.

32. Kolodkin-Gal, I.; Romero, D.; Cao, S.; Clardy, J.; Kolter, R.; Losick, R., D-Amino acids trigger biofilm disassembly. *Science* **2010,** *328* (5978), 627-629.

33. Fujii, N., D-amino acids in living higher organisms. *Origins Life Evol B* **2002,** *32* (2), 103-127.

34. Sasabe, J.; Suzuki, M.; Miyoshi, Y.; Tojo, Y.; Okamura, C.; Ito, S.; Konno, R.; Mita, M.; Hamase, K.; Aiso, S., Ischemic acute kidney injury perturbs homeostasis of serine enantiomers in the body fluid in mice: early detection of renal dysfunction using the ratio of serine enantiomers. *PLoS One* **2014,** *9* (1), e86504.

35. Ketting, D.; Wadman, S. K.; Spaapen, L. J.; Van der Meer, S. B.; Duran, M., Gas chromatography method for the separation of amino acids enantiomers in plasma and urine. Application in a case of short bowel syndrome. *Clin Chim Acta* **1991,** *204* (1-3), 79-86.

36. Bendikov, I.; Nadri, C.; Amar, S.; Panizzutti, R.; De Miranda, J.; Wolosker, H.; Agam, G., A CSF and postmortem brain study of D-serine metabolic parameters in schizophrenia. *Schizophr Res* **2007,** *90* (1), 41-51.

37. Heresco-Levy, U.; Javitt, D. C.; Ebstein, R.; Vass, A.; Lichtenberg, P.; Bar, G.; Catinari, S.; Ermilov, M., D-serine efficacy as add-on pharmacotherapy to risperidone and olanzapine for treatment-refractory schizophrenia. *Biol Psychiatry* **2005,** *57* (6), 577-585.

38. Tsai, G.; Yang, P.; Chung, L.-C.; Lange, N.; Coyle, J. T., D-serine added to antipsychotics for the treatment of schizophrenia. *Biol Psychiatry* **1998,** *44* (11), 1081-1089.

39. Weil, Z. M.; Huang, A. S.; Beigneux, A.; Kim, P. M.; Molliver, M. E.; Blackshaw, S.; Young, S. G.; Nelson, R. J.; Snyder, S. H., Behavioural alterations in male mice lacking the gene for D-aspartate oxidase. *Behav Brain Res* **2006,** *171* (2), 295-302.

40. Pätzold, R.; Schieber, A.; Brückner, H., Gas chromatographic quantification of free D-amino acids in higher vertebrates. *Biomed Chromatogr* **2005,** *19* (6), 466-473.

41. Nagata, Y.; Horiike, K.; Maeda, T., Distribution of free D-serine in vertebrate brains. *Brain Res* **1994,** *634* (2), 291-295.

42. Kartvelishvily, E.; Shleper, M.; Balan, L.; Dumin, E.; Wolosker, H., Neuron-derived D-serine release provides a novel means to activate N-methyl-D-aspartate receptors. *J Biol Chem* **2006,** *281* (20), 14151-14162.

43. Hashimoto, A.; Oka, T.; Nishikawa, T., Anatomical distribution and postnatal changes in endogenous free D-aspartate and D-serine in rat brain and periphery. *Eur J Neurosci* **1995,** *7* (8), 1657-1663.

44. Dunlop, D. S.; Neidle, A.; McHale, D.; Dunlop, D. M.; Lajtha, A., The presence of free D-aspartic acid in rodents and man. *Biochem Biophys Res Commun* **1986,** *141* (1), 27-32.

45. Hashimoto, A.; Kumashiro, S.; Nishikawa, T.; Oka, T.; Takahashi, K.; Mito, T.; Takashima, S.; Mizutani, Y.; Yamazaki, T.; Kaneko, T., Embryonic development and postnatal changes in free D-aspartate and D-serine in the human prefrontal cortex. *J Neurochem* **1993,** *61* (1), 348-351.

46. Morikawa, A.; Hamase, K.; Ohgusu, T.; Etoh, S.; Tanaka, H.; Koshiishi, I.; Shoyama, Y.; Zaitsu, K., Immunohistochemical localization of D-alanine to β-cells in rat pancreas. *Biochem Biophys Res Commun* **2007,** *355* (4), 872-876.

47. Etoh, S.; Hamase, K.; Morikawa, A.; Ohgusu, T.; Zaitsu, K., Enantioselective visualization of D-alanine in rat anterior pituitary gland: localization to ACTH-secreting cells. *Anal Bioanal Chem* **2009,** *393* (1), 217-223.

48. Brückner, H.; Schieber, A., Determination of amino acid enantiomers in human urine and blood serum by gas chromatography-mass spectrometry. *Biomed Chromatogr* **2001,** *15* (3), 166-172.

49. Brückner, H.; Hausch, M., Gas chromatographic characterization of free D-amino acids in the blood serum of patients with renal disorders and of healthy volunteers. *J Chromatogr B Biomed Sci Appl* **1993,** *614* (1), 7-17.

50. Huang, Y.; Nishikawa, T.; Satoh, K.; Iwata, T.; Fukushima, T.; Homma, H.; Imai, K., Urinary excretion of D-serine in human: comparison of different ages and species. *Biol Pharm Bull* **1998,** *21* (2), 156-162.

51. Hamase, K.; Morikawa, A.; Ohgusu, T.; Lindner, W.; Zaitsu, K., Comprehensive analysis of branched aliphatic D-amino acids in mammals using an integrated multi-loop two-dimensional column-switching high-performance liquid chromatographic system combining reversed-phase and enantioselective columns. *J Chromatogr A* **2007,** *1143* (1-2), 105-111.

52. Ohide, H.; Miyoshi, Y.; Maruyama, R.; Hamase, K.; Konno, R., D-Amino acid metabolism in mammals: Biosynthesis, degradation and analytical aspects of the metabolic study. *J Chromatogr B Analyt Technol Biomed Life Sci* **2011,** *879* (29), 3162-3168.

53. Krebs, H. A., Metabolism of amino-acids: deamination of amino-acids. *Biochem J* **1935,** *29* (7), 1620-1644.

54. Still, J.; Buell, M. V.; Knox, W. E.; Green, D., Studies on the cyclophorase system VII. D-Aspartic oxidase. *J Biol Chem* **1949,** *179* (2), 831-837.

55. Lehmann, W. D.; Theobald, N.; Fischer, R.; Heinrich, H. C., Stereospecificity of phenylalanine plasma kinetics and hydroxylation in man following oral application of a stable isotope-labelled pseudo-racemic mixture of L-and D-phenylalanine. *Clinica Chimica Acta* **1983,** *128* (2), 181-198.

56. Wolosker, H.; Blackshaw, S.; Snyder, S. H., Serine racemase: a glial enzyme synthesizing D-serine to regulate glutamate-N-methyl-D-aspartate neurotransmission. *Proc Natl Acad Sci U S A* **1999,** *96* (23), 13409-13414.

57. Kim, P. M.; Duan, X.; Huang, A. S.; Liu, C. Y.; Ming, G.-l.; Song, H.; Snyder, S. H., Aspartate racemase, generating neuronal D-aspartate, regulates adult neurogenesis. *Proc Natl Acad Sci U S A* **2010,** *107* (7), 3175-3179.

58. Friedman, M., Chemistry, nutrition, and microbiology of D-amino acids. *J Agric Food Chem* **1999,** *47* (9), 3457-3479.

59. Brückner, H.; Hausch, M., D-Amino acids in dairy products: detection, origin and nutritional aspects. I. Milk, fermented milk, fresh cheese and acid curd cheese. *Milchwissenschaft* **1990,** *45* (6), 357-360.

60. Brückner, H.; Hausch, M., Detection of free D-amino acids in food by chiral phase capillary gas chromatography. *J High Resolut Chromatogr* **1989,** *12* (10), 680-684.

61. Brückner, H.; Hausch, M., Gas chromatographic detection of D-amino acids as common constituents of fermented foods. *Chromatographia* **1989,** *28* (9), 487-492.

62. Brückner, H.; Westhauser, T., Chromatographic determination of D-amino acids as native constituents of vegetables and fruits. *Chromatographia* **1994,** *39* (7-8), 419-426.

63. Gandolfi, I.; Palla, G.; Delprato, L.; Nisco, F.; Marchelli, R.; Salvadori, C., D-Amino acids in milk as related to heat treatments and bacterial activity. *J Food Sci* **1992,** *57* (2), 377-379.

64. Ollivaux, C. l.; Soyez, D.; Toullec, J.-Y., Biogenesis of D-amino acid containing peptides/proteins: where, when and how? *J Pept Sci* **2014,** *20* (8), 595-612.

65. Jilek, A.; Kreil, G., D-amino acids in animal peptides. *Monatsh Chem Chem Mon* **2008,** *139* (1), 1-5.

66. Fujii, N., D-amino acid in elderly tissues. *Biol Pharm Bull* **2005,** *28* (9), 1585-1589.

67. Masters, P. M.; Bada, J. L.; Zigler, J. S., Aspartic acid racemisation in the human lens during ageing and in cataract formation. *Nature* **1977,** 268 (5615), 71-73.

68. D'Aniello, S.; Somorjai, I.; Garcia-Fernàndez, J.; Topo, E.; D'Aniello, A., D-Aspartic acid is a novel endogenous neurotransmitter. *FASEB J* **2011,** *25* (3), 1014-1027.

69. Snyder, S. H.; Kim, P. M., D-Amino acids as putative neurotransmitters: focus on D-serine. *Neurochem Res* **2000,** *25* (5), 553-560.

70. Mothet, J.-P.; Parent, A. T.; Wolosker, H.; Brady, R. O.; Linden, D. J.; Ferris, C. D.; Rogawski, M. A.; Snyder, S. H., D-serine is an endogenous ligand for the glycine site of the N-methyl-D-aspartate receptor. *Proc Natl Acad Sci U S A* **2000,** *97* (9), 4926-4931.

71. Panatier, A.; Theodosis, D. T.; Mothet, J.-P.; Touquet, B.; Pollegioni, L.; Poulain, D. A.; Oliet, S. H., Glia-derived D-serine controls NMDA receptor activity and synaptic memory. *Cell* **2006,** *125* (4), 775-784.

72. Henneberger, C.; Papouin, T.; Oliet, S. H.; Rusakov, D. A., Long-term potentiation depends on release of D-serine from astrocytes. *Nature* **2010,** *463* (7278), 232-236.

73. D'Aniello, A.; Di Fiore, M. M.; Fisher, G. H.; Milone, A.; Seleni, A.; D'Aniello, S.; Perna, A. F.; Ingrosso, D., Occurrence of D-aspartic acid and N-methyl-D-aspartic acid in rat neuroendocrine tissues and their role in the modulation of luteinizing hormone and growth hormone release. *FASEB J* **2000,** *14* (5), 699-714.

74. Olverman, H.; Jones, A.; Mewett, K.; Watkins, J., Structure/activity relations of N-methyl-D-aspartate receptor ligands as studied by their inhibition of [3 H] d2-amino-5-phosphonopentanoic acid binding in rat brain membranes. *Neuroscience* **1988,** *26* (1), 17-31.

75. Schell, M. J.; Cooper, O. B.; Snyder, S. H., D-aspartate localizations imply neuronal and neuroendocrine roles. *Proc Natl Acad Sci U S A* **1997,** *94* (5), 2013-2018.

76. D'Aniello, A.; Di Cosmo, A.; Di Cristo, C.; Annunziato, L.; Petrucelli, L.; Fisher, G., Involvement of D-aspartic acid in the synthesis of testosterone in rat testes. *Life Sci* **1996,** *59* (2), 97-104.

77. Nagata, Y.; Homma, H.; Lee, J.-A.; Imai, K., D-Aspartate stimulation of testosterone synthesis in rat Leydig cells. *FEBS Lett* **1999,** *444* (2), 160-164.

78. Ishio, S.; Yamada, H.; Hayashi, M.; Yatsushiro, S.; Noumi, T.; Yamaguchi, A.; Moriyama, Y., D-Aspartate modulates melatonin synthesis in rat pinealocytes. *Neurosci Lett* **1998,** *249* (2), 143-146.

79. Wang, H.; Wolosker, H.; Pevsner, J.; Snyder, S.; Selkoe, D., Regulation of rat magnocellular neurosecretory system by D-aspartate: evidence for biological role (s) of a naturally occurring free D-amino acid in mammals. *J Endocrinol* **2000,** *167* (2), 247-252.

80. Steinberger, E., Hormonal control of mammalian spermatogenesis. *Physiol Rev* **1971,** *51* (1), 1-22.

81. Sakai, K.; Homma, H.; Lee, J.-A.; Fukushima, T.; Santa, T.; Tashiro, K.; Iwatsubo, T.; Imai, K., Localization of D-aspartic acid in elongate spermatids in rat testis. *Arch Biochem Biophys* **1998,** *351* (1), 96-105.

82. D'Aniello, A.; Di Fiore, M. M.; D'Aniello, G.; Colin, F. E.; Lewis, G.; Setchell, B. P., Secretion of D-aspartic acid by the rat testis and its role in endocrinology of the testis and spermatogenesis. *FEBS Lett* **1998,** *436* (1), 23-27.

83. Nagata, Y.; Masui, R.; Akino, T., The presence of free D-serine, D-alanine and D-proline in human plasma. *Experientia* **1992,** *48* (10), 986-988.

84. Hashimoto, K.; Engberg, G.; Shimizu, E.; Nordin, C.; Lindström, L. H.; Iyo, M., Reduced D-serine to total serine ratio in the cerebrospinal fluid of drug naive schizophrenic patients. *Prog Neuropsychopharmacol Biol Psychiatry* **2005,** *29* (5), 767-769.

85. Corvin, A.; McGhee, K.; Murphy, K.; Donohoe, G.; Nangle, J.; Schwaiger, S.; Kenny, N.; Clarke, S.; Meagher, D.; Quinn, J., Evidence for association and epistasis at the DAOA/G30 and D-amino acid oxidase loci in an Irish schizophrenia sample. *Am J Med Genet B Neuropsychiatr Genet* **2007,** *144* (7), 949-953.

86. Chumakov, I.; Blumenfeld, M.; Guerassimenko, O.; Cavarec, L.; Palicio, M.; Abderrahim, H.; Bougueleret, L.; Barry, C.; Tanaka, H.; La Rosa, P., Genetic and physiological data implicating the new human gene G72 and the gene for D-amino acid oxidase in schizophrenia. *Proc Natl Acad Sci U S A* **2002,** *99* (21), 13675-13680.

87. Hons, J.; Zirko, R.; Ulrychova, M.; Cermakova, E.; Libiger, J., D-serine serum levels in patients with schizophrenia: relation to psychopathology and comparison to healthy subjects. *Neuro Endocrinology Lett* **2008,** *29* (4), 485-492.

88. Verrall, L.; Burnet, P.; Betts, J.; Harrison, P., The neurobiology of D-amino acid oxidase and its involvement in schizophrenia. *Mol Psychiatry* **2010,** *15* (2), 122-137.

89. Hudson, M.; Pocknee, R.; Mowat, N., D-lactic acidosis in short bowel syndrome - an examination of possible mechanisms. *QJ Med* **1990,** *74* (274), 157-63.

90. Haan, E.; Brown, G.; Bankier, A.; Mitchell, D.; Hunt, S.; Blakey, J.; Barnes, G., Severe illness caused by the products of bacterial metabolism in a child with a short gut. *Eur J Pediatr* **1985,** *144* (1), 63-65.

91. Van Eys, J.; Judge, M.; Judd, J.; Hill, W.; Bozian, R.; Abrahams, S., A reinvestigation of methylglyoxal accumulation in thiamine deficiency. *J Nutr* **1962,** *76* (4), 375-384.

92. Giesecke, D.; Stangassinger, M.; Henle, K., D-Milchsäure - ein Stoffwechselproblem. *Z Ernährungswiss* **1985,** *24* (3), 172-186.

93. Tubbs, P.; Greville, G., The oxidation of D-α-hydroxy acids in animal tissues. *Biochem J* **1961,** *81* (1), 104-114.

94. Spaapen, L.; Ketting, D.; Wadman, S.; Bruinvis, L.; Duran, M., Urinary D-4-hydroxyphenyllactate, D-phenyllactate and D-2-hydroxyisocaproate, abnormalities of bacterial origin. *J Inherit Metab Dis* **1987,** *10* (4), 383-390.

95. Van Der Werf, P.; Orlowski, M.; Meister, A., Enzymatic conversion of 5-oxo-L-proline (L-pyrrolidone carboxylate) to L-glutamate coupled with cleavage of adenosine triphosphate to adenosine diphosphate, a reaction in the γ-glutamyl cycle. *Proc Natl Acad Sci U S A* **1971,** *68* (12), 2982-2985.

96. Daniel, J. W., The Metabolism of L- and DL-Malic Acids by Rats. *Food Cosmet Toxicol* **1969,** *7* (2), 103-106.

97. Rzem, R.; Veiga-da-Cunha, M.; Noel, G.; Goffette, S.; Nassogne, M. C.; Tabarki, B.; Scholler, C.; Marquardt, T.; Vikkula, M.; Van Schaftingen, E., A gene encoding a putative FAD-dependent L-2-hydroxyglutarate dehydrogenase is mutated in L-2-hydroxyglutaric aciduria. *Proc Natl Acad Sci U S A* **2004,** *101* (48), 16849-16854.

98. Achouri, Y.; Noël, G.; Vertommen, D.; Rider, M.; Veiga-Da-Cunha, M.; Van Schaftingen, E., Identification of a dehydrogenase acting on D-2-hydroxyglutarate. *Biochem J* **2004,** *381*, 35-42.

99. Struys, E. A.; Salomons, G. S.; Achouri, Y.; Van Schaftingen, E.; Grosso, S.; Craigen, W. J.; Verhoeven, N. M.; Jakobs, C., Mutations in the D-2-hydroxyglutarate dehydrogenase gene cause D-2-hydroxyglutaric aciduria. *Am J Hum Genet* **2005,** *76* (2), 358-360.

100. Dang, L.; White, D. W.; Gross, S.; Bennett, B. D.; Bittinger, M. A.; Driggers, E. M.; Fantin, V. R.; Jang, H. G.; Jin, S.; Keenan, M. C., Cancer-associated IDH1 mutations produce 2-hydroxyglutarate. *Nature* **2009,** *462* (7274), 739-744.

101. Patel, K. P.; Ravandi, F.; Ma, D.; Paladugu, A.; Barkoh, B. A.; Medeiros, L. J.; Luthra, R., Acute myeloid leukemia with IDH1 or IDH2 mutation frequency and clinicopathologic features. *Am J Clin Pathol* **2011,** *135* (1), 35-45.

102. Janin, M.; Mylonas, E.; Saada, V.; Micol, J.-B.; Renneville, A.; Quivoron, C.; Koscielny, S.; Scourzic, L.; Forget, S.; Pautas, C.; Caillot, D.; Preudhomme, C.; Dombret, H.; Berthon, C.; Barouki, R.; Rabier, D.; Auger, N.; Griscelli, F.; Chachaty, E.; Leclercq, E.; Courtier, M.-H.; Bennaceur-Griscelli, A.; Solary, E.; Bernard, O. A.; Penard-Lacronique, V.; Ottolenghi, C.; de Botton, S., Serum 2-hydroxyglutarate production in IDH1-and IDH2-mutated de novo acute myeloid leukemia: a study by the Acute Leukemia French Association Group. *J Clin Oncol* **2013,** *32* (4), 297-305.

103. Caldwell, J., Do single enantiomers have something special to offer? *Hum Psychopharm Clin* **2001,** *16* (S2), S67-S71.

104. Flack, H., Louis Pasteur's discovery of molecular chirality and spontaneous resolution in 1848, together with a complete review of his crystallographic and chemical work. *Acta Crystallogr Sect A: Found Crystallogr* **2009,** *65* (5), 371-389.

105. Trapp, G. Bestimmung der Interkonversionsbarrieren von Enantiomeren und Isomeren mit dynamischen Elektromigrationsmethoden und Computersimulation. Ph. D. Thesis, Eberhard-Karls-Universität Tübingen, **2001**.

106. Lottspeich, F.; Engels, J. W., *Bioanalytik*. 2. ed.; Elsevier Spektrum Akademischer Verlag: **2006**; p 169-174.

107. Gil-Av, E.; Feibush, B.; Charles-Sigler, R., Separation of enantiomers by gas liquid chromatography with an optically active stationary phase. *Tetrahedron Lett* **1966,** *7* (10), 1009-1015.

108. Gil-Av, E., Present status of enantiomeric analysis by gas chromatography. *J Mol Evol* **1975,** *6* (2), 131-144.

109. Voet, D.; Voet, J. G., *Biochemie*. 1 ed.; VCH Verlagsgesellschaft mbH: **1994**; p 65-68.

110. Bijvoet, J.; Peerdeman, A.; Van Bommel, A., Determination of the absolute configuration of optically active compounds by means of X-rays. *Nature* **1951,** *168* (4268), 271-272.

111. Herwig, P.; Zawatzky, K.; Grieser, M.; Heber, O.; Jordon-Thaden, B.; Krantz, C.; Novotný, O.; Repnow, R.; Schurig, V.; Schwalm, D.; Vager, Z.; Wolf, A.; Trapp, O.; Kreckel, H., Imaging the absolute configuration of a chiral epoxide in the gas phase. *Science* **2013,** *342* (6162), 1084-1086.

112. Soda, K., Microdetermination of D-amino acids and D-amino acid oxidase activity with 3,methyl-2-benzothiazolone hydrazone hydrochloride. *Anal Biochem* **1968,** *25* (1), 228-235.

113. Varadi, M.; Adanyi, N.; Szabo, E. E.; Trummer, N., Determination of the ratio of D- and L-amino acids in brewing by an immobilised amino acid oxidase enzyme reactor coupled to amperometric detection. *Biosens Bioelectron* **1999,** *14* (3), 335-340.

114. Domínguez, R.; Serra, B.; Reviejo, A.; Pingarron, J., Chiral analysis of amino acids using electrochemical composite bienzyme biosensors. *Anal Biochem* **2001,** *298* (2), 275-282.

115. Dixon, M.; Kleppe, K., D-Amino acid oxidase. II. Specificity, competitive inhibition and reaction sequence. *Biochim Biophys Acta* **1965,** *96*, 368–382.

116. Waldhier, M. C.; Gruber, M. A.; Dettmer, K.; Oefner, P. J., Capillary electrophoresis and column chromatography in biomedical chiral amino acid analysis. *Anal Bioanal Chem* **2009,** *394* (3), 695-706.

117. Dettmer-Wilde, K.; Engewald, W., *Practical Gas Chromatographie. A Comprehensive Reference*. Springer: **2014**; p 530-536.

118. Schurig, V., *Differentiation of Enantiomers I*. Springer: **2013**; p 21-40.

119. Waldhier, M. C. Analysis of Amino Acid Enantiomers by Gas Chromatography - Mass spectrometry in physiological fluids. diploma thesis, University of Regensburg, **2008**.

120. Barbaro, E.; Zangrando, R.; Vecchiato, M.; Turetta, C.; Barbante, C.; Gambaro, A., D-and L-amino acids in Antarctic lakes: assessment of a very sensitive HPLC-MS method. *Anal Bioanal Chem* **2014,** *406* (22), 5259-5270.

121. Miyoshi, Y.; Hamase, K.; Tojo, Y.; Mita, M.; Konno, R.; Zaitsu, K., Determination of D-serine and D-alanine in the tissues and physiological fluids of mice with various D-amino-acid oxidase activities using two-dimensional high-performance liquid chromatography with fluorescence detection. *J Chromatogr B* **2009,** *877* (24), 2506-2512.

122. Zahradnickova, H.; Husek, P.; Simek, P.; Hartvich, P.; Marsalek, B.; Holoubek, I., Determination of D- and L-amino acids produced by cyanobacteria using gas chromatography on Chirasil-Val after derivatization with pentafluoropropyl chloroformate. *Anal Bioanal Chem* **2007,** *388* (8), 1815-1822.

123. Schurig, V.; Juza, M.; Preschel, M.; Nicholson, G.; Bayer, E., Gas chromatographic enantiomer separation of proteinogenic amino acid derivatives: comparison of Chirasil-Val and Chirasil-γ-Dex used as chiral stationary phases. *Enantiomer* **1999,** *4*, 297-303.

124. Han, Y.; Chen, Y., On-column labeling technique and chiral CE of amino acids with mixed chiral selectors and UV detection. *Electrophoresis* **2007,** *28* (15), 2765-2770.

125. Grob, R. L.; Barry, E. F., *Modern Practice of Gas Chromatography*. Wiley Interscience: **2004**; p 26-214.

126. Skoog, D. A.; Leary, J. J., *Instrumentelle Analytik*. Springer: **1996**; p 463-465,650-655.

127. Kaspar, H. Amino acid analysis in biological fluids by GC-MS. Ph.D. Thesis, University of Regensburg, **2009**.

128. Liu, Z.; Phillips, J. B., Comprehensive two-dimensional gas chromatography using an on-column thermal modulator interface. *J Chromatogr Sci* **1991,** *29* (6), 227-231.

129. Dettmer, K.; Almstetter, M. F.; Wachsmuth, C. J.; Oefner, P. J., Comprehensive Two-Dimensional Gas Chromatography for Metabolomics. In *The Handbook of Plant Metabolomics*, Wiley-VCH Verlag GmbH & Co. KGaA: **2013**; pp 77-91.

130. Mondello, L.; Tranchida, P.; Dugo, P.; Dugo, G., Comprehensive two dimensional gas chromatography mass spectrometry: a review. *Mass Spectrom Rev* **2008,** *27* (2), 101-124.

131. Beens, J.; Udo, A. T., Comprehensive two-dimensional gas chromatography-a powerful and versatile technique. *Analyst* **2005,** *130* (2), 123-127.

132. Górecki, T.; Harynuk, J.; Panić, O., The evolution of comprehensive two-dimensional gas chromatography (GC × GC). *J Sep Sci* **2004,** *27*, 359-379.

133. Poliak, M.; Kochman, M.; Amirav, A., Pulsed flow modulation comprehensive two-dimensional gas chromatography. *J Chromatogr A* **2008,** *1186* (1), 189-195.

134. Phillips, J. B.; Gaines, R. B.; Blomberg, J.; van der Wielen, F. W.; Dimandja, J.-M.; Green, V.; Granger, J.; Patterson, D.; Racovalis, L.; de Geus, H.-J.; Haglund, P.; Lipsky, J.; Sinha, V.; Ledford, E. B., A robust thermal modulator for comprehensive two-dimensional gas chromatography. *J High Resolut Chromatogr* **1999,** *22* (1), 3-10.

135. Kinghorn, R. M.; Marriott, P. J., High speed cryogenic modulation-a technology enabling comprehensive multidimensional gas chromatography. *J High Resolut Chromatogr* **1999,** *22* (4), 235-238.

136. Kristenson, E. M.; Korytár, P.; Danielsson, C.; Kallio, M.; Brandt, M.; Mäkelä, J.; Vreuls, R. J.; Beens, J.; Brinkman, U. A. T., Evaluation of modulators and electron-capture detectors for comprehensive two-dimensional GC of halogenated organic compounds. *J Chromatogr A* **2003,** *1019* (1), 65-77.

137. Marriott, P.; Shellie, R., Principles and applications of comprehensive two-dimensional gas chromatography. *TrAC Trends Anal Chem* **2002,** *21* (9), 573-583.

138. Good, A.; Durden, D.; Kebarle, P., Ion-molecule reactions in pure nitrogen and nitrogen containing traces of water at total pressures 0.5-4 Torr. Kinetics of clustering reactions forming H+ (H2O) n. *J Chem Phys* **1970,** *52* (1), 212-221.

139. Horning, E.; Horning, M.; Carroll, D.; Dzidic, I.; Stillwell, R., New picogram detection system based on a mass spectrometer with an external ionization source at atmospheric pressure. *Anal Chem* **1973,** *45* (6), 936-943.

140. Dzidic, I.; Carroll, D.; Stillwell, R.; Horning, E., Comparison of positive ions formed in nickel-63 and corona discharge ion sources using nitrogen, argon, isobutane, ammonia and nitric oxide as reagents in atmospheric pressure ionization mass spectrometry. *Anal Chem* **1976,** *48* (12), 1763-1768.

141. Wachsmuth, C. Evaluation of gas chromatography/atmospheric pressure chemical ionization time-of-flight mass spectrometry for qualitative and quantitative metabolomics. Master thesis, University of Regensburg, **2011**.

142. Carrasco-Pancorbo, A.; Nevedomskaya, E.; Arthen-Engeland, T.; Zey, T.; Zurek, G.; Baessmann, C.; Deelder, A. M.; Mayboroda, O. A., Gas chromatography/atmospheric pressure chemical ionization-time of flight mass spectrometry: analytical validation and applicability to metabolic profiling. *Anal Chem* **2009,** *81* (24), 10071-10079.

143. McEwen, C. N.; McKay, R. G., A combination atmospheric pressure LC/MS: GC/MS ion source: advantages of dual AP-LC/MS: GC/MS instrumentation. *J Am Soc Mass Spectrom* **2005,** *16* (11), 1730-1738.

144. Schiewek, R.; Lorenz, M.; Giese, R.; Brockmann, K.; Benter, T.; Gäb, S.; Schmitz, O. J., Development of a multipurpose ion source for LC-MS and GC-API MS. *Anal Bioanal Chem* **2008,** *392* (1-2), 87-96.

145. Bristow, T.; Harrison, M.; Sims, M., The application of gas chromatography/atmospheric pressure chemical ionisation time-of-flight mass spectrometry to impurity identification in Pharmaceutical Development. *Rapid Commun Mass Spectrom* **2010,** *24* (11), 1673-1681.

146. García-Villalba, R.; Pacchiarotta, T.; Carrasco-Pancorbo, A.; Segura-Carretero, A.; Fernández-Gutiérrez, A.; Deelder, A. M.; Mayboroda, O. A., Gas chromatography-atmospheric pressure chemical ionization-time of flight mass spectrometry for profiling of phenolic compounds in extra virgin olive oil. *J Chromatogr A* **2011,** *1218* (7), 959-971.

147. Pacchiarotta, T.; Nevedomskaya, E.; Carrasco-Pancorbo, A.; Deelder, A. M.; Mayboroda, O. A., Evaluation of GC-APCI/MS and GC-FID as a complementary platform. *J Biomol Tech* **2010,** *21* (4), 205-213.

148. Wachsmuth, C. J.; Almstetter, M. F.; Waldhier, M. C.; Gruber, M. A.; Nürnberger, N.; Oefner, P. J.; Dettmer, K., Performance evaluation of gas chromatography-atmospheric pressure chemical ionization-time-of-flight mass spectrometry for metabolic fingerprinting and profiling. *Anal Chem* **2011,** *83* (19), 7514-7522.

149. Wachsmuth, C. J.; Dettmer, K.; Lang, S. A.; Mycielska, M. E.; Oefner, P. J., Continuous water infusion enhances atmospheric pressure chemical ionization of methyl chloroformate derivatives in gas chromatography coupled to time-of-flight mass spectrometry-based metabolomics. *Anal Chem* **2014,** *86* (18), 9186-9195.

150. Nagata, Y.; Yamamoto, K.; Shimojo, T.; Konno, R.; Yasumura, Y.; Akino, T., The presence of free D-alanine, D-proline and D-serine in mice. *Biochim Biophys Acta* **1992,** *1115* (3), 208-11.

151. Pawlowska, M.; Chen, S.; Armstrong, D. W., Enantiomeric separation of fluorescent, 6-aminoquinolyl-N-hydroxysuccinimidyl carbamate, tagged amino acids. *J Chromatogr A* **1993,** *641* (2), 257-265.

152. Hinze, W.; Riehl, T.; Armstrong, D.; DeMond, W.; Alak, A.; Ward, T., Liquid chromatographic separation of enantiomers using a chiral. beta.-cyclodextrin-bonded stationary phase and conventional aqueous-organic mobile phases. *Anal Chem* **1985,** *57* (1), 237-242.

153. Roussel, C.; Favrou, A., Cationic ß-cyclodextrin: a new versatile chiral additive for separation of drug enantiomers by high-performance liquid chromatography. *J Chromatogr A* **1995,** *704* (1), 67-74.

154. Pinjari, R. V.; Joshi, K. A.; Gejji, S. P., Molecular electrostatic potentials and hydrogen bonding in α-, β-, and γ-cyclodextrins. *J Phys Chem A* **2006,** *110* (48), 13073-13080.

155. Lindner, W.; Böhs, B.; Seidel, V., Enantioselective capillary electrophoresis of amino acid derivatives on cyclodextrin evaluation of structure-resolution relationships. *J Chromatogr A* **1995,** *697* (1-2), 549-560.

156. Pinjari, R. V.; Khedkar, J. K.; Gejji, S. P., Cavity diameter and height of cyclodextrins and cucurbit [n] urils from the molecular electrostatic potential topography. *J Incl Phenom Macrocycl Chem* **2010,** *66* (3-4), 371-380.

157. Sicoli, G.; Pertici, F.; Jiang, Z.; Jicsinszky, L.; Schurig, V., Gas-chromatographic approach to probe the absence of molecular inclusion in enantioseparations by carbohydrates. Investigation of linear dextrins ("acyclodextrins") as novel chiral stationary phases. *Chirality* **2007,** *19* (5), 391-400.

158. Waldhier, M. C.; Dettmer, K.; Gruber, M. A.; Oefner, P. J., Comparison of derivatization and chromatographic methods for GC-MS analysis of amino acid enantiomers in physiological samples. *J Chromatogr B Analyt Technol Biomed Life Sci* **2010,** *878* (15-16), 1103-1112.

159. Frank, H.; Woiwode, W.; Nicholson, G.; Bayer, E., Determination of the rate of acidic catalyzed racemization of protein amino acids. *Liebigs Ann Chem* **1981,** *3*, 354-365.

160. Bada, J. L., Kinetics of racemization of amino acids as a function of pH. *J Am Chem Soc* **1972,** *94* (4), 1371-1373.

161. Masters, P. M.; Friedman, M., Racemization of amino acids in alkali-treated food proteins. *J Agric Food Chem* **1979,** *27* (3), 507-511.

162. Liardon, R.; Hurrell, R. F., Amino acid racemization in heated and alkali-treated proteins. *J Agric Food Chem* **1983,** *31* (2), 432-437.

163. Geiger, T.; Clarke, S., Deamidation, isomerization, and racemization at asparaginyl and aspartyl residues in peptides. Succinimide-linked reactions that contribute to protein degradation. *J Biol Chem* **1987,** *262* (2), 785-794.

164. Warrack, B. M.; Hnatyshyn, S.; Ott, K.-H.; Reily, M. D.; Sanders, M.; Zhang, H.; Drexler, D. M., Normalization strategies for metabonomic analysis of urine samples. *J Chromatogr B* **2009,** *877* (5), 547-552.

165. Chen, Y.; Shen, G.; Zhang, R.; He, J.; Zhang, Y.; Xu, J.; Yang, W.; Chen, X.; Song, Y.; Abliz, Z., Combination of injection volume calibration by creatinine and MS signals' normalization to overcome urine variability in LC-MS-based metabolomics studies. *Anal Chem* **2013,** *85* (16), 7659-7665.

166. Tang, K. W. A.; Toh, Q. C.; Teo, B. W., Normalisation of urinary biomarkers to creatinine for clinical practice and research - when and why. *Singapore Med J* **2015,** *56* (1), 7-10.

167. Ferguson, M. A.; Vaidya, V. S.; Waikar, S. S.; Collings, F. B.; Sunderland, K. E.; Gioules, C. J.; Bonventre, J. V., Urinary liver-type fatty acid-binding protein predicts adverse outcomes in acute kidney injury. *Kidney Int* **2010,** *77* (8), 708-714.

168. Benjamini, Y.; Hochberg, Y., Controlling the false discovery rate: a practical and powerful approach to multiple testing. *J R Stat Soc Series B Stat Methodol* **1995,** *57* (1), 289-300.

169. Salkind, N. J.; Rasmussen, K., *Encyclopedia of Measurement and Statistics*. SAGE Publications: **2007**; Vol. 1.

170. Šidák, Z., Rectangular confidence regions for the means of multivariate normal distributions. *J Am Stat Assoc* **1967,** *62* (318), 626-633.

171. Jombart, T.; Devillard, S.; Balloux, F., Discriminant analysis of principal components: a new method for the analysis of genetically structured populations. *BMC Genetics* **2010,** *11* (1), 94-108.

172. Bland, J.; Altman, D., Statistical methods for assessing agreement between two methods of clinical assessment. *Lancet* **1986,** *1* (8476), 307-310.

173. Villas-Bôas, S.; Delicado, D.; Lkesson, M.; Nielsen, J., Simultaneous analysis of amino and nonamino organic acids as methyl chloroformate derivatives using gas chromatography–mass spectrometry. *Anal Biochem* **2003,** *322* (1), 134-138.

174. Waldhier, M. C.; Almstetter, M. F.; Nürnberger, N.; Gruber, M. A.; Dettmer, K.; Oefner, P. J., Improved enantiomer resolution and quantification of free D-amino acids in serum and urine by comprehensive two-dimensional gas chromatography-time-of-flight mass spectrometry. *J Chromatogr A* **2011,** *1218* (28), 4537-4544.

175. Landfried, K.; Zhu, W.; Waldhier, M. C.; Schulz, U.; Ammer, J.; Holler, B.; Wolff, D.; Edinger, M.; Peter, K.; Kreutz, M.; Andreesen, R.; Oefner, P. J.; Holler, E., Tryptophan catabolism is associated with acute GVHD after human allogeneic stem cell transplantation and indicates activation of indoleamine 2,3-dioxygenase. *Blood* **2011,** *118* (26), 6971-6974.

176. Armbruster, D. A.; Tillman, M. D.; Hubbs, L. M., Limit of detection (LOD)/limit of quantitation (LOQ): comparison of the empirical and the statistical methods exemplified with GC-MS assays of abused drugs. *Clin Chem* **1994,** *40* (7), 1233-1238.

177. Anderson, D. J., Determination of the lower limit of detection. *Clin Chem* **1989,** *35* (10), 2152-2153.

178. Pauling, L.; Robinson, A. B.; Teranishi, R.; Cary, P., Quantitative analysis of urine vapor and breath by gas-liquid partition chromatography. *Proc Natl Acad Sci U S A* **1971,** *68* (10), 2374-2376.

179. Thomas, A.; Stevens, A. P.; Klein, M. S.; Hellerbrand, C.; Dettmer, K.; Gronwald, W.; Oefner, P. J.; Reinders, J., Early changes in the liver-soluble proteome from mice fed a nonalcoholic steatohepatitis inducing diet. *Proteomics* **2012,** *12* (9), 1437-1451.

180. Kaspar, H.; Dettmer, K.; Gronwald, W.; Oefner, P., Automated GC–MS analysis of free amino acids in biological fluids. *J Chromatogr B Analyt Technol Biomed Life Sci* **2008,** *870* (2), 222-232.

181. Hušek, P., Derivatization and gas chromatographic determination of hydroxycarboxylic acids treated with chloroformates. *J Chromatogr A* **1991,** *547*, 307-314.

182. Grob, K., *Split and Splitless Injection for Quantitative Gas Chromatography*. 4 ed.; Wiley-VCH Verlag GmbH: **2001**; p 90-100.

183. Xia, F.; Bronowska, A. K.; Cheng, S.; GralÎˆter, F., Base-catalyzed peptide hydrolysis is insensitive to mechanical stress. *J Phys Chem B* **2011,** *115* (33), 10126-10132.

184. König, W.; Kernebeck, K., Acidic removal of S-trityl groups as demonstrated for synthetic insulin fragments. *Liebigs Ann Chem* **1979,** *2*, 227-247.

185. Neuberger, A., Stereochemistry of amino acids. *Adv Protein Chem* **1948,** *4*, 297-383.

186. Moschen, A. R.; Kaser, S.; Tilg, H., Non-alcoholic steatohepatitis: a microbiota-driven disease. *Trends Endocrin Met* **2013,** *24* (11), 537-545.

187. Tilg, H.; Moschen, A. R., Evolution of inflammation in nonalcoholic fatty liver disease: the multiple parallel hits hypothesis. *Hepatology* **2010,** *52* (5), 1836-1846.

188. Basaranoglu, M.; Kayacetin, S.; Yilmaz, N.; Kayacetin, E.; Tarcin, O.; Sonsuz, A., Understanding mechanisms of the pathogenesis of nonalcoholic fatty liver disease. *World J Gastroenterol* **2010,** *16* (18), 2223-2226.

189. Miele, L.; Valenza, V.; La Torre, G.; Montalto, M.; Cammarota, G.; Ricci, R.; Masciana, R.; Forgione, A.; Gabrieli, M. L.; Perotti, G.; Vecchio, F. M.; Rapaccini, G.; Gasbarrini, G.; Day, C. P.; Grieco, A., increased intestinal permeability and tight junction alterations in nonalcoholic fatty liver disease. *Hepatology* **2009,** *49* (6), 1877-1887.

190. Hamase, K.; Inoue, T.; Morikawa, A.; Konno, R.; Zaitsu, K., Determination of free D-proline and D-leucine in the brains of mutant mice lacking D-amino acid oxidase activity. *Anal Biochem* **2001,** *298* (2), 253-258.

191. Hamase, K.; Takagi, S.; Morikawa, A.; Konno, R.; Niwa, A.; Zaitsu, K., Presence and origin of large amounts of D-proline in the urine of mutant mice lacking D-amino acid oxidase activity. *Anal Bioanal Chem* **2006,** *386* (3), 705-711.

192. Fukushima, T.; Kawai, J.; Imai, K.; Toyo'oka, T., Simultaneous determination of D-and L-serine in rat brain microdialysis sample using a column-switching HPLC with fluorimetric detection. *Biomed Chromatogr* **2004,** *18* (10), 813-819.

193. Morikawa, A.; Hamase, K.; Zaitsu, K., Determination of D-alanine in the rat central nervous system and periphery using column-switching high-performance liquid chromatography. *Anal Biochem* **2003,** *312* (1), 66-72.

194. Lee, A.; Bartle, K.; Lewis, A., A model of peak amplitude enhancement in orthogonal two-dimensional gas chromatography. *Anal Chem* **2001,** *73* (6), 1330-1335.

195. Junge, M.; Huegel, H.; Marriott, P. J., Enantiomeric analysis of amino acids by using comprehensive two-dimensional gas chromatography. *Chirality* **2007,** *19* (3), 228-234.

196. Kaspar, H.; Dettmer, K.; Chan, Q.; Daniels, S.; Nimkar, S.; Daviglus, M.; Stamler, J.; Elliott, P.; Oefner, P., Urinary amino acid analysis: A comparison of iTRAQ®-LC-MS/MS, GC-MS, and amino acid analyzer. *J Chromatogr B Analyt Technol Biomed Life Sci* **2009,** *877* (20-21), 1838-1846.

197. Dettmer, K.; Almstetter, M.; Appel, I.; Nürnberger, N.; Schlamberger, G.; Gronwald, W.; Meyer, H.; Oefner, P., Comparison of serum versus plasma collection in gas chromatography–mass spectrometry based metabolomics. *Electrophoresis* **2010,** *31* (14), 2365-2373.

198. Cipollina, C.; ten Pierick, A.; Canelas, A. B.; Seifar, R. M.; van Maris, A. J.; van Dam, J. C.; Heijnen, J. J., A comprehensive method for the quantification of the non-oxidative pentose phosphate pathway intermediates in Saccharomyces cerevisiae by GC-IDMS. *J Chromatogr B* **2009,** *877* (27), 3231-3236.

199. Armstrong, D. W.; Gasper, M.; Lee, S. H.; Zukowski, J.; Ercal, N., D-amino acid levels in human physiological fluids. *Chirality* **1993,** *5* (5), 375-378.

200. Almstetter, M. F.; Oefner, P. J.; Dettmer, K., Comprehensive two-dimensional gas chromatography in metabolomics. *Anal Bioanal Chem* **2012,** *402* (6), 1993-2013.

201. Heil, M.; Podebrad, F.; Beck, T.; Mosandl, A.; Sewell, A.; Böhles, H., Enantioselective multidimensional gas chromatography-mass spectrometry in the analysis of urinary organic acids. *J Chromatogr B Analyt Technol Biomed Life Sci* **1998,** *714* (2), 119-126.

202. Lindstedt, S.; Norberg, K.; Steen, G.; Wahl, E., Structure of some aliphatic dicarboxylic acids found in the urine of an infant with congenital lactic acidosis. *Clin Chem* **1976,** *22* (8), 1330-1338.

203. Jin, S. J.; Tserng, K. Y., Identification of isomeric unsaturated medium-chain dicarboxylic acids in human urine. *J Lipid Res* **1989,** *30* (10), 1611-1619.

204. Klein, M. S.; Dorn, C.; Saugspier, M.; Hellerbrand, C.; Oefner, P. J.; Gronwald, W., Discrimination of steatosis and NASH in mice using nuclear magnetic resonance spectroscopy. *Metabolomics* **2011,** *7* (2), 237-246.

205. Lippold, B. C.; Garrett, E. R., Kinetics and mechanisms of lactonization of coumarinic acids and hydrolysis of coumarins. II. *J Pharm Sci* **1971,** *60* (7), 1019-1027.

206. Fassberg, J.; Stella, V. J., A kinetic and mechanistic study of the hydrolysis of camptothecin and some analogues. *J Pharm Sci* **1992,** *81* (7), 676-684.

207. Rousseau, G., Medium ring lactones. *Tetrahedron* **1995,** *51* (10), 2777-2849.

208. Teiber, J. F.; Draganov, D. I.; Du, B. N. L., Lactonase and lactonizing activities of human serum paraoxonase (PON1) and rabbit serum PON3. *Biochem Pharmacol* **2003,** *66* (6), 887-896.

209. das Neves, H. J. C.; Noronha, J. P.; Rufino, H., A new method for the chiral HRGC assay of L-2-hydroxyglutaric acid in urine. *J High Resolut Chromatogr* **1996,** *19* (3), 161-164.

210. Duran, M.; Kamerling, J.; Bakker, H.; Van Gennip, A.; Wadman, S., L-2-Hydroxyglutaric aciduria: an inborn error of metabolism? *J Inherit Metab Dis* **1980,** *3* (1), 109-112.

211. An, Y.; Xu, W.; Li, H.; Lei, H.; Zhang, L.; Hao, F.; Duan, Y.; Yan, X.; Zhao, Y.; Wu, J.; Wang, Y.; Tang, H., High-fat diet induces dynamic metabolic alterations in multiple biological matrices of rats. *J Proteome Res* **2013,** *12* (8), 3755-3768.

212. Thomas, A.; Klein, M. S.; Stevens, A. P.; Reinders, Y.; Hellerbrand, C.; Dettmer, K.; Gronwald, W.; Oefner, P. J.; Reinders, J., Changes in the hepatic mitochondrial and membrane proteome in mice fed a non-alcoholic steatohepatitis inducing diet. *J Proteomics* **2013,** *80C*, 107-122.

213. Wang, Q.; Jiang, L.; Wang, J.; Li, S.; Yu, Y.; You, J.; Zeng, R.; Gao, X.; Rui, L.; Li, W., Abrogation of hepatic ATP-citrate lyase protects against fatty liver and ameliorates hyperglycemia in leptin receptor-deficient mice. *Hepatology* **2009,** *49* (4), 1166-1175.

214. Kojima, H.; Sakurai, S.; Uemura, M.; Fukui, H.; Morimoto, H.; Tamagawa, Y., Mitochondrial abnormality and oxidative stress in nonalcoholic steatohepatitis. *Alcohol Clin Exp Res* **2007,** *31* (1 Suppl), S61-S66.

215. Richardson, C. L.; Delehanty, L. L.; Bullock, G. C.; Rival, C. M.; Tung, K. S.; Kimpel, D. L.; Gardenghi, S.; Rivella, S.; Goldfarb, A. N., Isocitrate ameliorates anemia by suppressing the erythroid iron restriction response. *J Clin Invest* **2013,** *123* (8), 3614-3623.

216. Mehta, V.; Namboodiri, M. A., N-Acetylaspartate as an acetyl source in the nervous system. *Brain Res Mol Brain Res* **1995,** *31* (1-2), 151-157.

217. Tserng, K. Y.; Jin, S. J.; Hoppel, C. L.; Kerr, D. S.; Genuth, S. M., Urinary 3-hydroxyadipic acid 3,6-lactone: structural identification and effect of fasting in adults and children. *Metabolism* **1989,** *38* (7), 655-661.

218. Liebich, H.; Först, C., Basic profiles of organic acids in urine. *J Chromatogr B: Biomed Sci Appl* **1990,** *525*, 1-14.

11 APPENDIX

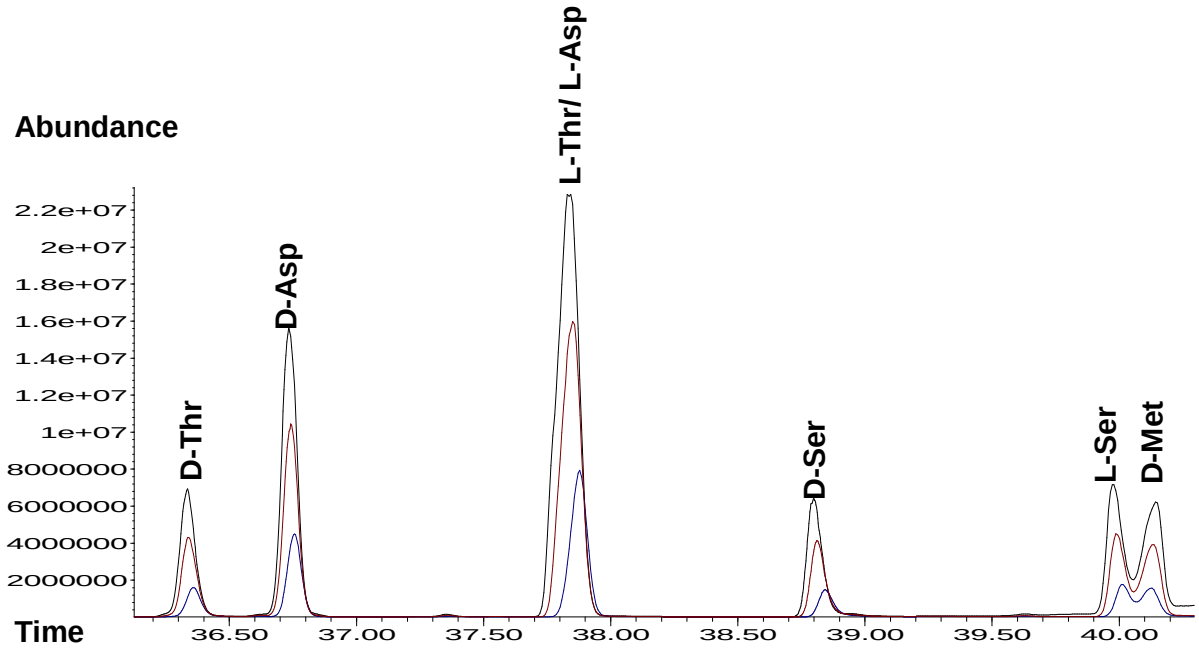

Figure S1. Overlaid chromatogram section of late eluting MeOH/MCF AAEs of MM I, after GC-qMS measure in SIM mode, accomplished with three different splitless times and remaining GC-MS parameters installed like in method II.

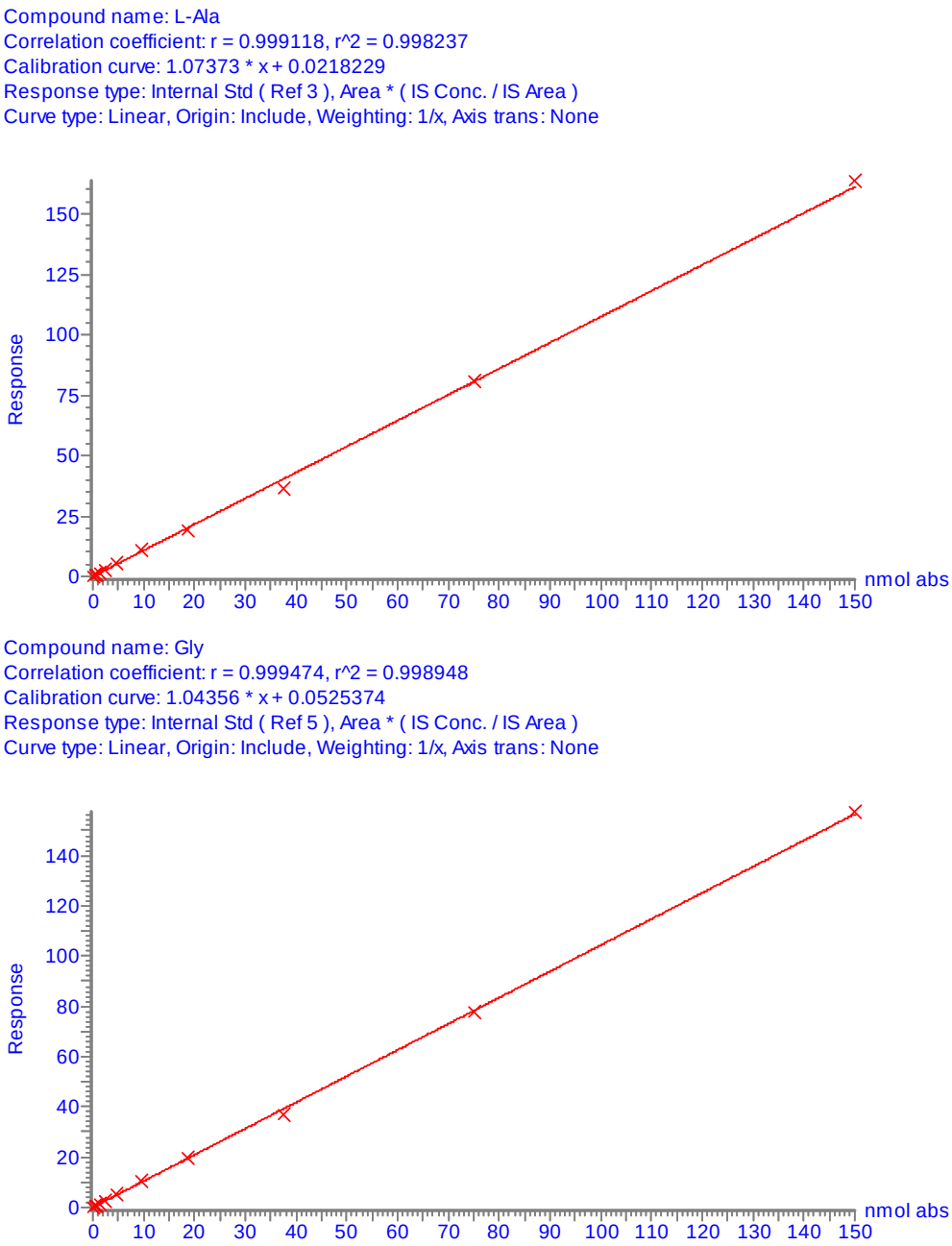

Figure S2. Characteristic calibration curves for MeOH/MCF L-Ala and Gly generated by chiral GC-qMS analysis of a dilution series of MM II with method II and a splitless time of 1.0 minutes except for the highest calibration point that was generated using method II and a splitless time of 0.5 minutes.

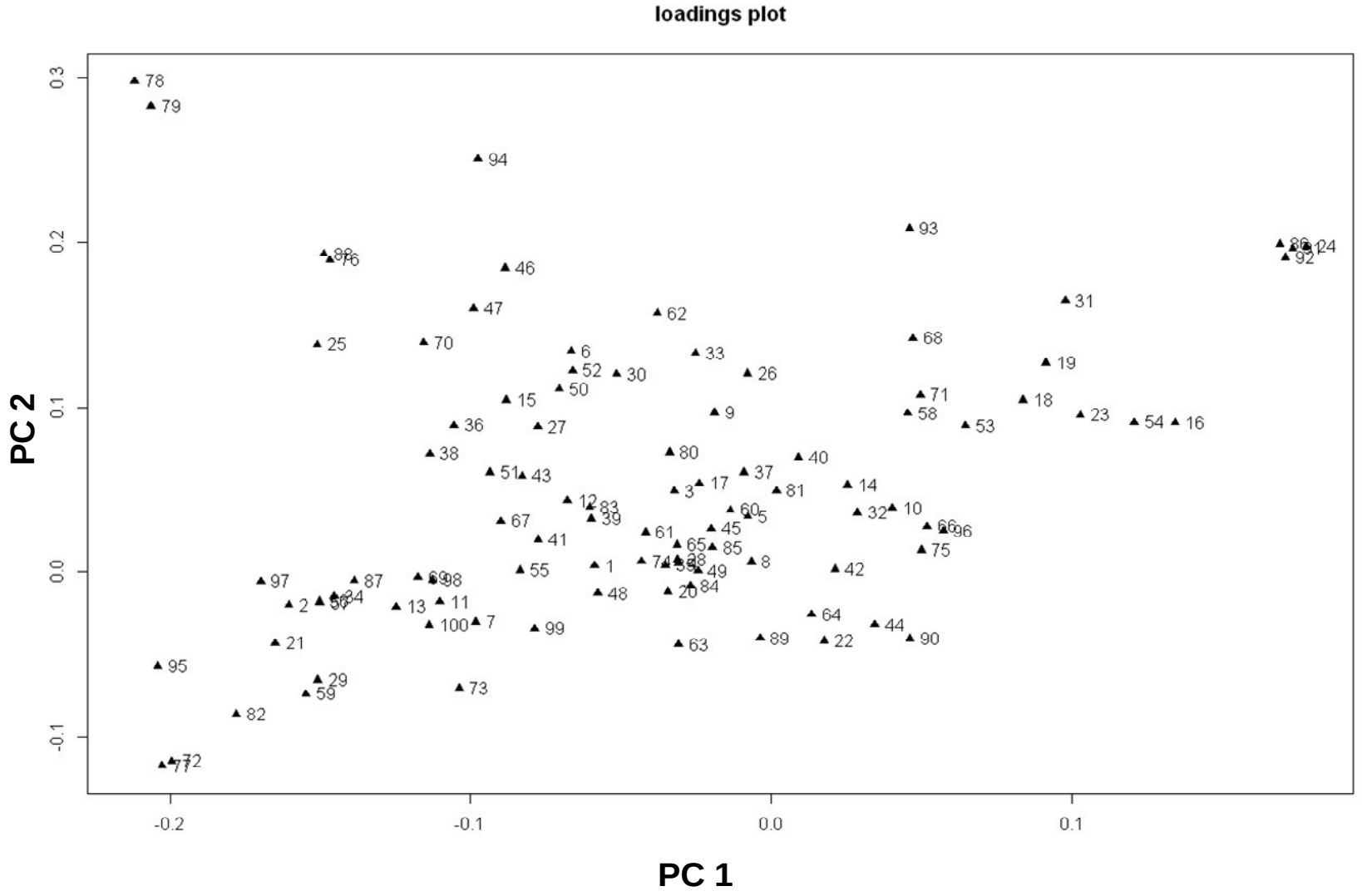

Figure S3. Loadings plot of PCA of discriminating metabolites shown in Figure 29 of chapter 8. Dots were marked by numbers given in Table 7, Table S1, Table S2 and Table S3.

Table S1. Identification results of 'Unknowns' subjected to sf analysis: Retention times, picked *m/z* and sf results of 88 features, significantly differentiating the groups in at least one comparison after repeated univariate statistical analysis.

Nr	assigned metabolite(s)	identified by	ret.t (GC-qMS)	picked m/z (GC-qMS)	Elemental composition derivative+H	calculated m/z of M+H	Δ [mDa]	mSigma
1	unknown	-	10.83	89	-	-	-	-
2	Fumaric acid (or Maleic acid)	NIST; sf; std	11.55	113	$C_6H_9O_4$	145.0501	0.03	24.6
3	Benzaldehyde	NIST; sf	11.89	106	C_7H_7O	107.04969	-2.45	43.7
4	Malonic acid	NIST; sf; std	12.77	101	$C_5H_9O_4$	133.0501	-0.32	8.2
6	unknown	-	13.38	105	-	-	-	-
-	df: Succinic acid	NIST; sf; std	14.43	115	$C_6H_{11}O_4$	147.0657	-0.69	7.8
7	Succinic acid	NIST; sf; std	14.44	115	$C_6H_{11}O_4$	147.0657	-0.69	7.8
8	unknown	-	15.14	127	-	-	-	-
9	DL-1-Acetoxy-1-ethoxyethane, 4,4-Dimethoxy-2-butanone, S- or 1-Butanol, Isobutanol, Erythronilic acid, 3-Hydroxy-2-methyl-[R-(R,S)]-butanoic acid, DL-3/4-Hydroxyisovaleric acid, DL- 2-Hydroxy-2/3-methylbutyric acid, 2-Methylpropan-2-ol (hydroxyacids and alcohols as 1-fold derivatives)	sf	16.21	87	$C_6H_{13}O_3$	133.0865	-0.54	71.9
10	see feature above	sf	16.23	74	$C_6H_{13}O_3$	133.0865	-0.54	71.9
11	Itaconic acid	NIST; sf; std	16.37	127	$C_7H_{11}O_4$	159.0657	-0.72	22.4
12	2-Methylbutylamine, 3-Methylbutylamine	sf	16.44	88	$C_7H_{16}NO_2$	146.1181	-0.96	13.3
13	Glutaric acid, D(L)-Methylsuccinic acid, Dimethylmalonic acid, DL-2-Aceto-2-hydroxybutanoic acid (1-fold derivative)	sf	16.85	100	$C_7H_{13}O_4$	161.0814	-0.76	6.9
14	Phenylacetic acid	NIST; sf; std	16.88	91	$C_9H_{11}O_2$	151.0759	-0.25	4.9
15	Adipate semialdehyde, 2/3-Oxohexanoic acid,DL-2/(3)-Methyl-3/(2)-oxovaleric acid, Ketoleucine	sf	17.53	114	$C_7H_{13}O_3$	145.0865	-1.03	20.3
16	cis/(trans)-2-Hexenedioic acid, cis-3-Hexenedioic acid, trans-2-Methylglutaconic acid, trans-3-Methylglutaconic acid	sf, sf, sf; NIST, sf;NIST	18.66	107	$C_8H_{13}O_4$	173.0814	-0.51	21.6
17	unknown	-	19.08	87	-	-	-	-
18	Carbamic acid or 3/2-Furoic acid	sf	19.36	99	$C_4H_8NO_4$ or $C_6H_7O_3$	134.0453 or 127.0395	-1.12 or 1.00	14.4 or 6.2
19	see feature above	sf	19.37	98	$C_4H_8NO_4$ or $C_6H_7O_3$	134.0453 or 127.0395	-1.12 or 1.00	14.4 or 6.2
21	Benzylamine	sf	20.04	72	$C_9H_{12}NO_2$	166.0868	2.53	58.5
22	DL-Citramalic acid (2-fold derivative)	NIST; sf; std	20.13	117	$C_7H_{13}O_5$	177.0763	-0.18	6

Table S1. continued.

Nr	assigned metabolite(s)	identified by	ret.t (GC-qMS)	picked m/z (GC-qMS)	Elemental composition derivative+H	calculated m/z of M+H	Δ [mDa]	mSigma
23	trans-2-Hexenedioic acid	NIST; sf; std	20.27	74	$C_8H_{13}O_4$	173.0814	-0.17	10.8
24	cis/(trans)-2-Hexenedioic acid, cis/trans-3-Hexenedioic acid, cis/trans-1-Carboxycyclopropane-2-acetic acid, cis/trans-2-Methylglutaconic acid, cis/trans-3-Methylglutaconic acid, (Succinylacetone)	NIST; sf	20.51	98	$C_8H_{13}O_4$	173.0814	-0.89	18.2
25	Ethyl-2-furoate, Ethyl-3-furoate, Furfuryl acetate, 5-Methylfuran-2-carboxylic acid	sf	20.82	99	$C_7H_9O_3$	141.0552	0.26	24.4
27	Diethanolamin (1-fold derivative)	sf	22.14	111	$C_6H_{14}NO_4$	164.092284	-3.15	39.9
-	L-Malic acid (2-fold derivatized)	NIST; sf; std	22.26	71	C6H11O5	163.06065	-1.7	1
29	3-Hydroxymethylglutaric acid (2-fold derivative), 2/3-DL-Hydroxyadipic acid (2-fold derivative), 2-Hydroxy-2-ethylsuccinic acid (2-fold derivative)	sf;NIST, sf, sf, sf	22.42	117	$C_8H_{15}O_5$	191.092	-0.32	12.5
30	Pimelic acid	NIST; sf; std	22.57	125	$C_9H_{17}O_4$	189.112685	0	18.6
31	Isopropylmaleate	sf	22.87	84	$C_9H_{15}O_4$	187.097035	0.3	20.6
32	3-Aminopropionaldehyde, Aminoacetone, (N-Acetylglycine) or (DL-Ile,) (D-*allo*-Ile), DL-Norleucine, β-Leucine	sf	23.49	88	$C_5H_{10}NO_3$ or $C_9H_{18}NO_4$	132.0661 or 204.1236	-0.27 or -1.49	12.1 or 20.3
-	df: α-Ketoglutarate	NIST; sf; std	24.41	87	$C_7H_{11}O_5$	175.0607	-0.72	91.7
34	α-Ketoglutarate	NIST; sf; std	24.42	115	$C_7H_{11}O_5$	175.0607	-0.72	91.7
36	unknown	-	25.22	112	-	-	-	-
37	(2/)3-Hydroxyglutaric acid (2-fold derivative),(DL-Citramalic acid (2-fold derivative))	sf	25.83	102	$C_7H_{13}O_5$	177.0763	-0.12	26.3
38	Acetamidopropanal (1-fold derivative)	sf	26.14	114	$C_7H_{12}NO_4$	174.0766	-0.73	14.6
42	trans/cis-2/3/4-Octenedioic acid	sf	27.51	136	$C_{10}H_{17}O_4$	201.1127	-1.4	24.9
43	4-Aminobutyraldehyde (, N-Acetyl-DL-Ala), Propionylglycine	sf	27.72	86	$C_6H_{12}NO_3$	146.081719	-1.11	11.8
44	2-Keto-3-deoxy-DL-gluconic acid (1fold derivative)	sf	27.75	116	$C_7H_{13}O_6$	193.0712	-0.31	7.1
45	Nonic acid, Azelaic acid	sf	28.29	88	$C_{11}H_{21}O_4$	217.144	-0.25	8.5
46	1,2,3-Propanetricarboxylic acid	NIST; sf	29.49	187	$C_9H_{15}O_6$	219.086865	-0.88	52.8
47	N-Acetylserine, O-Acetylethanolamine	sf	29.62	105	$C_6H_{12}NO_4$	162.0766	0.9	62.7
48	cis (/trans)-Aconitic acid	NIST; sf; std	29.80	153	C9H13O6	217.0712	-2.14	9.6

Table S1. continued.

Nr	assigned metabolite(s)	identified by	ret.t (GC-qMS)	picked m/z (GC-qMS)	Elemental composition derivative+H	calculated m/z of M+H	Δ [mDa]	mSigma
50	2,4,6-Trihydroxybenzoic acid methyl ester (underivatized), 2,4,6-Trihydroxybenzoic acid (1-fold derivative)	sf	31.25	152	$C_8H_9O_5$	185.045	-0.5	8.4
51	N-Acetylvaline, Valerylglycine, 5-Acetamidovalerate, 2-Methylbutyrylglycine, Isovalerylglycine, 3-Dehydrocarnitine	sf	31.78	109	$C_8H_{16}NO_3$	174.113	0.79	8
52	Benzoquinone acetic acid	sf	31.82	145	$C_9H_9O_4$	181.0501	0.18	20.7
53	2/3(*l*4)-Hydroxyphenylacetic acid, 4-Hydroxy-3-methylbenzoic acid, p-Anisic acid, (DL-Mandelic acid), Homovanillin (without derivatized OH-groups)	sf	31.99	153	$C_9H_{11}O_3$	167.07082	0.28	56.5
54	see feature above	sf	32.05	143	$C_9H_{11}O_3$	167.0708	0.28	56.5
55	unknown	-	32.29	94	-	-	-	-
56	cis/trans-2-Hydroxy-2-penteneglutaric acid (Enol byproduct of MCF derivatization of 2-Ketoglutaric acid, 2-fold derivative)	sf; std	32.89	115	$C_7H_{11}O_5$	175.06065	-0.75	7.2
57	see feature above	sf; std	33.28	115	$C_7H_{11}O_5$	175.06065	-1.49	5.9
58	unknown	-	34.31	121	-	-	-	-
59	Citric acid (3-fold derivative)	NIST; sf; std	34.73	175	$C_9H_{15}O_7$	235.08178	-3.57	19.6
60	Isovaleryl-DL-alanine, Isovalerylsarcosine, Hexanoylglycine, N-Acetyl-DL-Leu	sf	35.02	131	$C_9H_{18}NO_3$	188.128669	0.1	58.7
62	unknown	-	35.96	151	-	-	-	-
63	Hexanoylglycine,DL-Isovalerylalanine, Isovalerylsarcosine	sf	36.46	131	$C_9H_{18}NO_3$	188.1287	-1.79	7
-	D-2-HG-γ-lactone (1-fold derivative)	sf; std	37.47	85	$C_6H_9O_4$	145.0501	-0.37	8.5
66	DL-(*threo*)-Isocitric acid (3-fold derivatized)	sf	37.55	139	$C_9H_{15}O_7$	235.0818	0.1	59.8
67	N-Acetyl-D-Asp	NIST; sf; std	37.85	102	$C_8H_{14}NO_5$	204.087199	-1.82	50.8
68	Ethyl hydrogen fumarate, 3-Hydroxyadipic acid 3,6-lactone(, Itaconic acid)(, Citraconic acid), Mesaconic acid, Glutaconic acid	sf	38.51	90	$C_7H_{11}O_4$	159.0657	-0.97	4.7
69	N-Acetyl-L-Asp	NIST; sf; std	38.62	102	$C_8H_{14}NO_5$	204.0872	-0.9	11.8
70	DL-β-aspartyl-glycine	sf	38.79	224	$C_{10}H_{17}N_2O_7$	277.1036	3.05	25.4
71	unknown	-	38.82	67	-	-	-	-
72	(DL-Malic acid (3fold derivative)),DL-1-Deoxy-erythro-hexo-2,3-diulose (1fold derivative), DL-1,5-Anhydrofructose	sf	38.99	101	$C_8H_{13}O_7$	221.0661	-0.2	37.5
73	Phenylglyoxylic acid	sf	39.00	105.18	$C_9H_9O_3$	165.06	-0.7	56.5
74	2/3(*l*4)-Hydroxyphenylacetic acid, 4-Hydroxy-3-methylbenzoic acid, p-Anisic acid, (DL-Mandelic acid), Homovanillin (all without derivatized OH-groups)	sf	39.20	98	$C_9H_{11}O_3$	167.0708	-0.5	6
75	4-Hydroxyphenylacetic acid (1-fold derivative)	NIST; sf, std	39.50	107	$C_9H_{11}O_3$	167.0708	-0.4	6.4
76	(DL-3-Phenyllactic acid)(, Desaminotyrosine), 3-(3-Hydroxyphenyl)propanoic acid, 4-Methoxyphenylacetic acid, Coniferyl alcohol (without derivatized OH-groups)	sf	39.53	121	$C_{10}H_{13}O_3$	181.08647	-3.96	16.1

Table S1. continued.

Nr	assigned metabolite(s)	identified by	ret.t (GC-qMS)	picked m/z (GC-qMS)	Elemental composition derivative+H	calculated m/z of M+H	Δ [mDa]	mSigma
77	(DL-Malic acid (3fold derivative)),DL-1-Deoxy-erythro-hexo-2,3-diulose (1fold derivative), DL-1,5-Anhydrofructose	sf	40.02	101	$C_8H_{13}O_7$	221.0661	-1.3	22.3
78	unknown	-	40.21	238	-	-	-	-
79	Elenolic acid	sf	40.22	135	$C_{12}H_{17}O_6$	257.1025	1.23	11.7
80	Phenylglyoxylic acid	sf	40.27	78	$C_9H_9O_3$	165.0552	-2.75	21
81	Vanilpyruvic acid	sf	40.28	224	$C_{11}H_{13}O_5$	225.0763	0.67	69.4
-	L-2-HG-γ–lactone (1-fold derivative)	sf; std	40.33	85	$C_6H_9O_4$	145.0501	-1.32	13
82	Acetyl citrate	sf	40.47	115	$C_{10}H_{13}O_8$	261.061	-0.8	15.3
83	Austdiol (underivatized), Dillapional	sf	41.58	90	$C_{12}H_{13}O_5$	237.0763	-0.39	29.7
84	(Phe) unknown	sf	41.76	149	$C_{12}H_{16}NO_4$	238.1079	-0.08	9.8
86	N-cyclohexylcarbonyl-Gly, Neotussilagine	NIST; sf, sf	42.38	83	$C_{10}H_{18}NO_3$	200.128669	-3.33	6.9
87	DL-5-Amino-3-oxohexanoic acid, DL-2-Amino-6-oxohexanoate, 6-Amino-2-oxohexanoic acid	sf	43.17	121	$C_9H_{16}NO_5$	218.1028	-0.77	8.6
88	see feature above	sf	43.18	120	$C_9H_{16}NO_5$	218.1028	-0.77	8.6
89	(D)L-*threo*-Isocitric acid (4-fold derivative)	sf; std	44.25	129	$C_{11}H_{17}O_9$	293.0873	-0.4	7.5
-	df: (D)L-*threo*-Isocitric acid (4-fold derivative)	sf; std	44.27	101	$C_{11}H_{17}O_9$	293.0873	-0.4	7.5
90	N-Formyl-DL-Glu, cis(/trans)-4-D(L)Hydroxy-Pro (2-fold derivative), cis/trans-3-Hydroxy-DL-Pro (2-fold derivative), 5-Amino-2-oxopentanoic acid, 5-Aminolevulinic acid, DL-Glutamic-g-semialdehyde	sf	45.78	115	$C_8H_{14}NO_5$	204.0871	0.25	6.9
91	Isovalerylglutamic acid, Suberylglycine, N-Heptanoylglycine	sf	46.34	108	$C_{12}H_{22}NO_5$	260.1498	0.96	25.3
92	see feature above	sf	46.35	109	$C_{12}H_{22}NO_5$	260.1498	0.96	25.3
93	3-Succinoylpyridine (, Hippuric acid)	sf	47.49	131	$C_{10}H_{12}NO_3$	194.081719	-2.54	15.4
94	Hippuric acid	NIST; sf; std	48.79	77	$C_{10}H_{12}NO_3$	194.0817	-0.4	6.8
95	unknown	-	53.31	143	-	-	-	-
96	Phenylacetylglycine	NIST; sf	53.88	88	$C_{11}H_{14}NO_3$	208.0974	-1.7	8.6

Identification by NIST database relied on a match >65% for resolved peaks and a match >50% for disturbed and low abundant peaks (S/N<50). Identification by sf relied on Δm <5mDa and mSigma <50 for separated peaks and mSigma <100 for disturbed and low abundant peaks. Identification by standard (std) relied on similar relative ret.t. (relative to IS) and similar mass spectra. Metabolites given in brackets were rejected after standard injection**.** df refers to double feature. Double features were not assigned to a feature Nr as they were not used for PCA analysis. Metabolites yielding two derivatization products were not assigned to a feature Nr as only their summed areas, listed in Table S3, were used for PCA analysis. Feature Nr refer to the numbers in the loadings plot (Figure S3).

Table S2. Adjusted P-values (FDRs) for t-tests of the three group comparisons and respective fcs of the 88 differentiating features of which identification results were shown in Table S1. For metabolites for which less than three quantifiable values (S/N>8) were detected in a group, the respective counts per group were noted in brackets.

		steatosis/ controls		NASH/ controls		NASH/ steatosis	
Nr	ret.t $_{(GC\text{-}qMS)}$	fc	FDR	fc	FDR	fc	FDR
1	10.83	0.30	1.79E-02	0.43	4.98E-02	1.40	>0.05
2	11.55	0.04	2.94E-02	0.13	3.21E-02	3.45	>0.05
3	11.89	0.56	3.29E-02	0.40	7.87E-03	0.71	>0.05
4	12.77	0.55	2.97E-06	0.67	1.41E-04	1.21	>0.05
6	13.38	0.34 (6/ 6)	3.89E-06	0.09 (2/ 6)	1.43E-05	0.28 (2/ 6)	>0.05
-	14.43	0.14	1.62E-06	0.41	1.62E-04	2.93	4.63E-02
7	14.44	0.14	1.62E-06	0.41	1.62E-04	2.93	4.63E-02
8	15.14	not av. (6/ 0)	not av.	not av. (0/ 0)	not av.	not av. (0/ 6)	not av.
9	16.21	0.86	>0.05	0.30	4.55E-03	0.35	3.24E-02
10	16.23	2.39	4.89E-05	1.16	>0.05	0.49	4.59E-04
11	16.37	0.16 (1/ 6)	1.69E-02	0.33 (6/ 6)	2.60E-03	2.12 (6/ 1)	>0.05
12	16.44	0.28	2.87E-03	0.26	3.48E-03	0.93	>0.05
13	16.85	0.09	3.25E-05	0.27	5.53E-04	3.08	>0.05
14	16.88	1.72	8.54E-04	0.80	>0.05	0.46	2.56E-04
15	17.53	0.20	4.34E-05	0.11	2.20E-04	0.51	>0.05
16	18.66	18.97	1.61E-05	2.82	>0.05	0.15	8.90E-05
17	19.08	not av. (0/ 6)	not av.	not av. (0 / 6)	not av.	not av. (0/ 0)	not av.
18	19.36	6.74	1.14E-10	0.99	>0.05	0.15	1.12E-10
19	19.37	9.22	1.75E-08	1.05	>0.05	0.11	1.59E-09
21	20.04	not av. (0/ 6)	not av.	0.18 (3/ 6)	>0.05	not av.(3/ 0)	not av.
22	20.13	1.38	1.24E-02	1.92	1.84E-05	1.39	3.93E-03
23	20.27	10.52	1.59E-07	1.52	>0.05	0.14	2.27E-07
24	20.51	71.03 (6/ 1)	1.50E-07	1.90 (6/ 1)	>0.05	0.03 (6/ 6)	4.28E-10
25	20.82	0.07 (5/ 6)	3.99E-06	0.02 (1/ 6)	3.95E-04	0.33 (1/ 5)	>0.05
27	22.14	0.23	8.18E-05	0.15	8.97E-05	0.67	>0.05
-	22.26	0.04	1.06E-02	0.11	2.01E-02	2.87	>0.05
29	22.42	0.05	6.66E-04	0.32	4.55E-03	6.19	>0.05
30	22.57	0.44	9.82E-06	0.16	5.85E-07	0.38	1.45E-02
31	22.87	9.55	1.50E-14	0.65	>0.05	0.07	8.03E-15
32	23.49	1.96	4.02E-05	1.02	>0.05	0.52	1.55E-04
-	24.41	0.06	2.83E-03	0.17	8.09E-03	2.94	>0.05
34	24.42	0.05	2.67E-03	0.16	8.05E-03	3.25	>0.05
36	25.22	0.15	9.82E-06	0.11	8.97E-05	0.70	>0.05
37	25.83	not av. (0/ 6)	not av.	not av. (0/ 6)	not av.	not av. (0/ 0)	not av.
38	26.14	0.10 (1/ 6)	2.46E-02	0.09 (1/ 6)	2.80E-02	0.85 (1/ 1)	>0.05
42	27.51	not av. (6/ 0)	not av.	not av. (0/ 0)	not av.	not av. (0/ 6)	not av.
43	27.72	0.22	4.87E-07	0.21	1.27E-06	0.96	>0.05
44	27.75	1.84	5.29E-03	2.15	8.89E-04	1.17	>0.05
45	28.29	not av. (0/ 6)	not av.	not av. (0/ 6)	not av.	not av. (0/ 0)	not av.
46	29.49	0.25 (6/ 6)	2.23E-05	0.03 (1/ 6)	7.23E-04	0.11 (1/ 6)	>0.05
47	29.62	0.18 (6/ 6)	2.37E-05	0.03 (1/ 6)	1.39E-03	0.18 (1/ 6)	>0.05
48	29.80	0.33	9.82E-06	0.57	1.19E-03	1.75	>0.05

Table S2. continued.

		steatosis/ controls		NASH/ controls		NASH/ steatosis	
Nr	ret.t $_{(GC\text{-}qMS)}$	fc	FDR	fc	FDR	fc	FDR
50	31.25	0.28 (6/ 6)	>0.05	not av. (0 / 6)	not av.	not av. (0/ 6)	not av.
51	31.78	0.14 (1/ 6)	>0.05	not av. (0 / 6)	not av.	not av. (0 / 1)	not av.
52	31.82	0.35	6.43E-03	0.15	1.63E-03	0.43	>0.05
53	31.99	4.35	1.61E-05	1.00	>0.05	0.23	4.95E-05
54	32.05	13.56	2.31E-06	1.80	>0.05	0.13	1.06E-05
55	32.29	0.13 (1/ 6)	>0.05*	not av. (0/ 6)	not av.	not av. (0/ 1)	not av.
56	32.89	0.04	2.67E-03	0.16	8.05E-03	3.59	>0.05
57	33.28	0.04	2.67E-03	0.16	8.05E-03	3.60	>0.05
58	34.31	3.08	2.19E-04	0.69	>0.05	0.22	2.07E-04
59	34.73	0.05	1.12E-06	0.33	8.97E-05	6.67	>0.05
60	35.02	0.82	>0.05	0.55	1.84E-03	0.68	>0.05
62	35.96	0.61 (6/ 6)	2.85E-02	0.08 (1/ 6)	1.08E-02	0.13 (1/ 6)	>0.05
63	36.46	0.49	5.13E-05	1.02	>0.05	2.10	1.00E-04
-	37.47	0.22	1.61E-05	0.57	4.31E-03	2.61	3.09E-02
66	37.55	3.03	2.73E-03	1.58	>0.05	0.52	4.63E-02
67	37.85	0.18	8.40E-06	0.25	5.06E-05	1.34	>0.05
68	38.51	3.41	1.95E-07	0.43	4.01E-02	0.13	1.70E-08
69	38.62	0.10	5.00E-06	0.25	7.79E-05	2.39	>0.05
70	38.79	0.13	7.22E-09	0.06	1.46E-08	0.50	>0.05
71	38.82	3.51 (6/ 2)	3.77E-03	0.61 (1/ 2)	>0.05	0.18 (1/ 6)	2.07E-02
72	38.99	0.02	9.82E-06	0.30	4.98E-04	14.46	>0.05
73	39.00	0.10 (4/ 6)	>0.05	not av. (0/ 6)	not av.	not av. (0/ 4)	not av.
74	39.20	0.45	1.66E-04	0.55	1.78E-03	1.24	>0.05
75	39.50	2.89	7.10E-05	1.83	3.38E-02	0.63	2.15E-02
76	39.53	0.08	5.37E-07	0.02	1.28E-06	0.31	>0.05
77	40.02	0.02	8.40E-06	0.30	4.25E-04	14.59	>0.05
78	40.21	0.03	1.59E-07	0.003	1.88E-06	0.12	>0.05
79	40.22	0.03	1.30E-07	0.004	1.32E-06	0.15	>0.05
80	40.27	0.58	7.45E-04	0.34	3.01E-05	0.59	>0.05
81	40.28	1.10	>0.05	0.66	>0.05	0.61	4.24E-02
-	40.33	0.08	5.42E-04	0.31	6.55E-03	3.93	>0.05
82	40.47	0.03	7.56E-06	0.28	2.68E-04	8.68	>0.05
83	41.58	0.33	6.07E-04	0.32	9.47E-04	0.97	>0.05
84	41.76	0.56	1.69E-03	0.80	>0.05	1.42	>0.05
86	42.38	42.37	1.92E-16	1.15	>0.05	0.03	2.03E-16
87	43.17	0.07 (6/ 6)	>0.05	not av. (0/ 6)	not av.	not av. (0/ 6)	not av.
88	43.18	0.08 (6/ 6)	1.04E-05	0.01 (2/ 6)	2.26E-04	0.17 (2/ 6)	>0.05
89	44.25	0.88	>0.05	1.46	8.20E-03	1.66	4.09E-03
-	44.27	0.89	>0.05	1.45	8.05E-03	1.62	4.18E-03
90	45.78	2.22	2.97E-06	2.54	7.08E-07	1.15	>0.05
91	46.34	45.94	1.14E-11	1.28	>0.05	0.03	9.80E-13
92	46.35	41.26	1.50E-14	1.19	>0.05	0.03	8.03E-15
93	47.49	not av. (6/ 0)	not av.	not av. (1/ 0)	not av.	0.04 (1/ 6)	>0.05*
94	48.79	0.21	7.89E-08	0.02	1.46E-08	0.11	4.63E-02
95	53.31	0.02	2.25E-02	0.12	2.76E-02	6.44	>0.05
96	53.88	3.30	1.95E-07	1.58	3.13E-02	0.48	1.15E-05

not. av. refers to not available for the calculation of fcs due to less than three quantifiable values in one of the two compared groups. The R 'limma' package was able to determine adjusted p-values (FDRs) if at least one value was available as it estimates a SD from the SDs of the other features.

Table S3. Identification results, retention times (ret.t.), integrated *m/z*, adjusted P-values (FDRs) and fcs for three group comparisons of 11 additional features of interest. For metabolites for which less than three quantifiable values (S/N>8) were detected in minimum one of the groups, the respective counts of compared groups were noted in brackets.

							steatosis/ controls		NASH/ controls		NASH/ steatosis	
Nr	assigned metabolite(s)	identified by	ret.t $_{(GC\text{-}qMS)}$	Integrated m/z $_{(GC\text{-}qMS)}$	calculated m/z of M+H	Δ[mDa]	fc	FDR	fc	FDR	fc	FDR
5	DL-3-Methyl-2-oxovalerate	std	13.36	85	-	-	0.92	>0.05	0.66	8.05E-03	0.71	>0.05
20	Adipic acid	std	19.59	114	175.0970	-0.07	0.52	1.67E-02	0.74	>0.05	1.43	>0.05
33	D-*allo*-Ile	sf; std	23.53	144	204.1236	-1.49	0.86	>0.05	0.22	1.78E-03	0.26	1.42E-02
39	N-Acetyl-L-Ala	std	26.58	86	-	-	0.21 (1/4)	n.av.	n.av. (0/4)	n.av.	n.av. (0/1)	n.av.
40	Suberic acid	NIST; std	26.87	129	203.1283	-0.17	1.40	>0.05	0.63	>0.05	0.45	3.47E-02
41	N-Acetyl-D-Ala	std	27.06	86	-	-	0.28 (4/5)	n.av.	n.av. (0/5)	n.av.	n.av. (0/4)	n.av.
-	L-*threo*-Isocitric acid-γ-lactone	std	49.3	143	203.0556	-0.34	1.22	>0.05	1.23	>0.05	1.01	>0.05
97	D-Malate (2-fold+3fold)	std + std	22.00; 29.30	103; 75	221.0661 (2-fold)	-	0.06 (1/6)	>0.05	0.12 (4/6)	>0.05	1.93 (4/1)	>0.05
98	L-Malate (2-fold+3fold)	NIST; sf; std + std	22.20; 30.73	103; 75	221.0661 (2-fold)	-1.7	0.09	4.78E-03	0.22	1.41E-02	2.30	>0.05
99	D-2-HG (3-fold +lactone)	std + sf; std	33.52; 37.47	71; 85	145.0501 (lactone)	-0.37	0.21	1.27E-05	0.56	3.48E-03	2.62	2.92E-02
100	L-2-HG (3-fold +lactone)	std + sf; std	34.24; 40.34	71; 85	145.0501 (lactone)	-1.32	0.10	6.07E-04	0.33	7.27E-03	3.22	>0.05

n. av. refers to not available for the calculation of fcs due to less than three quantifiable values in one of the two compared groups. The R 'limma' package can determine adjusted p-values (FDRs) if at least one value was available as it estimates a SD from the SDs of the other features.

12 CURRICULUM VITAE

Persönliche Daten:	Magdalena Ch. Waldhier	**Name**
	22.07.1983	**Geburtsdatum**
	Hindenburg	**Geburtsort**
	Deutsch	**Staatsangehörigkeit**

Ausbildung

Promotion

Institut für funktionelle Genomik — **5/2009 – aktuell**

Fakultät Chemie und Pharmazie

–Universität Regensburg

Stipendium

Promotionsabschlussförderung — **10/2013 - 09/2014**

aus dem „Bayerischen Programm

zur Realisierung der Chancengleichheit für

Frauen in Forschung und Lehre“

Diplom-Chemie

Abschluss: Diplom — **10/2008**

Note: sehr gut

Vordiplom: — **10/2005**

Note: gut

Studium der Chemie — **08/2003 - 10/2008**

Universität Regensburg

Schwerpunkte: Analytik, Physikalische Chemie,

Naturwissenschaftliche Informatik

Schulbildung

Allgemeine Hochschulreife	**06/2003**
Note: gut	
Apian- Gymnasium Ingolstadt	**09/1994 - 06/2003**

Berufserfahrung

Mitarbeiterin der AGROLAB Laborgruppe GmbH	**seit 06/2015**

Besondere Kenntnisse

Englisch (sehr gute Kenntnisse in Wort und Schrift)	**Sprachkenntnisse**
Polnisch (Muttersprache)	
Spanisch (sehr gute Kenntnisse in Wort und Schrift)	
Französisch (gute Kenntnisse in Wort und Schrift)	
MS Office (sehr gute Kenntnisse), SPSS, R	**EDV**
Programmierung in HTML, MySQL, PHP, LabView	
Kenntnisse in uni- und multivariater Statistik	**Statistik**

Privates

Mutterschutz und Elternzeit	**08/2012 - 09/2013**
Schwimmen, Volleyball, Yoga	**Hobby**

13 PUBLICATIONS AND PRESENTATIONS

13.1 PUBLICATIONS

Waldhier MC, Wachsmuth CJ, Gruber MA, Hellerbrand C, Zhu W, Nürnberger N, Dettmer K, Oefner PJ. Chiralomics: adding a new dimension to metabolomics. In preparation.

Landfried K, Zhu W, **Waldhier MC**, Schulz U, Ammer J, Holler B, Wolff D, Edinger M, Peter K, Kreutz M, Andreesen R, Oefner PJ, Holler E. Tryptophan catabolism is associated with acute GvHD following human allogeneic stem cell transplantation and indicates activation of indole-amine-2,3-dioxygenase. *Blood* **2011**;118(26):6971-6974.

Wachsmuth CJ, Almstetter MF, **Waldhier MC**, Gruber MA, Nürnberger N, Oefner PJ, Dettmer K. Performance evaluation of gas chromatography-atmospheric pressure chemical ionization time-of-flight mass spectrometry for metabolic fingerprinting and profiling. *Analytical Chemistry* **2011**;83(19):7514-7522.

Waldhier MC, Almstetter MF, Nürnberger N, Gruber MA, Dettmer K, Oefner PJ. Improved enantiomer resolution and quantification of free D-amino acids in serum and urine by comprehensive two-dimensional gas chromatography-time-of-flight mass spectrometry. *Journal of Chromatography A* **2011**;1218(28):4537-4544.

Waldhier MC, Dettmer K, Gruber MA, Oefner PJ. Comparison of derivatization and chromatographic methods for GC-MS analysis of amino acid enantiomers in physiological samples. *Journal of Chromatography B* **2010**;878(15-16):1103–1112.

Waldhier MC, Gruber MA, Dettmer K, Oefner PJ. Capillary electrophoresis and column chromatography in biomedical chiral amino acid analysis. *Analytical and Bioanalytical Chemistry* **2009**;394(3):695–706.

Borisov SM, **Waldhier MC**, Klimant I, Wolfbeis OS. Optical carbon dioxide sensors based on silicone-encapsulated room-temperature ionic liquids. *Chemistry of Materials* **2007**;19(25):6187–6194.

13.2 Presentations

13.2.1 Oral Presentations

Waldhier MC, Wachsmuth CJ, Gruber MA, Hellerbrand C, Zhu W, Nürnberger N, Dettmer K, Oefner PJ
*'Chiralomics: adding a new dimension to metabolomics'***,** 12th Austrian Proteomic Research Symposium (APRS 2014) in Salzburg, Österreich.

Waldhier MC
'Enantioselective amino acid analysis of physiological fluids by GC-MS.' 21st Postgraduate Seminar of the Separation Science workgroup (GDCh),(2011) in Hohenroda, Deutschland.

13.2.2 Poster Presentation

Waldhier MC, Almstetter MF, Gruber MA, Dettmer K, Oefner PJ
'Chiral amino acid analysis of physiological fluids by GC-MS.', 34th International Symposium on Capillary Chromatography (ISCC 2010) in Riva del Garda, Italien.

14 SUMMARY

Chirality is not a rare phenomenon in metabolomes. Nevertheless, common metabolomics approaches still detect enantiomers as a single signal. However, they are individual metabolites due to different stereospecific enzymes catalyzing their metabolism. The here presented methods consider the configuration of chiral metabolites in the interpretation of metabolomics data to investigate the following biomedical hypotheses. D-AAs, albeit much lower abundant than their antipodes, are potential diagnostic markers for diseases affecting the liver, the gut and the gut flora. The other assumption of this thesis was that the comprehensive resolution of stereoisomers from metabolomes, providing more detailed metabolic fingerprints than conventional approaches, would facilitate the differentiation of groups.

In order to investigate the former hypothesis two different GC-MS techniques were used for the implementation, optimization and validation of quantitative AAE analysis, primarily in urine and serum. The GC-qMS method using MeOH/MCF derivatization and a γ-CD derivative for enantiomer separation was chosen, among several tested derivative/chiral selector combinations, in my diploma thesis as the most effective GC-qMS method for quantitative AAE analysis with respect to the number of baseline separated proteinogenic AAE pairs and peak intensities. Sample preparation was optimized to allow the accurate quantification of exclusively free AAEs. In addition injection parameter and IS contents were optimized to decrease LLOQs and the method was validated by comparison to a non-chiral GC-qMS method for AA quantification. Finally, the method was subjected to biomedical applications that underlined the potential of D-AAs as diagnostic markers due to changed D-AA levels found in mouse serum and mouse liver tissues as a consequence of pathological changes of the liver. The method separated ten pairs of AAEs, but it failed to separate Phe enantiomers, D-Ile/L-Leu, L-Thr/L-Asp, and L-Ser/D-Met. For L-Thr, L-Asp and D-Met a specific *m/z* enabled their accurate quantification in SIM mode but the quantification of the other coeluting enantiomers was impeded. Moreover, not each D-AA that was baseline separated from its antipode could be quantified in all samples of interest due to insufficient LLOQs. Thus, the potential of comprehensive GC×GC-TOFMS was tested for quantitative AAE analysis in urine and serum. The same derivative/chiral selector combination was used and a ZB-AAA column provided best AAE resolution as the second dimension selector from two different

selectors tested. Upon optimization of the temperature program, baseline separation was accomplished for all detected AAEs except for Phe enantiomers. The method was validated by comparison to the chiral GC-qMS method and pros and cons of both approaches were discussed. The application of chiral GC×GC-TOFMS revealed increased D-AA serum levels in patients with liver cirrhosis when compared to respective serum levels of healthy individuals. Finally, performing a chiral fingerprinting approach, it was demonstrated that comprehensive enantiomer resolution assisted with the differentiation of different NAFLD stages in the analysis of urine samples from respective mouse models. There was observed a clear group separation of the three investigated groups after PCA of differentiating features and D-Val, D-2-HG and D-*allo*-Ile levels significantly differentiated NASH from hepatic steatosis. There were identified further enantiomers of hydroxydiacids and AA derivatives that significantly differentiated the diseased groups from controls and besides D-Val six other separated AAEs differentiated the experimental groups. This chiral GC-qMS based fingerprinting approach introduced a new field of investigation that I named ‘chiralomics’ as it expanded metabolomics to the chiral dimension.

15 ZUSAMMENFASSUNG

Viele Stoffwechselprodukte sind chiral, werden aber in der Metabolomik meist nicht getrennt bestimmt. Stereoisomere sind jedoch auf Grund der Stereospezifizität der meisten Enzyme, die für ihren Auf- und Abbau verantwortlich sind, eigenständige Stoffwechselprodukte und Veränderungen in ihrer Abundanz können Aufschluss über gestörte Stoffwechselwege geben. So sind D-Aminosäuren (D-As), die zwar in deutlich geringeren Mengen vorkommen als ihre Spiegelbilder, potenzielle diagnostische Marker für Krankheiten, die beispielsweise die Funktion der Leber, des Darms und der Darmflora beeinträchtigen. Die zweite Annahme der Arbeit war, dass die Auflösung von allen erfassbaren Stereoisomeren, detailliertere metabolische Fingerabdrücke generiert, die die Differenzierung von Gruppen erleichtern.

Initiales Ziel der Dissertation war die Optimierung der GC-MS basierten, quantitativen Analysen von Aminosäure-Enantiomeren in biologischen Proben wie Blut und Urin. Ausgangspunkt war die Derivatisierung der Aminosäuren mit Methylchloroformat und Methanol, gefolgt von deren Trennung auf einer γ-CD basierten stationären Phase und anschließender Detektion mittels Quadrupol-Massenspektrometrie. Diese Kombination hatte sich im Rahmen meiner Diplomarbeit als die effektivste unter den getesteten Derivat/ Säule Kombinationen für die quantitative Bestimmung von Aminosäure-Enantiomeren erwiesen. Durchgeführte Verbesserungen betrafen die Probenvorbereitung (Vorabtrennung von Proteinen und Durchführung der Derivatisierung ohne Einsatz von NaOH, um die Bestimmung von protein- und peptidgebundenen AsE zu unterbinden), die Injektion und die Konzentration der internen Standards, wodurch eine bis zu 16-fache Verbesserung der unteren Bestimmungsgrenzen erzielt werden konnten. Die optimierte Methode wurde über einen Methodenvergleich mit einer etablierten achiralen GC-qMS Methode für quantitative As Analytik in Serum und Urin validiert. Die Methode ermöglichte die Trennung von zehn Aminosäure-Enantiomerenpaaren, schaffte es jedoch nicht Phe Enantiomere, sowie D-Ile/L-Leu, L-Thr/L-Asp, und L-Ser/D-Met aufzulösen. Von diesen konnten im SIM-Modus, anhand von charakteristischen *m/z* Werten L-Thr, L-Asp und D-Met quantifiziert werden, während die Bestimmung der anderen überlappenden Enantiomere gestört war. In der Anwendung an Serum und Leberproben aus Mausmodellen zur Fettleber erwiesen sich überdies die Bestimmungsgrenzen ungenügend, um alle D-As, die von ihrer L-Form getrennt

waren, in allen Proben zu quantifizieren. Deshalb wurde die Leistungsfähigkeit der allumfassenden zweidimensionalen Gaschromatographie (GC×GC-TOFMS) für die Bestimmung von AsE in Urin und Serum getestet. Es wurde die gleiche As Derivat/ chirale Säule Kombination verwendet und zudem eine ZB-AAA Säule, welche die beste Enantiomerenauflösung, von den zwei für die zweite Dimension getesteten Säulen, ermöglichte. Über die Optimierung des Temperaturprograms erreichte ich die Basislinien-Trennung aller erfassten AsE mit Ausnahme der Phe Enantiomere. Die Methode wurde über einen Methodenvergleich mit der chiralen GC-qMS validiert und Vor- und Nachteile beider Methoden wurden diskutiert. Die GC×GC Methode fand erhöhte D-As Serum Gehalte in Leberzirrhose Patienten im Vergleich zum D-As Serum Gehalt in gesunden Probanden und bekräftigte damit die untersuchte Hypothese. Die zweite Annahme dieser Arbeit wurde mit Hilfe eines erstmalig durchgeführten chiralen Fingerprintings untersucht. Es wurde gezeigt, dass die allgemeine Trennung von Enantiomeren zur Unterscheidung verschiedener NAFLD Stufen, anhand von Urin der entsprechenden Mausmodelle, beiträgt. Eine deutliche Gruppentrennung war mit Hilfe von PCA der differenzierenden Peaks sichtbar und D-Val, D-*allo*-Ile und D-2-HG Gehalte unterschieden NASH von der hepatischen Steatose deutlich. Es wurden weitere Enantiomere von Hydroxydisäuren und As Derivaten identifiziert, die die kranken von den gesunden Mäusen unterschieden und weitere sechs AsE differenzierten die experimentellen Gruppen. Dieser allumfassende enantioselektive Ansatz mittels GC-qMS eröffnete ein neues Wissenschaftsgebiet, welches ich „Chiralomics“ nannte, da es das Gebiet der „Metabolomics“ um die chirale Dimension erweitert.

Erklärung

Hiermit versichere ich, dass ich die vorliegende Arbeit selbst verfasst und keine anderen als die angegebenen Quellen und Hilfsmittel verwendet habe.

Regensburg, 15.10.2015

Magdalena Waldhier